Kurzschlusserkennung und Lokalisierung mittels Frauscher Tracking Solutions Kurzschlussortung

Ein Projekt finanziert im Rahmen der Verkehrsinfrastrukturforschung 2015 (**VIF2015**)

September 2015

Impressum:

Herausgeber und Programmverantwortung:
Bundesministerium für Verkehr, Innovation und Technologie
Abteilung Mobilitäts- und Verkehrstechnologien
Radetzkystraße 2
A – 1030 Wien

ÖBB-Infrastruktur AG
Nordbahnstraße 50
A – 1020 Wien

Autobahnen- und Schnellstraßen-Finanzierungs-Aktiengesellschaft
Rotenturmstraße 5-9
A – 1010 Wien

Für den Inhalt verantwortlich:
Frauscher Sensortechnik GmbH
Gewerbestraße 1
4774 St. Marienkirchen

Programmmanagement:
Österreichische Forschungsförderungsgesellschaft mbH
Thematische Programme
Sensengasse 1
A – 1090 Wien

Kurzschlusserkennung und Lokalisierung mittels Frauscher Tracking Solutions Kurzschlussortung

Ein Projekt finanziert im Rahmen der

Verkehrsinfrastrukturforschung

(VIF2015)

AutorInnen:

Florian Grünberger

Manuel Hemetsberger

Gavin Lancaster

Auftraggeber:

Bundesministerium für Verkehr, Innovation und Technologie

ÖBB-Infrastruktur AG

Autobahnen- und Schnellstraßen-Finanzierungs-Aktiengesellschaft

Auftragnehmer:

Frauscher Sensortechnik GmbH

Formale Vorgaben:

Einrichtung der Seite	**Abstand** in cm
Oben:	3,5
Unten:	3
Links:	3
Rechts:	2,5

Formatvorlage	**Schriftart**	**Schriftgröße**
Hauptkapitelüberschriften	Arial, fett, Großbuchstaben	13pt
Überschriften	Arial, fett	13pt
Standardtext	Arial, 1,5-zeilig, Blocksatz	11pt
Überschriften von Verzeichnissen	Arial, fett, Großbuchstaben	13pt
Inhaltsverzeichnis Abbildungsverzeichnis Tabellenverzeichnis Literaturverzeichnis	Arial	12pt
Fußnotenzeichen	Arial, hochgestellt	10pt
Fußnotentext	Arial	10pt
Untertitel von Tabellen und Abbildungen	Arial, fett	10pt
Quelle von Tabellen und Abbildungen	Arial	8pt
Seitennummerierung	Arial, zentriert, Seitenende	10pt

INHALTSVERZEICHNIS

Abbildungsverzeichnis

Tabellenverzeichnis

1 EXECUTIVE SUMMARY

Jährlich kommt es im Streckennetz der ÖBB zu über eintausend Kurzschlüssen an Oberleitungen. Diese Kurzschlussvorfälle sind durch Betriebsunterbrechungen und notwendige Prüf- und Wartungstätigkeiten ein signifikanter Kostenfaktor. Die momentan eingesetzte Technik in den Unterwerken erkennt zwar das Auftreten eines Kurzschlusses und ordnet ihm einen Speisebezirk zu, eine genauere Lokalisierung ist damit jedoch nicht möglich. Diese erfolgt in der Praxis mittels manueller Fehlereingrenzung durch den Dispatcher der Leitstelle. Das hier beschriebene Forschungsprojekt wurde mit dem Ziel ins Leben gerufen, das Potential der Distributed Acoustic Sensing Technologie (DAS) zur Lokalisierung von Kurzschlussorten zu evaluieren.

Das Prinzip von DAS basiert darauf, Veränderungen in der Reflexion von Laserimpulsen zu detektieren, die durch Schallwellen bzw. Vibration ausgelöst werden, wenn diese auf ein Glasfaserkabel treffen (Lichtwellenleiter, LWL). Dazu wird ein Laserimpuls in eine Single Mode Faser gesendet. Lokale Veränderungen des reflektierten Lichts bilden die Datengrundlage für DAS. Speziell entwickelte Algorithmen ermöglichen auf Basis der Rückstreuungsdaten die Klassifizierung der Ursachen solcher Veränderungen. Die Firma Frauscher hat das auf DAS basierende System FTS entwickelt (Frauscher Tracking Solutions). Dieses System wurde für die Klassifizierung bestimmter Ereignisse entlang von Eisenbahninfrastruktur entwickelt und wurde in Zusammenhang mit diesem Forschungsprojekt verwendet um die Erfassbarkeit von Oberleitungskurzschlüssen zu prüfen und Daten zu erfassen. FTS legte somit die Grundlage für das Erreichen der im Projekt definierten Ziele.

Primäres Ziel des Forschungsprojektes war es, die Einsatzgrenzen für Kurzschlusslokalisierung mittels Fibre Optic Sensing festzuhalten und nach Möglichkeit einen Algorithmus für die Lokalisierung von Oberleitungskurzschlüssen zu entwickeln. Im Rahmen des Verkehrsinfrastrukturforschungs-Programms wurden dazu folgende Forschungsfragen formuliert:

- Welchen Einfluss hat der Abstand des Kurzschlusses zum Unterwerk?
- Gibt es eine maximale Distanz zum Unterwerk, bis der eine Detektion möglich ist?
- Wie wirkt sich der Abstand des LWL am Boden zur Oberleitung aus?
- Welchen Einfluss hat der Abstand der Oberleitungsmasten zum LWL?
- Wirken sich verschiedene Verlegearten und Position der LWL auf die Detektionsfähigkeit aus?

Wenn ein LWL in der Nähe der Oberleitung installiert ist, wie unterscheiden sich die aufgenommenen Signale zu jenen des bodenverlegten LWL?

Zur Erreichung des Primärziels wurden die definierten Arbeitspakete systematisch abgearbeitet. Nach initialen Meetings zum besseren Verständnis der Kurzschlussthematik wurden in einer

gemeinsam mit der ÖBB ausgearbeiteten Mindmap (Abbildung 1) mögliche Einflussfaktoren auf die signaltechnische Ausprägung von Kurzschlussereignissen erarbeitet.

Abbildung 1: Mindmap zu den Einflussfaktoren auf die signaltechnische Ausprägung von Kurzschlussereignissen

Auf Basis dieser Mindmap wurde das Konzept für die später durchgeführten Praxisversuche entworfen. Verfolgt wurde dabei der Ansatz, Kurzschlüsse bewusst zu erzeugen, die aufgezeichneten Daten auszuwerten und über gemeinsame Charakteristika einen Algorithmus zur Erkennung von Oberleitungskurzschlüssen zu entwickeln. Kapitel 1 dieses Berichtes soll als Zusammenfassung des Projektverlaufs dienen. Ausführlichere Beschreibungen der einzelnen Arbeitspakete und daraus erlangten Erkenntnisse finden sich in den Kapiteln 3 bis 8.

1.1 Testreihe Allerding

Die ersten Praxisversuche wurden am Installationsort Allerding, welcher sich auf der Strecke Passau – Wels befindet, durchgeführt. Dabei wurden 63 selbstinduzierte Kurzschlüsse aufgenommen um das Kurzschlussereignis datentechnisch nachzuvollziehen und potentielle Einflussparameter auf die Detektierbarkeit eines Kurzschlusses zu untersuchen. Folgende Erkenntnisse ließen sich aus dieser Versuchsreihe ableiten:

- Identisch durchgeführte Kurzschlüsse zeigen unterschiedliche Signalausprägungen, die je nach Sichtbarkeit klassifiziert werden können.
- Kurzschlüsse sind abhängig vom betrachteten Frequenzbereich unterschiedlich gut zu erkennen
- Gleichzeitig zum Kurzschluss kommt es über mehrere Kilometer zu zeitgleichen Anregungen des Lichtwellenleiters.
- Positive Korrelation zwischen Energiegehalt und Sichtbarkeit des Kurzschlusses.
- Eine zunehmende Distanz zwischen Kurzschluss und FTS System übt eine dämpfende Wirkung auf das aufgezeichnete Signal aus.

- Die unterschiedliche Länge des Lichtpulses im LWL beeinflusst die Signalqualität.
- Die Verlegungsart ist entscheidend für die Signalqualität. Erdverlegte Kabel zeigen sich durch die bessere akustische Ankopplung als sensibler im Vergleich zur Verlegung in Betontrögen.

Zur Erhöhung der Datenquantität wurde eine zweite Versuchsreihe angesetzt. Diese wurde zum besseren Verständnis von Infrastruktureinflüssen auf der Güterzugumfahrung (GZU) in St. Pölten durchgeführt. Die GZU entspricht dem Aufbau nach einer modernen Eisenbahnstrecke im Netz der ÖBB und unterscheidet sich daher von Allerding.

1.2 Testreihe GZU

Auf der GZU wurden in der zweiten Versuchsreihe mehr als 70 neue Aufnahmen generiert. Dabei setzten sich diese aus selbstinduzierten Kurzschlüssen und zusätzlichen Signalquellen zusammen. Diese zusätzlichen Signalquellen wurden genutzt um die über den LWL potentiell messbaren Ereignisse eines Kurzschlusses isoliert zu betrachten:

- Schallereignis durch den Kurzschluss: Prangerschüsse (durch Schwarzpulver ausgelöste Explosionen).
- Vibration des anliegenden Oberleitungsaufbaus (Vibrationen der Oberleitungsmasten).

Durch die Versuche auf der GZU wurden einige Erkenntnisse aus Allerding bestätigt:

- Unterschiedliche Klassifizierungen der Kurzschlüsse.
- Frequenzabhängigkeit der Sichtbarkeit in den Daten.
- Zeitgleiche Anregungen entlang der Infrastruktur. Im Anschluss an diese Testreihe wurde ermittelt, dass die kilometerweiten, punktuellen Anregungen des LWL zur Kurzschlusszeit durch Bewegungen der Oberleitung erzeugt werden. Durch den schlagartigen Stromanstieg im Kurzschlussfall entstehen Magnetfelder und Kräfte, die sich entlang der Oberleitung in akustisch hörbaren Bewegungen niederschlagen. Diese Bewegungen erzeugen damit die beobachteten Signale.

Abweichungen zu Allerding und neue Erkenntnisse:

- Signale werden auf der GZU häufiger beobachtet, dafür mit einem deutlich geringer ausgeprägten V-Muster. Die Infrastruktur wirkt sich also dämpfend aus. Als naheliegende Ursache wurde die veränderte Installation der Kabeltröge ermittelt. Anstatt im Boden vergraben zu sein werden die Tröge auf Neubaustrecken auf Asphalt gelagert mit einer Matte aus Gummigranulat dazwischen. Um den Einfluss gezielt zu untersuchen wurde auf dem Frauscher Werksgelände ein Testaufbau geschaffen. Dieser Testaufbau konnte keinen signifikanten Einfluss der Gummimatten feststellen und ist daher im generellen Zusammenwirken aller örtlichen Gegebenheiten zu suchen.
- Auf der GZU korrelieren Energiegehalt und Sichtbarkeit von Kurzschlüssen nicht

- Eine höhere optische Distanz zwischen FTS und Kurzschlussort wirkt sich nicht auf das Verhältnis Signal-zu-Grundrauschen aus.
- Prangerschüsse sind datentechnisch deutlicher als V-Muster erkennbar und eigenen sich somit zur Kurzschlusssimulierung. in weitere Folge wird für dieses V-Muster der Begriff Chevron verwendet. Versuche, Oberleitungsmasten in Schwingung zu versetzen, waren nicht erfassbar.

1.3 Testreihe Allerding 2

Um weitere Versuchsdaten zu sammeln und bisherige Erkenntnisse zu überprüfen, wurde eine zweite Testreihe am Installationsort Allerding durchgeführt, wobei die Orte der Kurzschlusstests unverändert blieben. Um die Versuchsdurchführung schneller zu gestalten wurde Kurzschlüsse nicht mehr induziert, sondern nur mehr über Prangerschüsse und Mastvibration simuliert.

Bestätigte Ergebnisse:

- Unterschiedliche Klassifizierungen der Kurzschlüsse. Dies hat sich also in alle drei Testreihen bestätigt.
- Frequenzabhängigkeit der Sichtbarkeit in den Daten. Eine allgemeine Frequenzabhängigkeit mit einer optimalen Sichtbarkeit im niederfrequenten Bereich wird damit angenommen
- Prangerschüsse erzeugen einen klar erkennbaren Chevron ohne klare Abhängigkeit von der Schussrichtung aufzuweisen

Neue Erkenntnisse:

- Im Gegensatz zur GZU waren die Versuche, Oberleitungsmasten mit Hammerschlägen in Schwingung zu versetzen, datentechnisch sichtbar. Während Prangerschüsse das, für einen Kurzschluss charakteristische, V-Muster zeigen, wirken sich Hammerschläge nur als punktuelles Ereignis aus. Damit ist nachgewiesen, dass es das Knallereignis ist, welches die signaltechnische Grundlage für eine Lokalisierung liefert.

1.4 Algorithmusentwicklung und Implementierung

Anhand der gesammelten Versuchsdaten wurde ein Algorithmus entwickelt, der mittels Mustererkennung die zuvor bildbearbeitungstechnisch aufbereiteten Daten nach typischen Merkmalen (Features) untersucht. Dieser Algorithmus erreicht mit den jetzigen Daten der höchsten Klassifizierung (Sichtbarkeit) eine Erkennungsrate von 98%. Mit jedem zukünftig neu erzeugten Datensatz kann der Algorithmus getestet und ggf. angepasst werden.

Dieser Algorithmus wurde im Projektverlauf bereits in eine automatisierte Meldekette eingebunden. Ausgehend von einer im Kurzschlussfall automatisch von der ÖBB abgesetzten E-Mail-Benachrichtigung speichert FTS die Daten des betroffenen Zeitbereichs und stößt die Weiterverarbeitung und den Algorithmusablauf an. FTS gibt anschließend eine Rückmeldung der Lokalisierungsergebnisse aus. Diese Automatisierung bedeutet, dass über das Testsystem in

Allerding auftretende Kurzschlüsse bereits lokalisiert, oder zumindest für eine kontinuierliche Weiterentwicklung des Algorithmus verwendet werden können.

Probleme/Herausforderungen:
Die Einflussgrößen auf das am LWL ankommende Signal haben sich als sehr komplex erwiesen. Eine Durchführung selbstinduzierter Kurzschlüsse mit identischer Intensität ist in der Praxis nicht möglich. Somit zeigen die Referenzdaten bereits eine Abweichung. Selbst die Sammlung der Daten stellte sich als schwierig heraus, da der Zugang zur Strecke nur begrenzt möglich und die Arbeitsschritte während der Versuche sehr zeitaufwändig waren. Der Einfluss der Infrastruktur auf die Schallübertragung kann gar nicht hoch genug eingeschätzt werden und ist aktuell nicht quantitativ zu bewerten. Eine weitere Herausforderung stellten die zuvor nicht absehbaren Erkenntnisse dar, etwa die kilometerweiten Anregungen zur Kurzschlusszeit. Insgesamt lässt sich von einem sehr komplexen Forschungsprojekt sprechen.

1.5 Fazit

Trotz der weit gefächerten Aufgabenstellung konnte im Projektverlauf die grundsätzliche Eignung von DAS-basierenden System für die Lokalisierung von Oberleitungskurzschlüssen nachgewiesen werden. Die Technologie besitzt damit Potential für die Effizienzsteigerung der ÖBB Instandhaltungsprozesse und wird auch nach Ablauf des Förderprojektes weiterverfolgt. Einsatzgrenzen der Technologie wurden theoretisch erhoben und in Praxisversuchen untersucht. Die gestellten Forschungsfragen werden in Kapitel 3.4.6 beantwortet. Das Projekt hat bereits einen Prototyp eines automatisierten Lokalisierungssystems hervorgebracht, der zukünftig mit der ÖBB weiterentwickelt werden soll. Die intensive Zusammenarbeit im Zuge dieses Forschungsprojekts hat nicht nur die Partnerschaft zwischen der ÖBB und der Firma Frauscher erheblich bereichert, sondern auch die technologische Grundlagenarbeit auf den Weg gebracht für eine dem Zeitgeist der Digitalisierung entsprechende Möglichkeit der Infrastrukturüberwachung. Aufbauend auf den erlangten Erkenntnissen wurden bereits die nächsten Schritte definiert in Richtung eines anwendbaren Endproduktes zur Kurzschlusslokalisierung. Dazu zählt eine tiefere Einarbeitung in die technischen und physikalischen Grundlagen unter Berücksichtigung der verschiedenen gemessenen Signalausprägungen. Die Zusammenarbeit wird sich über die Grenzen des Forschungsprojekts hinaus auch in weiteren Veröffentlichungen von Ergebnissen niederschlagen. In den derzeitigen und auch zukünftigen Feldanwendungen geht es besonders darum weitere und vor allem echte Kurzschlussdaten zu gewinnen, zu analysieren und daraus Maßnahmen zur Algorithmusoptimierung abzuleiten und Leistungskennzahlen für die Systemwirksamkeit zu ermitteln. Für die Automatisierung gilt es vor allem Rechenzeiten zu verkürzen, Verfügbarkeit zu erhöhen und Lokalisierungsinformation effizient zu kommunizieren. Eine direkte Einbindung des Systems in die ÖBB Infrastruktur wurde bereits mit den Verantwortlichen diskutiert. Nach wie vor

sehen die Forschungspartner hohes Potential in der Technologie und werden auch nach Beendigung des Förderrahmens an einer Überführung in die operative Praxis arbeiten.

2 ARBEITSPAKETE UND MEILENSTEINE

AP Nr.	Arbeitspaket Bezeichnung	Fertigstellungsgrad	Basistermin		Aktuell		Erreichte Ergebnisse / Abweichungen
			Anf.	Ende	Anf.	Ende	
1	Projektmanagement	100%	06.16	05.18	06.16	05.18	Es finden regelmäßig Treffen mit dem AG statt in welchen das weitere Vorgehen und die Ergebnisse diskutiert werden. Diese Treffen werden in einem Protokoll festgehalten.
2	Auswahl eines geeigneten Erprobungsortes	100%	06.16	07.16	07.16	05.17	Als Erprobungsort wurde zu Projektbeginn die Frauscher Testanlage in Allerding an der ÖBB Strecke Passau – Wels gewählt. Weitere Tests erfolgten auf der Güterzugumfahrung nahe St. Pölten. Beide Strecken sind repräsentativ für eine typische zweigleisige ÖBB Infrastruktur.
3	Installationsphase	100%	07.16	08.16	08.16	08.16	Das FTS System wurde in der Testanlage montiert und für die Systemeinstellungen Kurzschlussversuche optimiert.
4	Algorithmus Entwicklung Level 1	100%	08.16	07.17	10.16	04.18	In vier Nächten wurden 63 Kurzschlüsse für Referenzmuster erzeugt. Die Ergebnisse und Muster sind im Bericht D5208-EN-0.1 festgehalten welcher an die ÖBB übergeben wurde.
5	Algorithmus Entwicklung Level 2	70%	12.16	12.17	12.16	12.17	Das FTS System in Allerding wurde zur automatisierten Aufzeichnung von Kurzschlüssen konfiguriert um aus diesen weitere Muster für die Erkennung ableiten zu können.
6	Schnittstellen-entwicklung	100%	12.16	03.17	12.17	03.18	Im Antrag wurde ein falscher Zeitraum in der Arbeitspaketübersicht angeführt. In der detaillierten Arbeitspaket-beschreibung wurde das richtige Datum nun angeführt.

Tabelle 1: Arbeitspakete

Meilen-stein Nr.	Meilenstein Bezeichnung	Basis-termin	Akt. Planung	Meilenstein erreicht am	Anmerkungen zu Abweichungen
1	Lieferung des Equipments an die Erprobungsstelle	29.07.16	-	19.08.16	Erster Testplan bzw. Testort wurden im Zuge des Treffens am 04.08.2016 in Abstimmung mit AG festgelegt.
2	Installationsbericht der Anlage	31.08.16	-	26.08.16	Frauscher interner Bericht zur Testanlage Allerding. Parameter für das FTS System sind im Bericht D5208-EN-0.1 festgehalten.
3	Aufzeichnung von Zugüberfahrten und weiteren Geräuschquellen	30.09.16	-	17.10.16	Aufzeichnung von zusätzlichen Geräuschen war nicht notwendig, da diese bereits vorliegen. Erstmalig wurden Kurzschlüsse am 15.10.2016 im Zuge der ersten Testreihe aufgezeichnet.
4	Entwicklungsbericht	31.12.16	-	21.12.16	Die Ergebnisse und Muster aus den beiden Testnächten wurden

					im Bericht D5208-EN-0.1 festgehalten welcher an die ÖBB übergeben wurde.
5	Dokumentierte Einsatzgrenzen der Erkennung	31.05.17	31.05.18		Im Zuge der Praxistests wurden unerwartete Einflussfaktoren zu Tage gefördert. Eine zusammenfassende Bewertung erfolgt im Zuge des Abschlussberichts.
6	Prototypen Algorithmus	31.08.17	31.08.17	15.12.2017	Algorithmus wurde in einem gemeinsamen Meeting präsentiert und diskutiert.
7	Anforderungsspezifikation der Schnittstelle	31.01.17	31.01.18	29.01.2018	Der Termin wurde im Antrag falsch aus dem Meilensteinplan übernommen.
8	Report über Algorithmusentwicklung	28.02.18		27.02.2018	erfüllt
9	Abnahme der Schnittstelle	31.03.18		29.01.2018	erfüllt
10	Forschungs-Endbericht	31.05.18	31.05.18	07.06.2018	erfüllt

Tabelle 2: Meilensteine

3 ZUSAMMENFASSUNG DER PROJEKTDURCHFÜHRUNG ANHAND DEFINIERTER ARBEITSPAKETE

AP Nr. 1 Projektmanagement

Das Kick Off Meeting mit dem Auftraggeber ÖBB fand am 4. August 2016 statt. Im Zuge des Meetings wurden die bisherigen Ergebnisse beziehungsweise Erfahrungen der ÖBB mit Frauscher geteilt um daraus einen Versuchsort, Szenarien für einen Testplan und weitere unmittelbar einwirkende Umgebungsbedingungen abzuleiten. Nach dem Kick Off Meeting wurde gemeinsam mit der ÖBB eine Mindmap über mögliche Einflussfaktoren für die datentechnische Sichtbarkeit von Kurzschlüssen erstellt. Folgende Faktoren wurden dabei erarbeitet:

- Stärke des Kurzschlusses (Abstand zum Unterwerk, elektrische Phase, Leitfähigkeit des Kurzschlussauslösers)
- Vibrationsübertragung auf den Lichtwellenleiter (Lichtwellenleitertyp, Verlegeart, Abstand zum Kurzschluss, Aufbau und Umgebung der Infrastruktur, Oberleitungstyp, Masttyp)
- Parameter des Messsystems (Abstand des Kurzschlussortes zur Messeinheit, Länge des Lichtpulses)
- Äußere Einflüsse (Temperatur, Niederschlag, Wind, Luftfeuchtigkeit, Umgebungsgeräusche)

Im Projektverlauf hat der Projektleiter folgende Tätigkeiten schwerpunktmäßig durchgeführt:

- Zuverlässige und regelmäßige Kommunikation mit den Projektpartnern
- Regelmäßiger persönlicher Austausch in Meetings/Workshops. Folgende Besprechungstermine fanden im Zusammenhang mit dem Förderprojekt statt: 04.08.2016, 29.08.2016, 10.10.2016, 11.11.2016, 21.12.2016, 23.03.2017, 11.04.2017, 15.12.2017, 18.01.2018, 13.03.2018. Der Inhalt der Treffen wurde in entsprechenden Minutes of Meetings protokolliert.

- Planung und Koordination von Feldversuchen
- Sicherstellen der Termintreue gegenüber definierter Meilensteine
- Berichtswesen

AP Nr. 2 Auswahl eines geeigneten Erprobungsortes

Abbildung 2: ÖBB Strecke Passau – Wels, Höhe Allerding mit Frauscher Testcenter (rot eingerahmt)

Im Zuge der detaillierten Planung zu Projektbeginn wurde als typische Strecke im Netz der ÖBB eine zweigleisige, doppelt gespeiste Gleisanlage identifiziert. Aufgrund der geografischen Nähe zur Firma Frauscher und der geeigneten Streckencharakteristik wurde im gemeinsamen Einverständnis die Strecke Passau – Wels als primärer Versuchsort gewählt. Das Frauscher Testgebäude direkt an der Strecke in Allerding wurde zur Installation eines ortsfesten DAS Systems genutzt. Von hier aus wurden Daten aus der angrenzenden ÖBB Infrastruktur erzeugt. Das Arbeitspaket wurde durch die Lieferung und Montage eines DAS - Systems abgeschlossen. Im Zuge des Projektverlaufs wiederholte sich das Auswahlverfahren, da aufgrund der erlangten Erkenntnisse weitere Versuchsreihen an verschiedenen Orten notwendig waren. Versuche fanden dabei auf der Güterzugumfahrung (GZU) in der Nähe von St. Pölten statt, sowie ein weiteres Mal in Allerding. Zudem wurde auf dem Frauscher Werksgelände ein Testaufbau installiert, auf welchem ebenfalls Versuchsdaten erzeugt wurden.

AP Nr. 3 Installationsphase

Während der Installationsphase wurde das DAS - System in Allerding auf die gegebenen Streckenbedingungen angepasst und signaltechnisch optimiert. Als Vorbereitung für die späteren Praxisversuche wurden leicht zugängliche und damit gut verwendbare Oberleitungsmasten bereits ortsmäßig georeferenziert. Eine detaillierte Inspektion der zu testenden Streckenabschnitte erfolgte am jeweiligen Tag der Praxisversuche. Dazu wurden Teile der Strecke mit einem Turmwagen befahren und auf projektbezogene Besonderheiten untersucht (Lage des LWL, freies Gelände oder Einkesselung der Strecke).

Um die Effizienz der Datenaufzeichnung zu steigern wurde das DAS - System redundant mit zwei Fasern eines Lichtwellenleiters in Richtung des Kurzschlussortes aufgeschaltet. Da auch der Abstand des Kurzschlussortes zur DAS - Einheit als ein möglicher Beeinflussungsfaktor identifiziert wurde, wurde die zweite Faser künstlich verlängert um einen unterschiedlichen Abstand zu simulieren und systematische Signalverluste entlang der Faserlänge zu ermitteln.

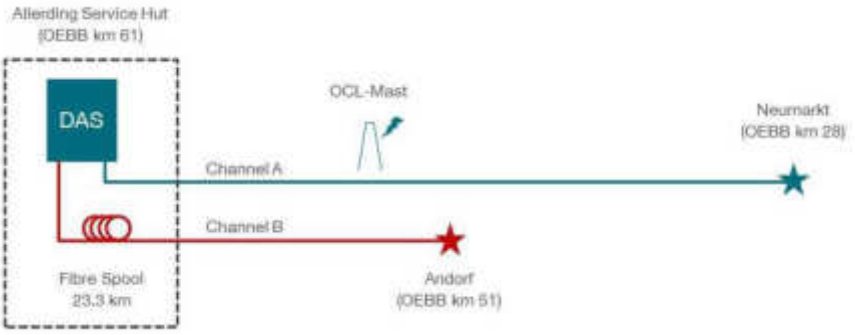

Abbildung 3: Schematische Darstellung des Messaufbaus von 15. bis 17. Oktober 2016.

AP Nr. 4 Algorithmus Entwicklung Level 1

Als Grundlage für eine spätere Algorithmuserarbeitung wurden in mehreren Schritten Felddaten erzeugt, gesammelt, aufbereitet und zur Analyse der Kurzschlussausprägungen verwendet. Die Datenaufzeichnung musste aufgrund im Projektverlauf wachsender Erkenntnisse mehrfach und an verschiedenen Standorten durchgeführt werden. Folgende Unterpunkte beschreiben die einzelnen Versuchsreihen sowie daraus abzuleitende Erkenntnisse.

AP Nr. 4.1. Versuchsreihe Allerding

Gemäß Task 4.1 im Arbeitspaket 4 wurden am Wochenende des 15. Oktobers 2016 sowie des 19. Novembers 2016 in Summe 63 Kurzschlüsse am unter Arbeitspaket 2 beschriebenen Versuchsort erzeugt. Diese sind im Testplan, welcher sich auf einem für Frauscher zugänglichen Internetserver der ÖBB befindet, dokumentiert. Die Durchführung erfolgte unter Einsatz massiver Personalressourcen auf Seiten der ÖBB und der Firma Frauscher in Nachtarbeit.

Der Einfluss von Umgebungssignaturen wurde im Laufe der Kurzschlusstests erprobt. So wurden Kurzschlüsse u.a. auch im Moment der Vorbeifahrt eines Zuges am Nachbargleis ausgelöst. Der Kurzschluss wurde über eine seitens der ÖBB gefertigte Kurzschlusseinrichtung initiiert. Folgender Abbildung ist der Versuchsaufbau zu entnehmen. Die Kurzschlusseinrichtung wurde am Mast (5) im Bereich der Oberleitung montiert. Eine Drahtbrücke (1), gehalten von einem Isolator (3) leitete den Kurzschlussstrom von der Oberleitung (2) auf einen Erdungswinkel (4) beim Einschalten der Spannung ein. Es wurden hierbei zwei verschiedene Drahtstärken, 2,5 mm² und 50 mm², als Brückenelement gewählt. Kurzschlüsse über den 2,5 mm² Draht lösten wesentlich lautere Schallereignisse aus, als jene des 50 mm². Auf die Kurzschlussstromstärke hat die Wahl des Querschnittes jedoch keinen Einfluss.

Abbildung 4: Kurzschlusseinrichtung am Mast mit 50 mm² Kupferkabel als Ableitung.

Ein sehr zeitintensiver Part war Task 4.2, die Analyse der Kurzschlussmuster. Die aufgezeichneten Daten, welche teilweise mehrere Minuten lang waren, mussten bis auf wenige Sekunden vor und nach einem Kurzschluss, ähnlich dem Videoschnitt, gekürzt werden. Eingelesen und analysiert wurden die Ausschnitte im Anschluss mit überwiegend selbstgeschriebenen MATLAB Scripts. Die Ergebnisse zu dieser Versuchsreihe sind im Dokument D5208-EN-0.1 ausführlich festgehalten, welches an die ÖBB übermittelt wurde.

Aus den initialen Versuchen und deren Datenauswertung konnten bereits mehrere Grunderkenntnisse der Kurzschlusscharakteristik abgeleitet werden:
Nach erfolgreicher Prozessierung der Daten kann ein Bild des aufgenommenen Signals für verschiedene Frequenzbereiche erstellt werden, als Beispiel dient hier Abbildung 5. Es kann ein signifikanter Unterschied im Signalanteil der unterschiedlichen Frequenzbereiche erkannt werden. Vor allem niederfrequente Bereiche zeigen einen eindeutigen Chevron. Es wurde berechnet, dass sich dieser Chevron mit einer Geschwindigkeit von etwa 340 m/s ausbreitet, welches annähernd der Geschwindigkeit von Schall in der Luft entspricht (343 m/s bei 20° C). Infolge dessen wird davon ausgegangen, dass der akustische Knall des Kurzschlusses welcher sich über die Luft, in Verbindung mit der Vibration des Mastes, welche sich über den Boden ausbreitet, dieses prägnante Signal erzeugt.

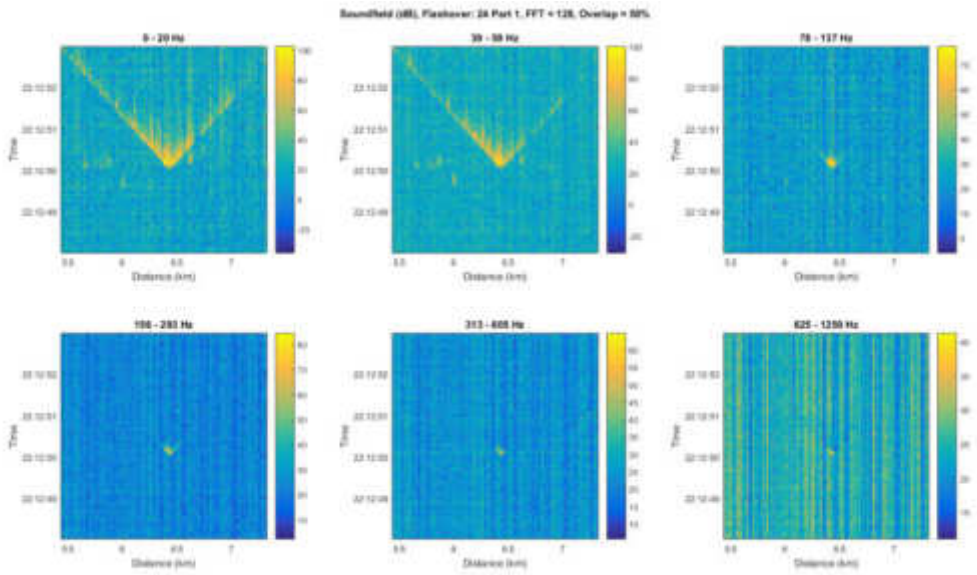

Abbildung 5: Signalausprägung eines Kurzschlusses nach Frequenzbereichen.

Stützend auf dieser Hypothese, wurde eine Untergliederung nach Schulnotensystem (Klassifizierung 1 – 5) erstellt:

- Klassifizierung 1: Deutlich sichtbares V in den Daten
- Klassifizierung 2: Sichtbares, aber deutlich kleineres V
- Klassifizierung 3: Ereignis sichtbar, aber nicht als V erkennbar“
- Klassifizierung 4: Ereignis kaum sichtbar
- Klassifizierung 5: Ereignis nicht sichtbar

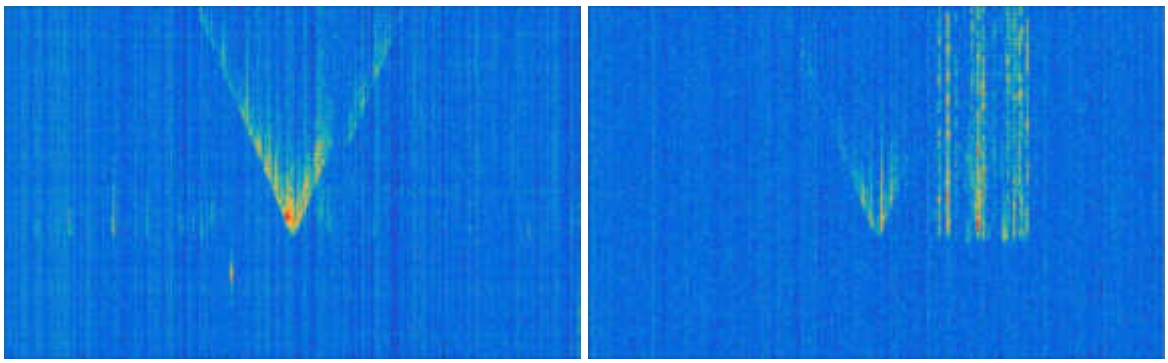

Abbildung 6: Vergleich von Kurzschlussdaten: Klassifizierung 1, Klassifizierung 2.

- Datentechnische Sichtbarkeit und Energieinhalt von Kurzschlüssen korrelieren in der Regel

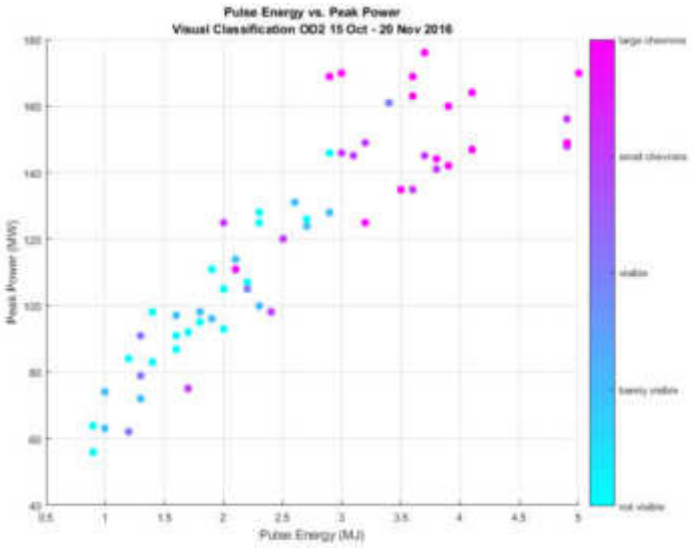

Abbildung 7: Kurzschlussenergie, Spitzenleistung und visuelle Klassifizierung.

- Neben dem örtlichen Kurzschlussereignis finden zeitgleich (und sogar mehrere Millisekunden früher) zum Kurzschluss Anregungen des LWLs statt, welche noch in mehreren Kilometern Entfernung sichtbar sind. Diese Erkenntnis war sehr überraschend und konnte zu diesem Zeitpunkt nicht erklärt werden

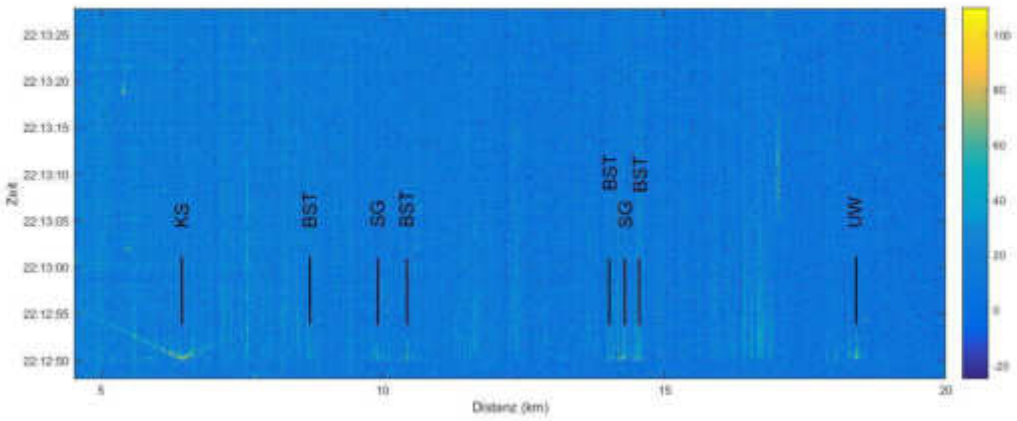

Abbildung 8: DAS-Signal und Auswirkungen der Stromkräfte an bestimmten Stellen im Oberleitungsnetz. KS-Ort des Kurzschlusses, BST-Bahnhof Streckentrennung, SG-Schaltgerüst, UW-Unterwerk.

- Die optische Distanz zwischen dem Kurzschlussort und dem Aufstellort des DAS Systems spielt eine Rolle bei der Signalbeschaffenheit. Ermittelt wurde diese durch die Überwachung mit zwei unterschiedlich langen LWL.

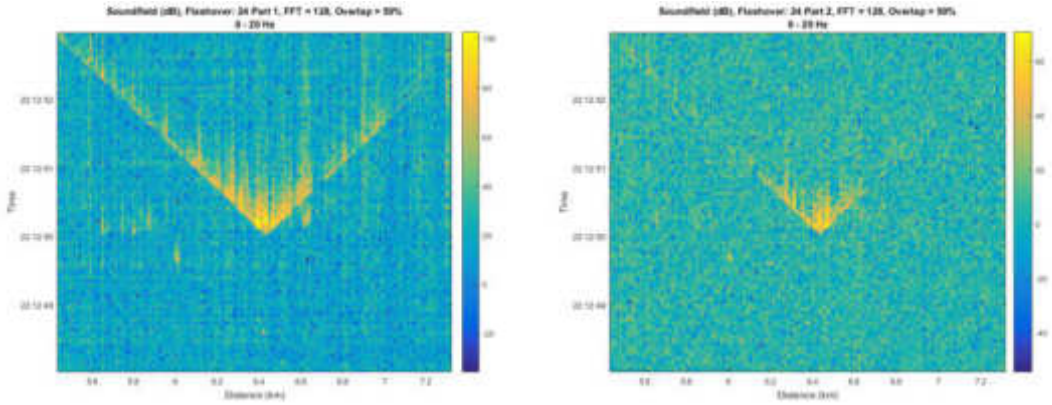

Abbildung 9: Auswirkung der optischen Distanz auf das Signal desselben Kurzschlusses (6400m links, 30200m rechts).

Folgende Grafik zeigt die systematischen Signalunterschiede bei verschiedenen Faserlängen, sowie die um 30dB unterschiedliche Auswirkung des Peaks beim Kurzschlussfall. Dies bezeugt einen dB Abfall von etwa 1.26 pro Kilometer.

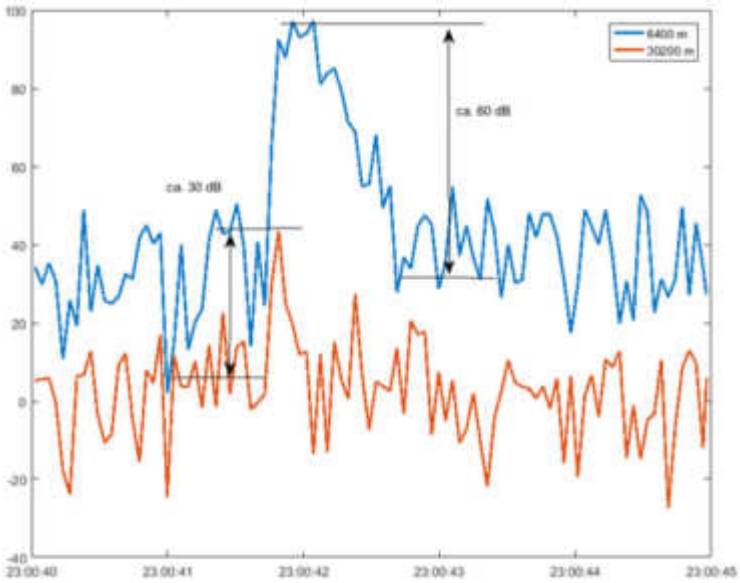

Abbildung 10: Signalverlauf für unterschiedliche Faserlängen am selben Ort.

- Ebenfalls eine Rolle für die Signalbeschaffenheit und den vom Ereignis angeregten dB, wenn auch eine eher untergeordnete, spielt die Breite der zur Aufzeichnung genutzten Laserimpulse in Nanosekunden

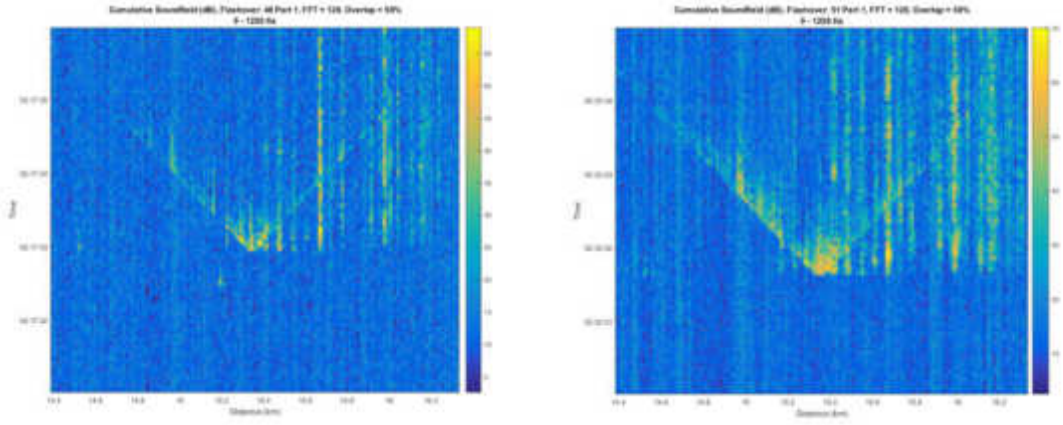

Abbildung 11: Auswirkung der Pulslänge auf das Signal desselben Kurzschlusses (100ns links, 200ns rechts).

Im Zuge dieser ersten Versuchsreihe wurde die Komplexität des Themas erstmals praktisch nachgewiesen, nachdem zuvor lediglich anhand einer Mindmap theoretische Einflussfaktoren ermittelt wurden. Verschiedenste Einflussgrößen für das aufgezeichnete Kurzschlusssignal konnten erhoben werden. Für eine statistische Auswertbarkeit einzelner Versuchsausprägungen waren deutlich mehr Datensätzen notwendig. Somit wurde beschlossen, dass für eine statistische Relevanz weitere Feldversuche zur Datenerhebung durchgeführt werden.

AP Nr. 4.2. Versuchsreihe St. Pölten – Güterzugumfahrung (GZU)

Aufgrund der Notwendigkeit weiterer Daten zur Klassifizierung der Einsatzgrenzen der Technologie und zur späteren Entwicklung des Algorithmus wurde eine zweite Testreihe beschlossen. Eine detaillierte Versuchs- und Ergebnisbeschreibung wurde im Dokument D6000-1 übermittelt. Die Messungen wurden im Mai 2017 auf der Güterzugumfahrung nahe St. Pölten durchgeführt und erbrachten mehr als 70 weitere Datensätze zur Analyse.

Im Vergleich zur ersten Testreihe in Allerding wurden bzgl. der Versuchsdurchführung folgende Änderungen vorgenommen:

- Als neuer Versuchsort wurde die Güterzugumfahrung nahe St. Pölten ausgewählt. Durch den Charakter einer modernen ÖBB Neubaustrecke sollten anhand von Signalunterschieden Einflüsse der Streckenbeschaffenheit auf das Schallübertragungsverhalten und die Kurzschlussausprägung untersucht werden
- Neben der unter 4.1 beschriebenen, gewollten Erzeugung echter Oberleitungskurzschlüsse wurden Daten mittels zusätzlicher Signalquellen aufgezeichnet. Hintergrund dieser Schritte war die Aufschlüsselung des komplexen Kurzschlussereignisses in seine Elemente, nämlich Luftschall durch die lokale Explosion und Körperschall durch die mechanische Ankopplung des Kurzschlussortes an die umliegende Infrastruktur. Folgende ergänzende Versuche fanden daher statt:
  1) Prangerschüsse: durch Schwarzpulver ausgelöste Explosionen, abgefeuert aus einem

sogenannten Prangerstutzen. Diese erzeugen einen lauten Knall und somit ein dem Oberleitungskurzschluss vergleichbares Luftschallereignis. Verschiedene Ladungsmengen wurden dabei getestet.

Abbildung 12: Prangerstutzen

2) Hammerschläge: Durch die mechanische Verbindung von Oberleitung und Mast sollten Kurzschlüsse auch mechanische Schwingungen zur Folge haben. Diese Schwingungen wurden mit einem Vorschlaghammer als Pendelaufbau am Mast simuliert.

Abbildung 13: Hammermontage am Oberleitungsmast.

3) Vorspannung der Masten: Ebenfalls mechanische Schwingungen wurden durch Vorspannung einzelner Masten mit anschließender ruckartiger Entlasten simuliert.

- Nutzung einer konstanten Pulslänge von 100ns, da die Variationen in Allerding einen eher untergeordneten Einfluss gezeigt haben und die zur Verfügung stehende Zeit genutzt werden sollte um möglichst viele statistische Daten für 100ns zu erzeugen.

Die Versuchsdurchführung und anschließende Datenauswertung bestätigten einerseits zahlreiche Beobachtungen aus den Erstversuchen in Allerding, förderten andererseits aber auch neue Erkenntnisse und Fragen zutage.

Bestätigte Ergebnisse aus den Initialversuchen:

- Sowohl Kurzschlüsse, mechanische Einwirkungen als auch Prangerschüsse zeigen jeweils unterschiedliche Klassifizierungen in der datentechnischen Sichtbarkeit.
- Unterschiedliche Sichtbarkeit in verschiedenen Frequenzspektren.

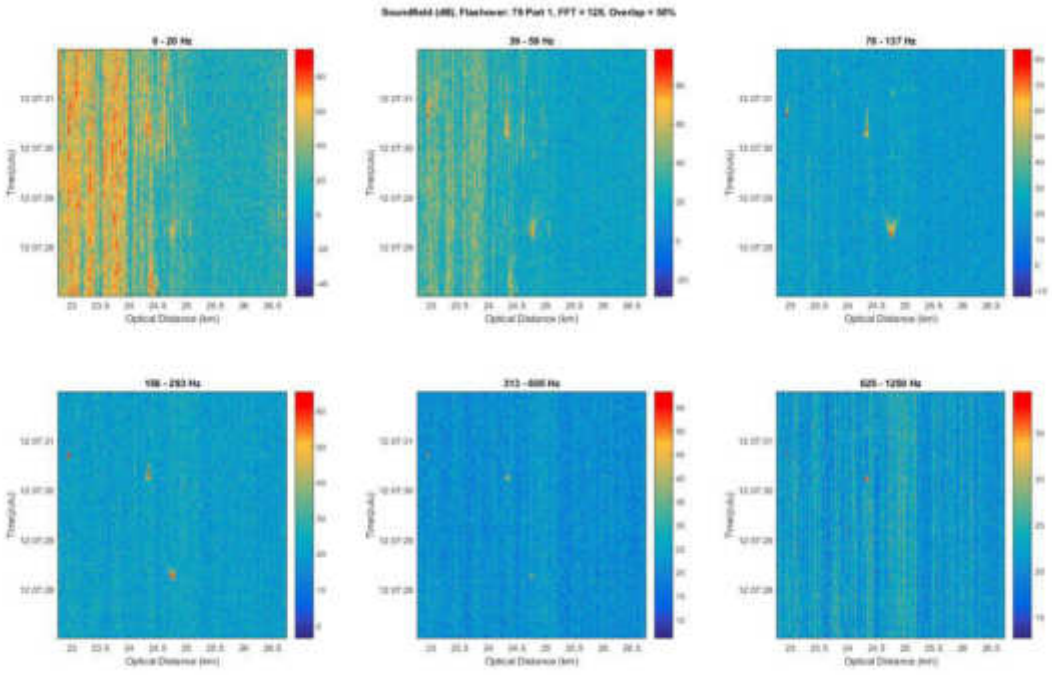

Abbildung 14: Gut sichtbares V eines Kurzschlussversuchs auf der GZU, dargestellt in verschiedenen Frequenzspektren.

- Zeitgleiche, mehrere Kilometer entfernte Anregungen zum Kurzschlusszeitpunkt wurden sichtbar. Im Nachgang zu den Versuchen wurde seitens der ÖBB schlussendlich die Ursache dieser Feststellungen ermittelt. Durch den fließenden Kurzschlussstrom entstehen durch die sich bildenden Magnetfelder Schwingungen in der Oberleitung, die von dem im Kabeltrog verlegten LWL als Vibrationsereignis erfasst werden können. Bei der GZU waren diese Ausprägungen schwächer, womöglich wegen der schwingungsresistenteren Infrastruktur.

Neue Erkenntnisse aus den GZ Versuchen:

- Signifikanter Einfluss der Infrastruktur auf die Signalqualität. Vibrationsintensive Ereignisse wurden zwar mit einer größeren Häufigkeit als in Allerding erfasst, allerdings war die Ausprägung der Chevrons jeweils deutlich geringer. Diese Beobachtung spricht für eine eher dämpfende Wirkung auf dem Signal zwischen Kurzschlussort und Faser. Nach Untersuchung der

Infrastrukturunterschiede wurde ein möglicher Einflussfaktor ermittelt: Im Gegensatz zu Allerding wird der Trog auf Gummigranulatplatten gelagert und steht auf einer mehrere Zentimeter dicken Asphaltschicht. Der Verdacht liegt damit nahe, dass sich diese Bauform vibrationsdämpfend und somit übertragungshemmend auswirkt. In Abstimmung mit der ÖBB wurde beschlossen, diese These in einem Testaufbau zu überprüfen. Die Durchführung wird unter Punkt 3.4.5 bzw. 7 gesondert beschrieben

- Abbildung 15 beschreibt einen Plot, der den Zusammenhang zwischen der Energie und Leistung eines selbstindizierten Kurzschlusses aufzeigt. Wie im Vorfeld erwartet, geht eine erhöhte Energie mit einer erhöhten Leistung einher. Anhand der farblichen Markierung der Beobachtungen, kann man eine Aussage darüber treffen, dass diese zwei Faktoren auf der GZU augenscheinlich keinen Einfluss auf die Sichtbarkeit eines Chevrons haben. Gut erkennbar ist diese Aussage anhand der Kategorie 2 (türkis – small chevron), welche über den ganzen Datensatz hinweg zu beobachten ist.

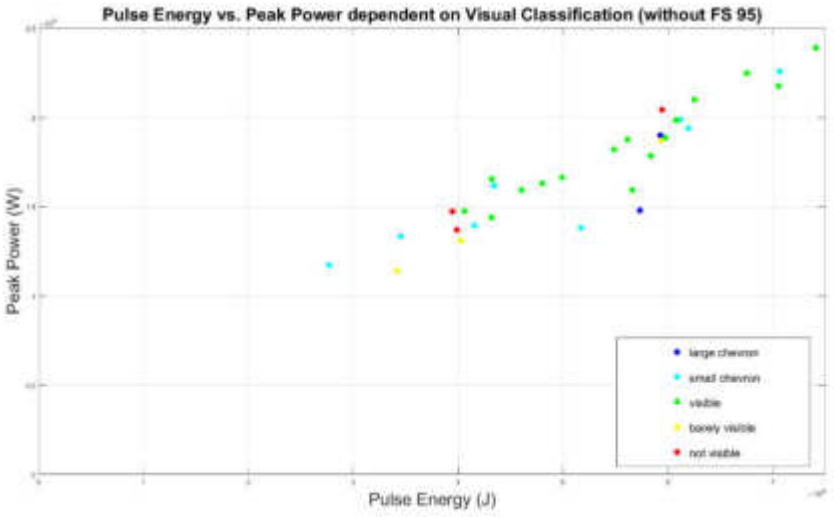

Abbildung 15: Darstellung Kurzschlussenergie, Spitzenleistung und visuelle Klassifizierung auf der GZU.

- Wie in Allerding wirkt sich ein größerer Ereignisabstand zum FTS System in der Sichtbarkeit des Signals aus.
- Resultate alternativer Signalquellen
  1) Prangerschüsse: Gute Sichtbarkeit. Die Prangerschüsse zeigen ausgeprägte Chevrons ähnlich der tatsächlichen Kurzschlüsse. Sie sind eine ausgezeichnete Alternative zu den tatsächlichen Kurzschlüssen, da sie weit weniger zeitintensiv in der Durchführung und risikofrei für die Infrastruktur sind.

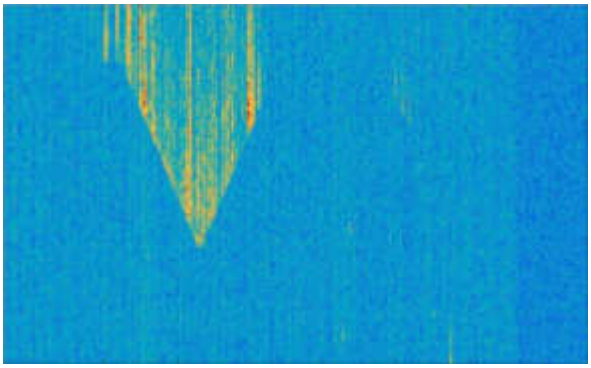

Abbildung 16: Beispiel der Visualisierung eines Prangerschusses auf der GZU.

2) Hammerschläge: die durchgeführten Hammerschläge waren auf der GZU kaum sichtbar. Die beobachteten Ausschläge wurden, wenn überhaupt, nur punktuell verzeichnet. Die Ursache kann in der bereits beschriebenen Lagerung des Troges zu finden sein. Es wurde entschieden diese Versuche in eine weitere Testreihe einzubinden.
3) Mastvorspannung: Das Lösen aus der Vorspannung war signaltechnisch nicht festzustellen. Der Ansatz wurde verworfen, da diese Art von Schwingung nicht mit den Schwingungen vergleichbar ist, in die der Mast bei einem Kurzschluss versetzt wird. Im Gegensatz zu der Amplitude der Schwingungen, die beim Vorspannen des Mastes entstehen, ist die Amplitude der Schwingungen beim Kurzschluss vergleichsweise klein. Vergleichbar mit den Schwingungen in die der Mast bei einem Hammerschlag versetzt wird.

Die Projektpartner haben festgelegt bis zum Ende des Förderprojekts eine weitere Testreihe in Allerding durchzuführen. Um möglichst viele Datensätze zu sammeln sollten diese nur mehr mittels Prangerschüssen und Hammerschlagtests erzeugt werden. Zudem wurden Versuche definiert um den Einfluss der Trogverlegung auf die Signalerkennung zu untersuchen.

AP Nr. 4.3. Versuchsreihe Allerding 2

Um den zu diesem Zeitpunkt bereits grundsätzlich entwickelten Basisalgorithmus zur Kurzschlusserkennung mit neuen Versuchsdaten zu erweitern wurden am 30.03.2018 weitere Versuche in Allerding durchgeführt. Sowohl der FTS Installationsort, als auch die Testorte entlang der Strecke blieben im Vergleich zur ersten Testreihe unverändert. Im Zuge dieser Versuche wurden mehr als 50 Datensätze erzeugt.

Im Vergleich zur Testreihe auf der GZU wurden bzgl. der Versuchsdurchführung (neben dem Ortswechsel) folgende Änderungen vorgenommen:

- Keine Erzeugung tatsächlicher Kurzschlüsse. Vibrations- und Schallereignisse wurden lediglich über Hammerschläge und Prangerschüsse simuliert.
- Keine zusätzlichen Tests mit Mastvorspannung, da diese als wenig erfolgversprechend beurteilt werden.

- Verzicht auf die Nutzung einer zweiten LWL Faser.
- Anpassung des Testablaufs für Prangerschüsse und Hammerschläge. Sowohl die Durchführung als auch die Häufigkeit der Signalerzeugung wurden angepasst. Der genaue Ablauf für jeden Datensatz ist dem gemeinsamen Excel File zu entnehmen. Grundgedanke war dabei die Signalauslösung in verschiedene Richtungen und mit unterschiedlichen Intensitäten, mit dem Zweck mögliche Abhängigkeiten aufzudecken.

Bestätigte Ergebnisse der bisherigen Versuche:

- Prangerschüsse zeigen unterschiedliche Klassifizierungen in der datentechnischen Sichtbarkeit.
- Prangerschüsse erzeugen zuverlässig gut sichtbare Signale.
- Unterschiedliche Qualität der Sichtbarkeit in verschiedenen Frequenzspektren.

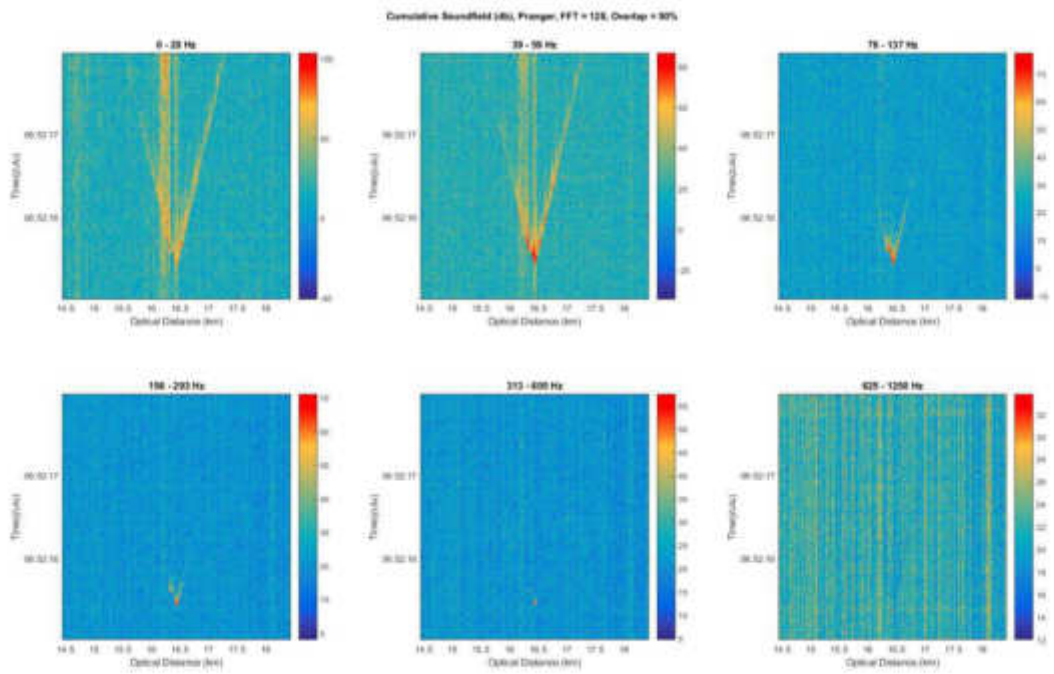

Abbildung 17: Chevron eines Prangerschusses mit 45g Schwarzpulver in Allerding, dargestellt in verschiedenen Frequenzspektren.

Neue Erkenntnisse:

- Wesentlich bessere Sichtbarkeit der Hammerschläge im Vergleich zur GZU. Weiterhin bilden sich die Versuche datentechnisch aber nur punktuell aus.

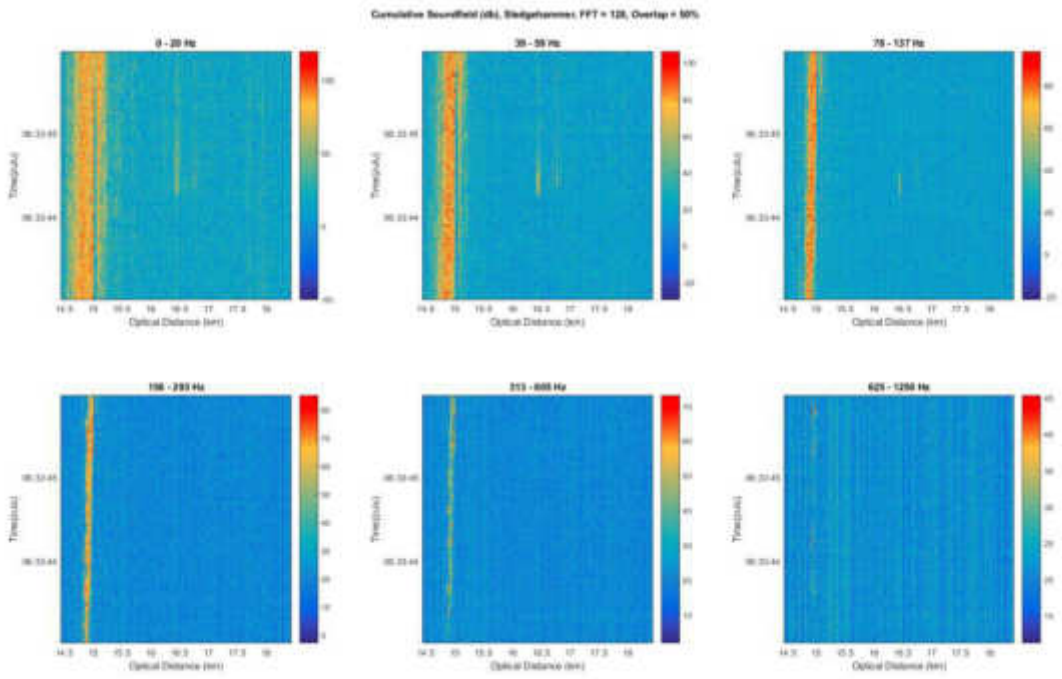

Abbildung 18: Signal für einen Hammerschlag in Allerding, dargestellt in verschiedenen Frequenzspektren.

- Prangerschüsse erzeugen weitestgehend richtungsunabhängig klar sichtbare Chevrons.
- Erkenntnis: klassische Chevrons der Kurzschlussversuche werden durch Knallgeräusche verursacht, da mechanische Einwirkungen im Signal lediglich punktuell wahrgenommen werden, rein akustische Signal aber als V verzeichnet werden.

AP Nr. 4.4. Deskriptive Statistik der Versuchsreihen

Tabelle 3 beschreibt eine deskriptive Auflistung der Versuche, die im Laufe der drei Testreihen durchgeführt wurden. Geordnet ist die Tabelle nach der visuellen Klassifizierung des aufgezeichneten Signals, sowie des Ortes der Testreihe. Zu unterscheiden sind dabei noch selbstinduzierte Kurzschlüsse und Prangerschüsse, wie in Kapitel 3.4.2 beschrieben. Insgesamt wurden 157 Ereignisse durchgeführt, davon Kurzschlüsse (104) und Prangerschüsse (53), wobei 16 davon aufgrund verschiedenster Umstände nicht aufgenommen werden konnten. 43 (47.25%) der selbstinduzierten Kurzschlüsse die aufgenommen wurden, fallen dabei in die visuelle Kategorie 1 bzw. 2 und konnten zum derzeitigen Stand für die Weiterverarbeitung der Daten verwendet werden. Dahingegen fallen 98% der Prangerschüsse in dieselben zwei Kategorien.

Visuelle Klassifikation	Allerding	St. Pölten	Gesamt
1	58	15	73
2	7	12	19
3	13	16	29

Visuelle Klassifikation	Allerding	St. Pölten	Gesamt
4	8	5	13
5	3	4	7
Nicht aufgenommen	7	9	16
Gesamt	96	61	157

Tabelle 3: Deskriptive Analyse der Testreihen in Allerding und St. Pölten.

AP Nr. 4.5. Zusätzliche Trogversuche

Die Versuche auf der GZU haben gezeigt, dass der Aufbau der Infrastruktur einen signifikanten Einfluss auf die Qualität der Signalübertragung vom Kurzschluss auf den Lichtwellenleiter hat. Es wurde vereinbart diesen Einfluss in gesonderten Versuchen näher zu analysieren um mögliche Auswirkungen in der Praxis besser einschätzen zu können. Über einen Testaufbau auf dem Frauscher Werksgelände sollten die baulichen Unterschiede zwischen der Allerding Strecke und der GZU nachgestellt und auf ihre Charakteristika in der Signalübertragung untersucht werden. GZU und Allerding unterscheiden sich bzgl. der Verlegung der Lichtwellenleiterkabel vor allem in zwei Belangen:

- Auf beiden Strecken liegen die Lichtwellenleiter in Betontrögen, allerdings mit unterschiedlicher Größe.
- Kabeltröge in Allerding sind in der Erde vergraben, auf der GZU werden sie auf Asphalt gelagert.
- Kabeltröge auf der GZU sind zwischen Beton und Asphalt auf zusätzlichen Kunststoffmatten gelagert.

Vor allem die Kunststoffmatten standen in Verdacht einen dämpfenden Einfluss auf die Vibrationsübertragung zu haben. Folgendes Testszenario wurde zur systematischen Untersuchung aufgebaut.

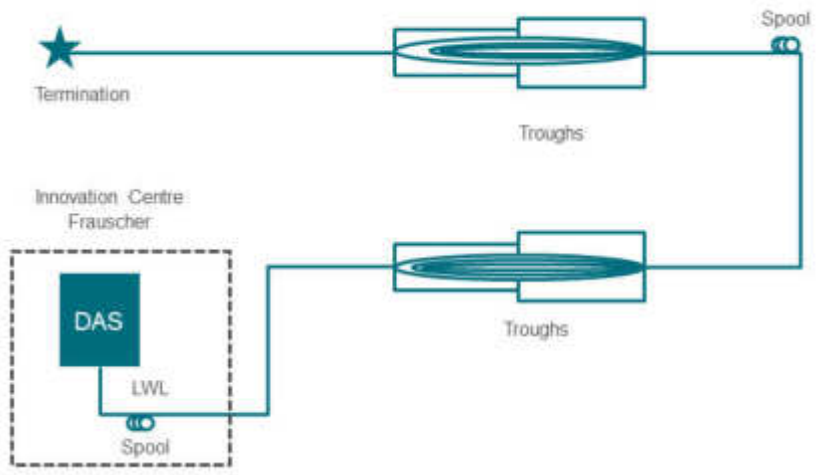

Abbildung 19: Testaufbau für Trogversuche auf dem Frauscher Werksgelände

Vier Original Betontröge der ÖBB wurden über ein im Frauscher Labor installiertes und zuvor konfiguriertes Messsystem überwacht. Dabei wurden zwei Tröge unterschiedlicher Größe in der Erde vergraben. Die beiden anderen Tröge, ebenfalls unterschiedlicher Größe, wurden analog zur GZU, auf Gummimatten und Asphalt gestellt. In die beiden Testinstallationen wurde jeweils eine Lichtwellenleiterspule von 33 Metern Länge gelegt, um datentechnisch ein längeres und damit besser sichtbares Signal zu erzeugen.

Im Versuch wurden insgesamt 76 Datensätze von unterschiedlichen Signalquellen aufgezeichnet:

- Definiertes Fallenlassen eines 20kg schweren Gewichts aus ca. 95cm Höhe
- Signalhupe
- Schritte
- Definiertes Fallenlassen einer 42 g schweren Schraube aus ca. 110 cm Höhe

Die Analyse der aufgezeichneten Daten ergab, dass bzgl. der Sichtbarkeit der erfassten Ereignisse kaum ein Intensitätsunterschied festzustellen ist. Es zeigt sich sogar, dass der eigentlich als dämpfend eingeschätzte Trog auf den Kunststoffunterlagen eine leichte Tendenz zu einer deutlicheren Abbildung in den Daten zeigt. Folgende Abbildung veranschaulicht exemplarisch den Gewichtsversuch Nummer 17. Im Bild lassen sich zwei getrennte Strukturen erkennen, wobei die linke Struktur den Asphaltaufbau zeigt und rechts der vergrabene Trog zu sehen ist. Somit liefern die Gummimatten keine Erklärung für das gedämpfte Signal auf der GZU. Diese ist im komplexen Zusammenwirken zwischen Infrastruktur und Umgebung zu suchen.

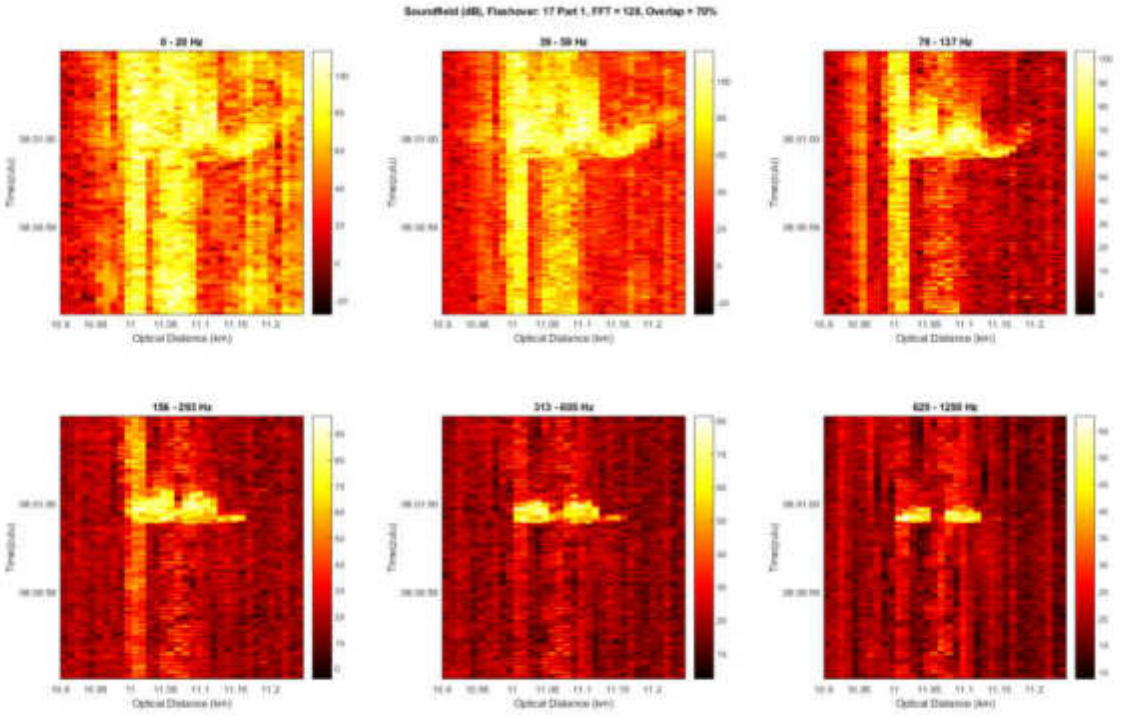

Abbildung 20: Visuelle Darstellung des Gewichtsversuchs Nummer 17 in verschiedenen Frequenzen.

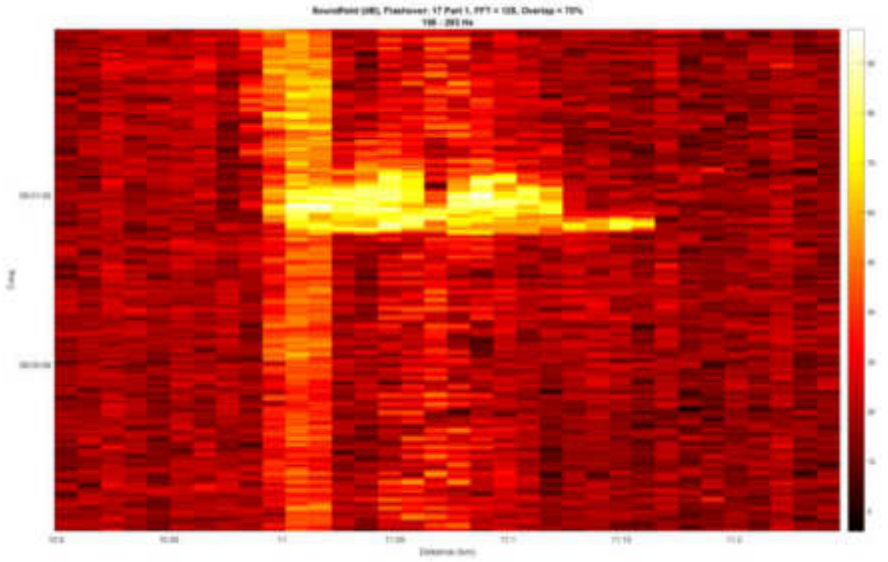

Abbildung 21: Gewichtsversuch Nummer 17 in 156 Hz – 293 Hz zeigt kaum einen Unterschied in den Signalausprägung.

AP Nr. 4.6. Signifikante Parameter und Beantwortung der im Vorfeld definierten Forschungsfragen

Anhand der Mindmap in Abbildung 1 wurden die in Tabelle 4 ersichtlichen Parameter ausgewählt, auf welche ein Hauptaugenmerk in der Analyse gelegt wurde. Ziel war es dabei herauszufinden, ob und welche dieser Faktoren einen signifikanten Einfluss auf die Detektion eines Kurzschlusses mithilfe der DAS Technologie haben können. Zu beachten ist hier etwa, dass trotz der hohen und positiven Korrelation zwischen Energie und Spitzenleistung (Abbildung 7), hat die Spitzenleistung einen signifikant schwächeren Einfluss auf die Sichtbarkeit eines Kurzschlusses. Erst wenn man den Einfluss auf die Klassifikation der Spitzenleistung in Verbindung mit der Energie analysiert, zeigt sich eine hohe Signifikanz.

Parameter	**Signifikanter Einfluss**
Pulsbreite	Ja
Optische Distanz	Ja
Wetter	Nein
Horizontaler Abstand von Mastvorderkante zu LWL	Ja
Art der Verlegung (LWL)	Ja
Art der Lage (LWL)	Ja
Fahrwegbeschreibung	Ja
Luftlinie von Kurzschluss zu LWL	Ja

Drahtstärke	Ja
Stromstärke (kA)	Ja
Spitzenleistungsgehalt (MW)	Ja (Infrastruktur beeinflusst Stärke der Abhängigkeit)
Energie (MJ)	Ja

Tabelle 4: Signifikanz einzelner Parameter für die Sichtbarkeit von Kurzschlüssen.

Folglich wird nun auf die im Vorfeld definierten Forschungsfragen eingegangen und versucht diese mit den Erkenntnissen der Testreihen bestmöglich zu beantworten.

- Welchen Einfluss hat der Abstand des Kurzschlusses zum Unterwerk?
  - Theoretisch betrachtet führt ein kürzerer Abstand zu einem höheren Energiegehalt. In Allerding befindet sich das betroffene Unterwerk in der Nähe des Bahnhofes Riedau. Die am LWL gemessene Distanz zwischen diesem Unterwerk und der Kurzschlussorte hat, wie erwartet, einen leicht negativen Einfluss auf den Energiegehalt. Das bedeutet somit, dass eine erhöhte Distanz zwischen Unterwerk und Kurzschluss mit einem verminderten Energiegehalt einhergeht.
- Gibt es eine maximale Distanz zum Unterwerk, bis der eine Detektion möglich ist?
  - Die technische Limitation eines DAS Systems wird durch die optische Bedämpfung, den Frequenzinhalt sowie die Stärke der Anregung bestimmt. Das FTS System ist bisher auf eine maximale Länge von 40 km ausgerichtet. Ein ausreichend energiereicher Kurzschluss ist über die komplette Länge erfassbar. Wie weit über den besagten 40 km noch eine Detektierbarkeit besteht, kann aber bis dato nicht getestet werden.
- Wie wirkt sich der Abstand des LWL am Boden zur Oberleitung aus?
  - Die Testreihen in Allerding und der GZU zeichnen ein gegensätzliches Bild. Während in St. Pölten, wie erwartet, die Detektierbarkeit mit steigender Distanz sinkt, ist steigt in Allerding der Anteil an Beobachtungen der Kategorie 1 und 2 mit höherem Abstand: für Distanzen unter 9 m konnten 3 Kurzschlüsse/Prangerschüsse erkannt werden. Dies entspricht 15.79% aller Beobachtungen unter 9 m. Dahingegen wurden 68 (89.47%) aller Beobachtungen größer oder gleich 9 m erkannt. Ob diese Resultate repräsentativ sind oder unter Mangel an zur Verfügung stehenden Daten bzw. undefinierten Einflüssen liegen, konnte nicht erhoben werden.

    Vergleicht man aber im Gegenzug die visuellen Klassifikationen derselben Kurzschlüsse zwischen optischer Distanz 1 und 2 (+ 10 km Vorlaufspule zu optischer Distanz 1), wird die Theorie bestätigt, dass eine erhöhte Distanz zwischen FTS System und Kurzschlussort die Sichtbarkeit des Kurzschlusses verschlechtert.

- Welchen Einfluss hat der Abstand der Oberleitungsmasten zum LWL?
    - Genau wie beim Abstand des LWL zur Oberleitung, zeichnet sich auch hier in den Daten ab, dass für Allerding entgegen der Erwartung eine anscheinend erhöhte Distanz zu einer besseren Detektierbarkeit führt.
- Wirken sich verschiedene Verlegearten und Position der LWL auf die Detektionsfähigkeit aus?
    - Verlegeart sowie Position des LWL haben einen Einfluss auf die Detektionsfähigkeit. So ist es laut den Daten etwa leichter mit einem erdverlegten als mit einem trogverlegten LWL einen Kurzschluss zu detektieren. Für die gesammelten Daten von Allerding und St. Pölten, zeigt der direkte Vergleich der Verlegeart *Trog* mit der Verlegeart *Trog mit Gummigranulatplatten*, keinen signifikanten Unterschied in der Detektionsrate.
- Wenn ein LWL in der Nähe der Oberleitung installiert ist, wie unterscheiden sich die aufgenommenen Signale zu jenen des bodenverlegten LWL?
    - Leider konnte auf beiden Teststrecken keine geeignete Position gefunden werden, an der ein passendes Experiment zur Beantwortung dieser Frage durchgeführt werden konnte.

AP Nr. 5 Algorithmus Entwicklung Level 2

Ein detaillierter Bericht zur Algorithmusentwicklung wurde im Zuge des Förderprojekts am 27.02.2018 an die ÖBB übermittelt („Catenary Short Circuit Detection and Localization using DAS and RUSBoost“). Dieses Dokument beschreibt im Detail die Erarbeitung und Umsetzung des Informationsverarbeitungsprozesses auf Basis der erzeugten Kurzschlussdaten. Alle aktuell und zukünftig erzeugten Kurzschlussdaten, egal ob natürlich oder künstlich simuliert, liefern statistische Grundlage zur iterativen Optimierung des Suchalgorithmus zur zuverlässigeren bzw. eindeutigeren Identifikation von Kurzschlussorten. Der Algorithmus zur Datenverarbeitung bildet damit das Herzstück im Konzept der Kurzschlusslokalisierung mittels DAS Technologie. Basis aller infrage kommenden Ansätze für die Algorithmusentwicklung ist die digitale Bildbearbeitung der visuellen Darstellung aufgezeichneter Rohdaten im Post Processing. Zunächst wurde eine Lösung über Kantenerkennung der Chevrons favorisiert. Vor allem durch die Erkenntnisse aus den Versuchen auf der GZU wurde aber klar, dass dieser Ansatz in mehrerlei Hinsicht problematisch ist:

- Chevrons zeigen nicht notwendigerweise gerade, homogene Kantenverläufe
- Chevrons auf der GZU bilden sich hinsichtlich ihrer Größe und Kantenlänge deutlich weniger prägnant aus
- Im Plot besteht eine Kante aus feinen Stufen. Zusätzliche Bildbearbeitung wäre nötig um diese zu glätten
- Störereignisse verfälschen den Kantenverlauf

Um diesen Einflüssen entgegenzuwirken basiert der derzeitige Algorithmus auf dem Prinzip der Pattern Recognition, wie im Bericht zum Aufbau und zur Entwicklung des Algorithmus beschrieben. Die Idee dahinter ist, das geplottete Signal auf den bereits beschriebenen Chevron, und vor allem dessen Ausprägung, zu untersuchen. Dabei wird der farbige Plot des Signals in verschiedenen Schritten in ein binäres (schwarz – weiß) Bild transformiert und morphologisch gesäubert. Auf diesem Bild werden nun alle übrig gebliebenen weißen Regionen untersucht und festgestellt, ob deren Features dem eines Kurzschlusssignals ähnlich sind. Wenn ja, werden diese Regionen markiert und die Information in einer Liste zusammengefasst. Dies geschieht auf Basis der bis dato vorhandenen Aufzeichnungen und wird über künftige neue Daten weiterentwickelt und verbessert.

Es folgt eine Kurzbeschreibung der grundsätzlichen Algorithmussystematik zum Entwicklungszeitpunkt (Februar 2018):

- Datengrundlage für Algorithmuserstellung: 101 simulierte Kurschlüsse im Netz der ÖBB, davon 16 rein akustische Tests via Prangerschüsse.
- Konzepterarbeitung und Entwicklung eines bildbearbeitungsbasierten Matlab Erkennungsalgorithmus auf Grundlage der als gut sichtbar klassifizierten Datensätze.
- 55% der aufgenommenen Kurzschlüsse wurden als gut sichtbar klassifiziert.
- Algorithmussystematik
  - Visueller Plot der Daten als Serie sich überlappender Farbbilder.
  - Umwandlung in Graubilder, anschließend schwarz/weiß Konvertierung
  - Auslesen der charakteristischen Objektfeatures.
  - Einteilung der Objekte in Gruppen.
  - Trainieren und Optimieren eines Klassifizierungsmodells.
  - Definition der Hauptmodelle inkl. Skalierungen.
  - Performance Tests für Optimierung durch 2.000 Testabläufe mit zufälliger Kombination von Trainings- und Fittingdatensätzen.
  - Ergebnis: der Algorithmus erreichte mit den verfügbaren Trainingsdaten der Klassifizierung 1 + 2 (entspricht 55% aller Kurzschlussdaten) folgende Ergebnisse:
    - True Positive Rate von 98%
    - False Positive Rate von 2%
  - Die Dauer des Algorithmusdurchlauf bei maximal genauem Zeitstempel lag bei ca. 30 Minute.
  - Dieser Basisalgorithmus wird zukünftig durch zusätzliche Felddaten iterativ optimiert.

Abbildung 22: Ein morphologisch gesäubertes, binäres Bild eines selbst-induzierten Kurzschlusses. Die Features aller weißen Regionen werden darauf geprüft, ein potentieller Kurzschluss zu sein.

AP Nr. 6 Schnittstellenentwicklung

In der operativen Praxis wird der Nutzen des Entwicklungsprojekts zur Kurzschlusslokalisierung nicht nur von der Zuverlässigkeit des Algorithmus bestimmt, sondern auch von der Zuverlässigkeit des Informationstransfers. Die erfolgreiche Lokalisierung eines Kurzschlussortes wirkt sich für den Betreiber nur dann positiv in Form einer Ressourcen- oder Verspätungsoptimierung aus, wenn die Information möglichst schnell an die entsprechenden Stellen gelangt. Da der Algorithmus mit Rohdaten arbeitet und diese nur begrenzt gespeichert werden, muss auch der Algorithmus möglichst zeitnah angestoßen werden. Somit wurde im Projektverlauf sehr schnell sichtbar, dass eine Automatisierung des Informationstransfers erforderlich ist. Diese Automatisierung wird im Folgenden als Meldekette bezeichnet.

Bestandteile der Meldekette:

- Erfassung des Kurzschlussereignisses und Kommunikation an FTS System:

Vorhandene ÖBB-Leittechnik wird verwendet um eine automatisierte Meldung inkl. Zeitstempel an das FTS System abzusetzen. Diese Meldung erfolgt derzeit per .csv File in einer E-Mail, allerdings werden auch andere Fileformate unterstützt.

- Empfang und Interpretation der Kurzschlussmeldung:

Entwicklung eines Parsing- und Triggerprogramms zur automatisierten Verarbeitung der Kurzschlussmeldung auf Basis einer Zeitinformation im .csv File.

- Datenspeicherung und Visualisierung:

Ausgelöst durch das Parsingprogramm werden die Rohdaten des betroffenen Zeitausschnitts permanent gespeichert und es erfolgt eine Umwandlung in einen visuellen Plot.

- Ablauf des Algorithmus:

Wie beschrieben erfolgen die Schritte zur Lokalisierung möglicher Kurzschlussorte über Mustererkennung.

- Zusammenstellung der Algorithmusergebnisse:

Identifizierte Kurzschlussorte werden inkl. Screenshots betroffener Stellen im Plot in ein .zip File verpackt.

- Rückmeldung der Lokalisierungsergebnisse:

Per E-Mail wird die Lokalisierungsinformation an frei definierbare Empfänger verteilt.

Das Funktionieren dieser automatisierten Meldekette wurde bereits sichergestellt. Somit kann der Lokalisierungsprozess für zukünftige reale und somit unangekündigte Kurzschlüsse grundsätzlich jederzeit erfolgen und trotz Forschungsstatus potentiell bereits einen Mehrwert für den Betreiber liefern. Automatisierung und derzeitiger Algorithmus sind beide auf dem Realsystem in Allerding aktiv in Betrieb und somit bereit zur Aufzeichnung. Dabei wird jeder zukünftig real oder künstlich verursachte Kurzschluss analysiert und zur weiteren Optimierung des Algorithmus genutzt.

Folgende Einsatzgrenzen der Automatisierung wurden im Zuge der Entwicklung ausgelotet:

- Funktionalität der Automatisierung ist nur gegeben sofern die gemeldete Zeitinformation für Kurzschlussfälle so präzise wie möglich an das System gesendet wird. Entscheidend ist dabei auch die zeitliche Synchronisierung zwischen Meldungsgeber und System.
- Hohe Berechnungszeit des Algorithmus (mind. 30 Min) limitiert durch die technische limitierte Rechenkapazität und die Notwendigkeit das komplette Datenspektrum zu analysieren.
- Limitierte Nutzbarkeit der Lokalisierungsinformation durch aktuell fehlende Einbindung von Bahnkilometrierungsinformationen.
- Limitierung des Informationsaustausches auf E-Mail-Kommunikation.
- Ausgabe mehrerer potentieller Kurzschlussorte, wobei identifizierte Ereignisse nicht priorisiert bzw. gewichtet werden sondern als reine Auflistung kommuniziert werden. Zur manuellen Beurteilung werden Bilder der lokalisierten Hotspots beigefügt.

Auf die Einsatzgrenzen der Kurzschlusslokalisierung selbst wurde bereits in den beschriebenen Ergebnissen aus Kapitel 1 eingegangen.

4 BESCHREIBUNG ERSTE VERSUCHSREIHE – ALLERDING

4.1 Introduction

This document provides interim results on experiments carried out in cooperation with ÖBB to assess the performance of a Frauscher Tracking Solutions (FTS) system using Distributed Acoustic Sensing (DAS) on the detection and location of a catenary flashover. The experiments were conducted in Austria on the main railway line between Schärding and Wels at a number of different locations between October and November 2016. A total of over 60 flashovers were induced over a period of 4 nights. This work is currently ongoing with the results to date being summarised in this document. Catenary flashovers are electrical short circuits between the high voltage (15 kV) catenary and ground typically causing an electrical spark and associated acoustic bang. These can occur for a number of reasons: faults within the locomotive, driver error, wildlife or natural occurrences such as a branch falling off a nearby tree, to name but a few. Circuit breakers in the respective substation cut the supply within a few milliseconds but in order to be able to reapply the electrical supply and resume operation, the cause of the flashover must be found and repaired if required. In certain cases the exact position of the flashover is not known and a considerable amount of time and effort is required to locate it. It is hoped FTS and DAS technology can help determine the source of a flashover event to within a few tens of meters which would be a vast improvement over the current accuracy. DAS operates by injecting pulses of laser light into an optical fibre which typical lies parallel to, and a few meters from, the railway track typically in a cable duct. Any acoustic disturbance of the fibre is detected and converted to an electrical signal which can be analysed using digital signal processing techniques. It is the acoustic bang caused by the flashover which can be measured using DAS.

The technical goal of this research is to determine the physical parameters which influence the creation, propagation and detectability of such flashovers and to quantify these thereby allowing limits on the usability of DAS technology to be determined. A small number of are numerous influencing parameters which can affect the signal strength detected at the optical fibre have been isolated for investigation in these initial experiments.

4.2 Measurement Time and Locations

The flashovers were conducted at a number of catenary support masts on the main railway line between Passau and Wels in the nights between 15th and 17th October 2016 and 19th and 21st November 2016. Detailed information on the masts where the flashovers occurred is shown in Tabelle 1.

Mast Number	Position (ÖBB km)	Distance between base of mast and fibre (m)
M 58/20	58.616	0.72
M 59/6	59.150	9.75
M 54/18	54.484	10.90
M 47/13	47.500	6.92

M 45/25	45.700	2.42
M 47/14	47.500	17.44
M 45/26	45.766	12.31

Tabelle 5: **Mast details of where flashovers were induced.**

4.3 Experimental Setup

Short Circuit

Three different experimental setups were used for the flashover tests. In the first setup, shown in Abbildung 23, the flashovers are induced by leading a conducting copper cable (wire cross section 50 mm^2) (1) from the catenary top cable (2) via an insulated mounting aid (3) to an iron bracket (4) mounted at the mast (5).

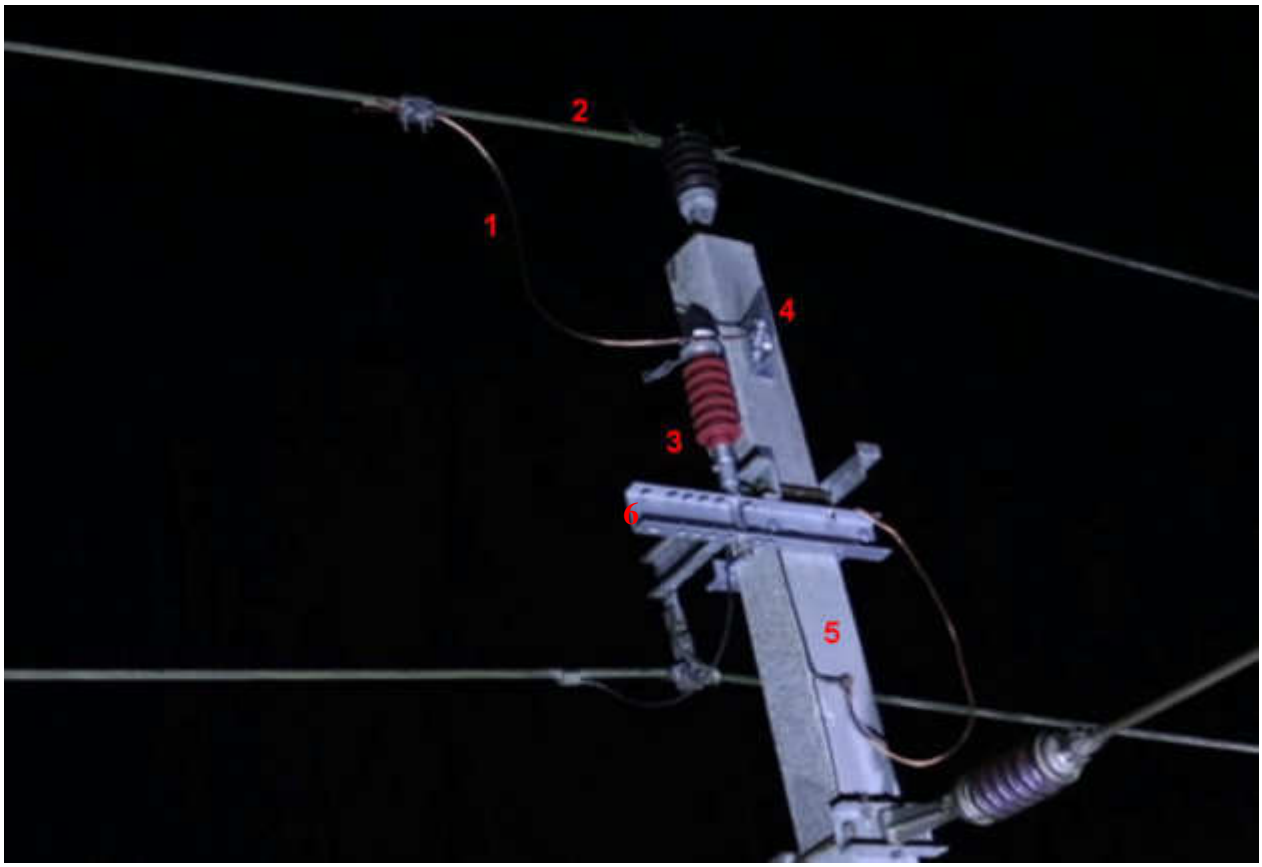

Abbildung 23: **Experimental setup with 50 mm² cross section cable.**

A small gap of 10-12 mm between the end of the copper cable and the iron bracket allowed high electric fields to be generated causing ionization of the air leading to an electric arc. A small amount of material is lost from the end of the copper cable after every flashover due to the high temperatures melting the copper. It was possible to generate up to three flashovers without intervention before the gap between copper cable and iron bracket became too large to allow a flashover to occur.

The second experimental setup was very similar to the first with a 50 mm^2 copper conducting cable being led from the Overhead Contact Line (OCL) to the insulated mounting aid. However, in this setup the mounting aid is moved to the furthest position from the iron bracket, (6) in Abbildung 24,

and a length of copper wire with 2.5 mm^2 cross section used to bridge the gap between the 50 mm^2 copper cable and the iron bracket. In the third experimental setup, copper wire with 2.5 mm² cross section was used but without the insulated mounting aid. The copper wire (1) was used to connect the catenary top cable (2) directly to the iron bracket (3), which was mounted at the mast (4), see Abbildung 25.

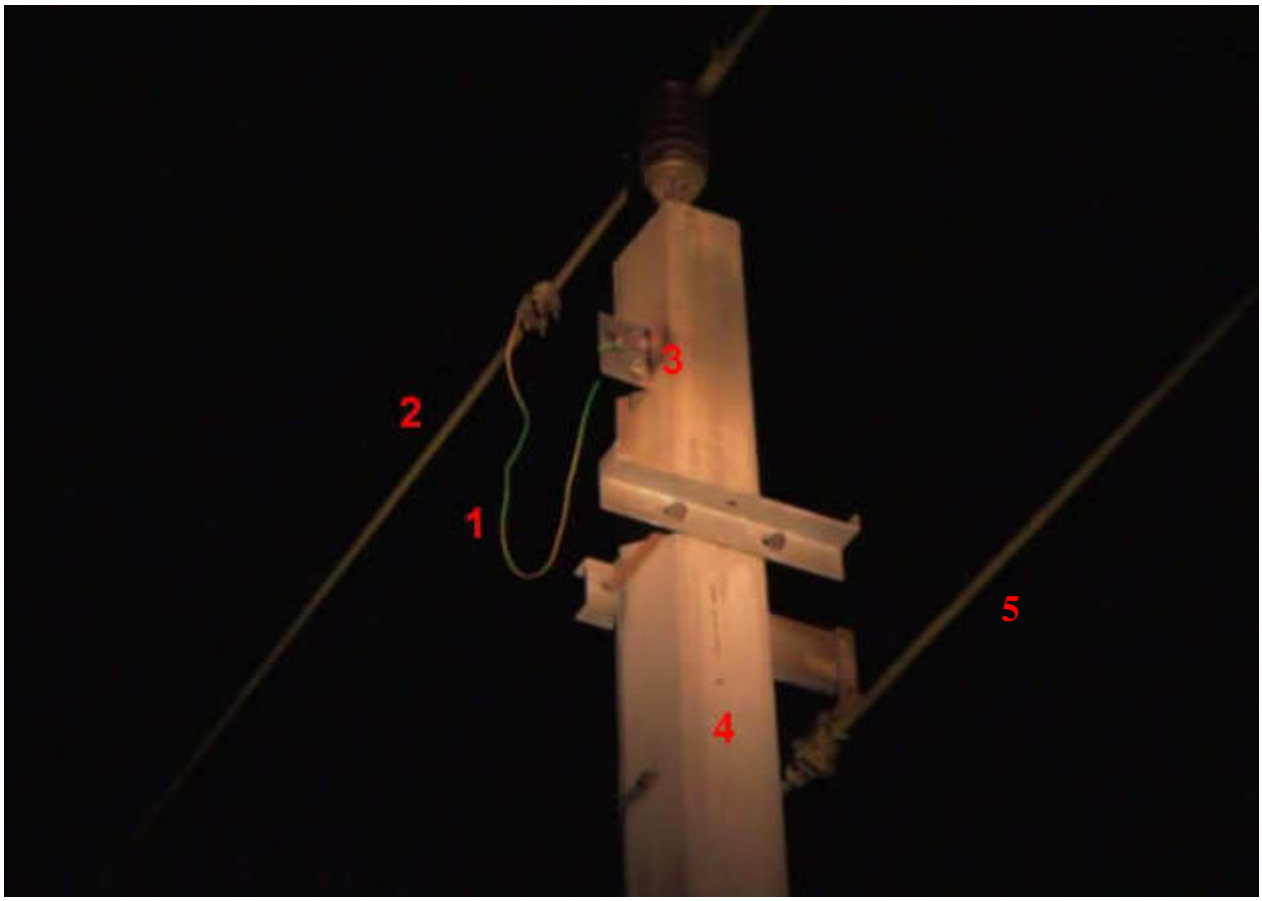

Abbildung 24: Experimental setup with 2.5 mm² cross section copper wire.

In all experimental setups the mast was earthed twice using copper cables with 50 mm² cross section. The first method connects the foot of the mast to the closest rail, see Abbildung 26, while the second method connects the upper part of the mast to the current return cable, see (5) in Abbildung 24. This defines two routes for current to flow back to the substation should one fail.

Abbildung 25: Experimental setup: Bracket and copper cable mounted to the foot of the mast.

Abbildung 26: **Experimental setup: copper cable firmly attached to one of the track rails.**

Current – Voltage

The energy of the induced flashover is calculated from measuring the current and voltage at the substation used to supply the catenary. The supply voltage was directly measured using an ÖBB voltage transformer with the ratio 175:1. The current was measured using an ÖBB current transformer with ratio 100:1 and current clamp with conversion factor 1A = 10V. These voltages are input to a Dewetron measurement system and then digitized using a National Instruments USB-6521 analogue to digital convertor (ADC) connected to a PC. The data was collected using DasyLab version 10. The software rescales the measured voltages to their original units of voltage and current.

Accelerometer

To assess the physical movement of the mast during and after a flashover is induced, an accelerometer of type MSR-165, see Abbildung 27, was mounted to the mast. This allowed acceleration in 3 mutually perpendicular axes at a maximum sample rate of 1600 Hz to be recorded. The sensor was physically mounted as shown in Abbildung 28 with the axes as defined and set to be triggered to record when one of the axes measured acceleration greater than 1.5g.

Abbildung 27: **MSR-165 accelerometer. Dimensions are 39 x 23 x 72 mm.**

Abbildung 28: **MSR-165 accelerometer mounted to the mast. The measurement axes are defined as indicated.**

DAS

The DAS measurement system is housed in a small service hut at km 60.656 directly beside the track and is built up of several constituent parts, see Abbildung 29. Up to two single mode optical fibres (Channel A and Channel B) with a maximum length of 40 km each can be connected to the optical unit. The optical unit generates and orchestrates the timing of the laser pulses and detects the reflected single from the fibres. The analogue signal is then fed to the processing unit which digitizes and saves the data (with a speed of up to 600MB/s) to the RAID. Additionally, it processes the data and forwards the results onto the display unit where it can be observed in real time via a web browser interface.

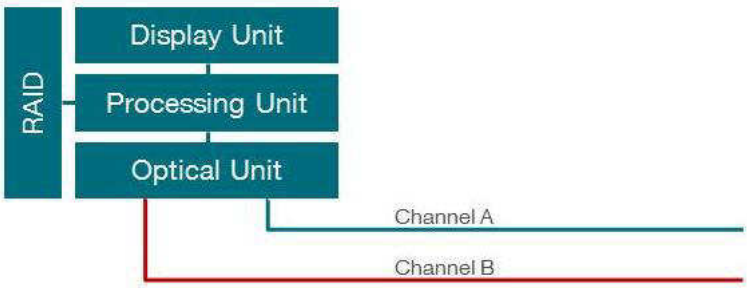

Abbildung 29: **The component parts of the DAS measurement system.**

For these experiments two single mode optical fibres were utilized for detection whereby a fibre spool was connected in series to one of the fibres prior to it exiting the service hut. This enabled the

same flashover to be simultaneously recorded at different optical distances. Schematics for the two measurement setups are shown in Abbildung 30 and Abbildung 31. The fibre identified as channel A was terminated in Neumarkt (~ OEBB km 28, approximately 33 km from the service hut) while the second, channel B, was terminated in Andorf (~ OEBB km 51) for the measurements between the 15th and 17th October 2016 and in Riedau (~ OEBB km 43) for the measurements between the 19th and 21st November 2016. The fibre spool lengths for the measurements in October and November were 23 km and 10 km respectively. The laser operates at 1550 nm while the pulse repetition rate was 2500 Hz and remained unaltered throughout the experiments. The pulse width varied between 100 ns and 200 ns.

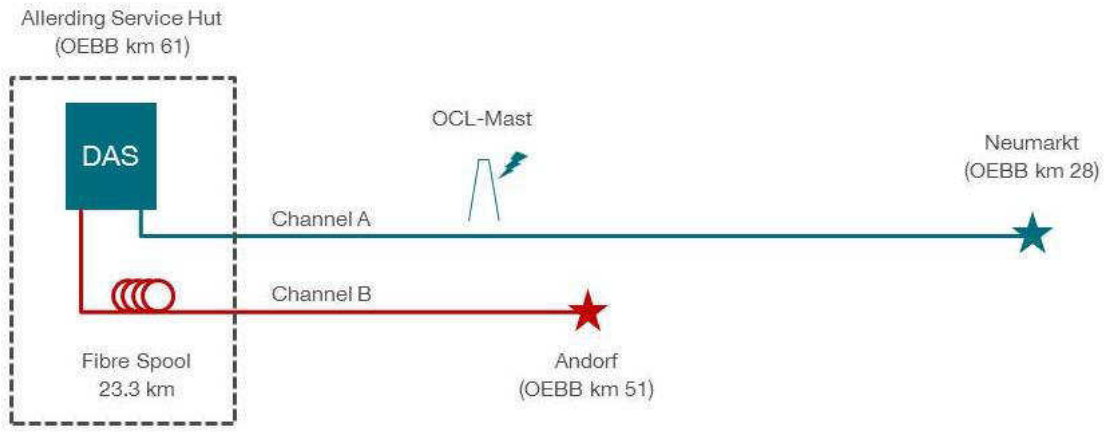

Abbildung 30: Schematic setup for the measurement period between 15th and 17th October 2016.

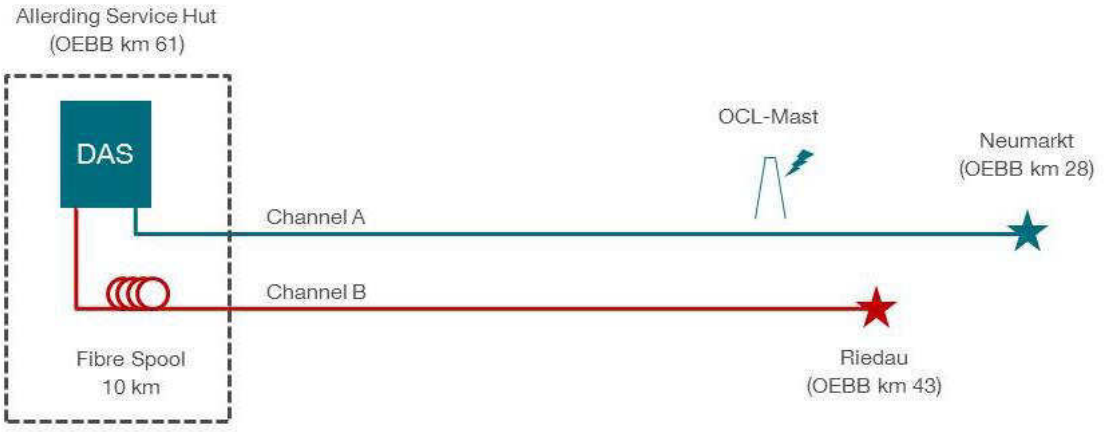

Abbildung 31: Schematic setup for the measurement period between 19th and 21st November 2016.

4.4 Results

A significant number of measurements, albeit not all, have been analysed to date. A number of tendencies can be identified which could be utilized in determining which flashovers can be detected

and/or located and those which cannot. Any algorithm written to detect and precisely locate a flashover in the future will be based on recognizing a characteristic pattern associated with such an event. This pattern should be distinct, unique and present in as many of the recorded signals as possible. It is therefore beneficial to visually determine if any patterns exist after a number of signal enhancement and pre-processing steps have been performed on the raw data and then isolate any parameters affecting these patterns. This qualitative analysis step, as detailed in chapter 8, was one of the first to be conducted allowing the multitude of flashovers to be grouped according to their visual characteristics. Tabelle 6 lists single measurements identified from each group for in depth analysis described in the following sections.

Measurement Number	Description	Ik (ÖBB) (kA)	Ppeak (MW)	Energy (MJ)
24	Chevrons	11.4	150	2.35
39	Small chevrons	6.5	98	1.23
10	Visible, no chevrons	5.8	76	0.9
15	Barely visible, no chevrons	5.3	82	1.08

Tabelle 6: Details of example measurements from each of the visual classification groups.

DAS

The sample rate of the raw DAS signal at each location is defined by the pulse repetition frequency of 2500 Hz. This limits the highest analysis frequency, or Nyquist frequency, to 1250 Hz. Some rudimentary signal processing steps are applied to each raw file to enhance the signal to noise ratio. The first step was to remove spatial data channels corresponding to any spools of fibre along the route which can cause optical artefacts. Additionally, a high-pass filter and a spatial decimator were applied to detrend the data and improve signal to noise ratio, respectively. Thereafter the frequency content was calculated using a Fast Fourier Transform (FFT) to allow a simplistic analysis of the frequency content of the flashover event. It is assumed that the majority of the signal energy resides in the lower part of the frequency spectrum and this allows an estimation of the noise. All signal processing was carried out in Matlab.

Octave Analysis

By dividing the energy content of the signal calculated from the FFT in to octaves, a crude frequency analysis can be conducted. For example, the upper octave contains energies in the range 625 – 1250 Hz; the next lower octave contains frequencies in the range 312.5 – 625 Hz, the next again in the range 156.25 – 312.5 Hz, etc. By plotting these energies calculated with an FFT length of 128 and an overlap of 50% we obtain Abbildung 32 to Abbildung 35. Each figure presents six octave

plots from 2 seconds before to 3 seconds after the flashover occurred. A distance of 1 km either side of the event is observed.

It can be seen that the frequency content differs substantially. Abbildung 32 shows a clear “V”, or chevron, as a result of the acoustic signal, or pressure wave, leaving the flashover location and travelling in both directions along the fibre route. The gradient of the “V” determines the speed of propagation and is experimentally found to be 340 m/s from the data. This matches the speed of sound in air very well (~343 m/s @ 20°C) and it can therefore be deduced with a high certainty that this signal results from the acoustic bang accompanying the short circuit.

From Abbildung 32 it can also be seen that only the low frequency components travel a substantial distance with the higher frequency components (150 Hz and upwards) remaining local to the short circuit.

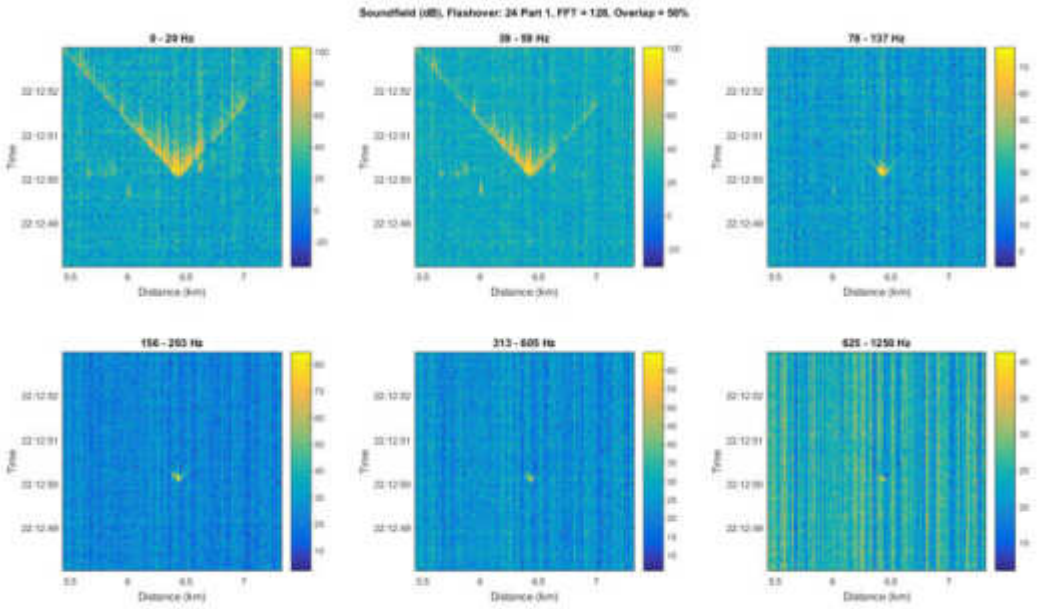

Abbildung 32: **Octave plot of measurement 24 showing the typical "chevrons" of a powerful event.**

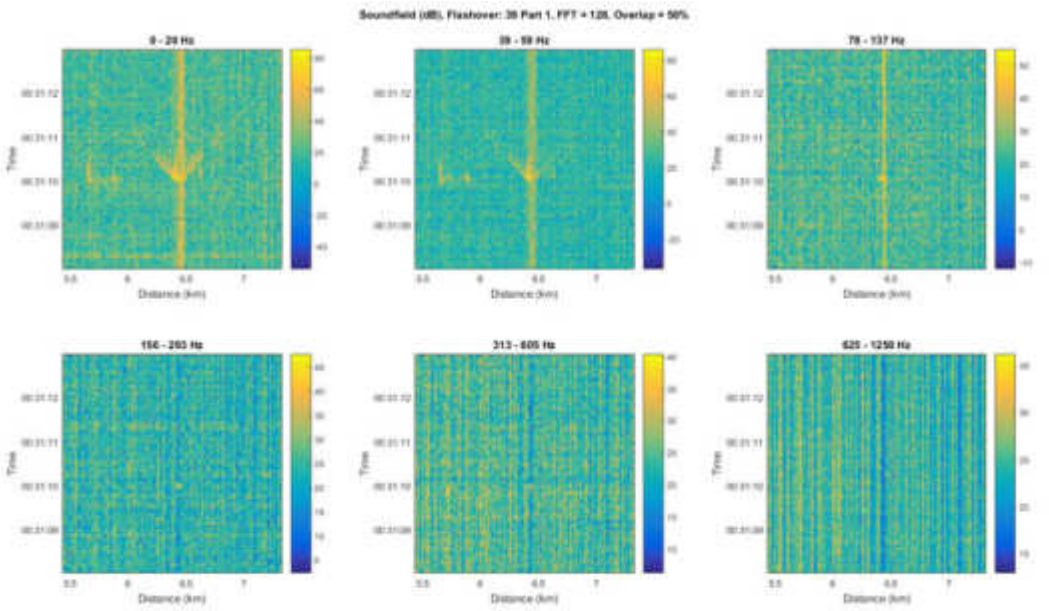

Abbildung 33: **Octave plot of Measurement 39 showing small chevrons. The yellow vertical bar in the upper three plots is the noise generated by engine of the service vehicle.**

As the energy content of the flashover is reduced the chevrons become less pronounced as can be seen for Measurement 39 in Abbildung 33. The high frequency content is still visible up to approximately the 5th octave after which it is swamped by the noise of the system.

Certain flashover events produced signal characteristics without any visible chevrons when applying the identical signal processing. These events caused a number of locations along the track to be excited simultaneously, particularly at low frequencies. After investigation those locations could be attributed to positions of other masts supporting the catenary along the track. Further information concerning these effects is detailed in chapter 5.

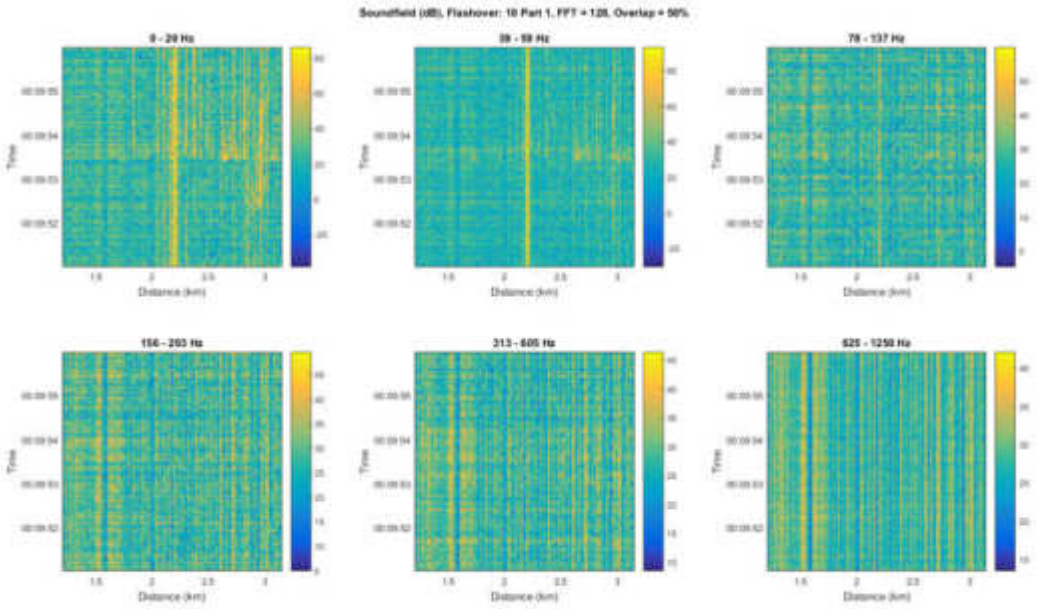

Abbildung 34: **Octave plots for Measurement 10. Several signal sources are visible and it is therefore unclear where the flashover occurred. The yellow, vertical bar visible in several subplots at approximately 2.1 km is the noise of the engine of the service vehicle.**

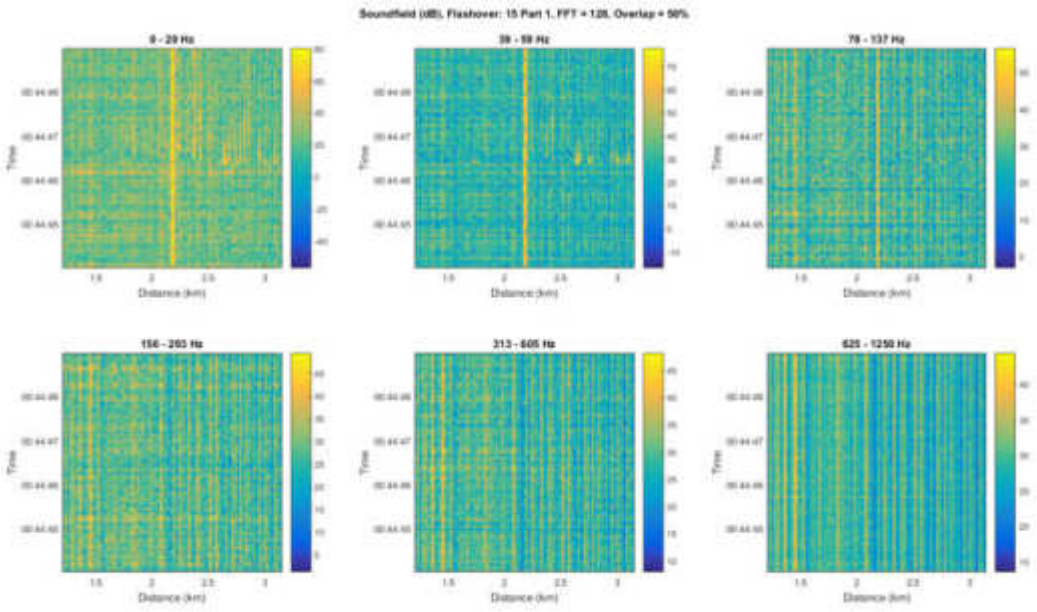

Abbildung 35: **Octave plots for Measurement 15. Signals from the flashover are barely visible when visually assessing the plot.**

Visual classification

It is obvious that the pre-processed DAS signal patterns can vary substantially from the case in which a chevron is clearly visible at the flashover location to producing no visible signal at all. Determining which of the many parameters affect this signal response is important in determining any limitations of a detection algorithm. A sensible assumption could be, for example, that those signals containing chevrons were produced by higher energy events. To asses this correlation the pre-processed data

from each measurement is visually classified and placed in one of the following groups describing the flashover as:

- having a large, clear chevron
- having small chevron
- being visible
- being barely visible
- being not visible

“Visible” was defined as being clearly able to see several locations of excitation which exactly coincide with the time of the flashover but with no other defining patterns. “Barely visible” is identical to “visible” but of less energy and a signal classified as being “not visible” contained no signal that could be visually detected with the current pre-processing steps. This is not to say that with another analysis methodology an improved digital signal processing routine could not extract more useful signal. However, at this early stage in the project it was decided to concentrate on classifying the various measurements and their dependent parameters and not focus on extracting the very last signal from the data. By plotting the peak power and pulse energy together with the visual classification, any correlation between power, energy content and the visibility of the DAS signal can be determined, see Abbildung 36.

Each data point represents a flashover. Those which are coloured have been visually classified in one of the aforementioned groups while those which are white have either yet to be classified or DAS data for the flashover does not exist (some measurements were simply missed due to a brief lapse in the communication between those present on the track, those persons initiating the flashover and those recording it). The shapes of the data points (circles or squares) indicate if the measured peak powers and pulse energies were saturated or not. The calculated powers and energies for saturated measurements are incorrect. Nevertheless these points have been included to indicate the present state of the data analysis. From this figure it can be seen that there is a tendency for the more powerful flashovers to generate chevrons but this is not always the case. Therefore, a complete analysis of all data is required to gain a better indication of this correlation.

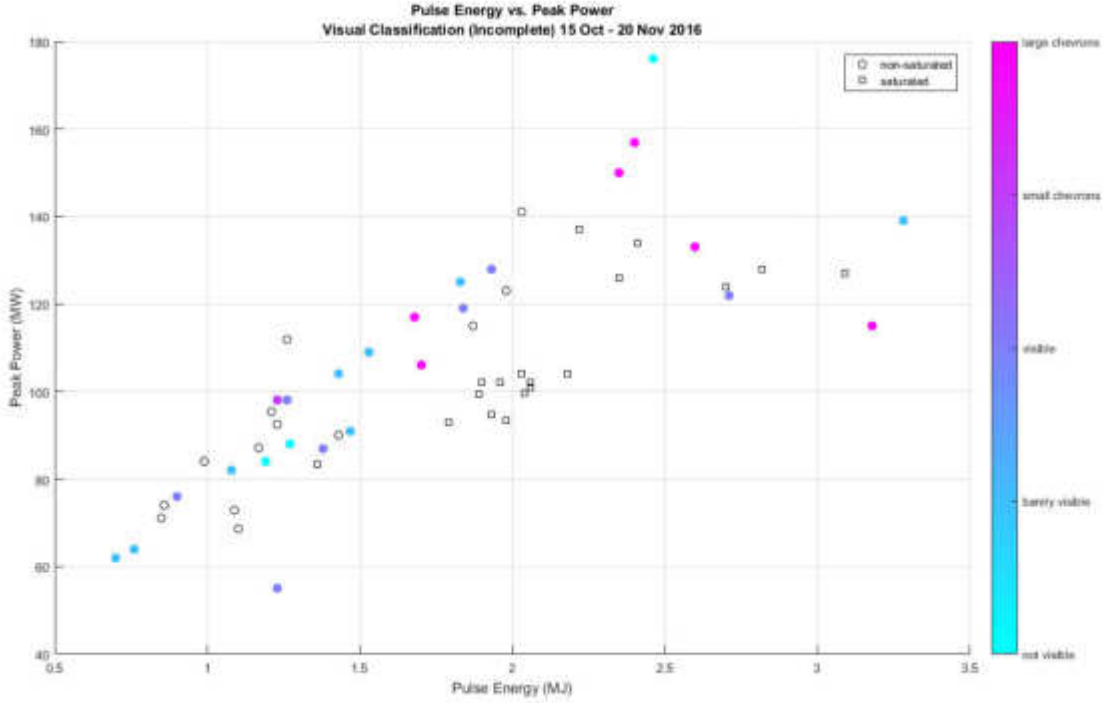

Abbildung 36: **Plot showing visual classification of the DAS signal plotted against peak power and energy. Colourless markers have either yet to be analysed or DAS data is unavailable. The marker shape signifies if the current measurements in the substation were saturated or not, details are given in 0.**

Optical Distance

The optical distance between the DAS system and the location of the flashover will also play a significant role in the strength of the measurable signal as the further the laser pulse has to travel in the fibre the weaker it becomes. This results in a decreased signal returning to the sensor.

Applying the identical pre-processing steps to a signal containing a clearly visible chevron pattern at two varying distances allow the attenuation of the signal to be determined. This methodology was applied to Measurements 24 and 28 to generate Abbildung 37 and Abbildung 39 for an optical distance of 6.5 km and Abbildung 38 and Abbildung 40 for an optical distance of 30 km. These figures show example data taken from the lowest frequency band, i.e. between 0 – 20 Hz. Both measurements were recorded with a laser pulse width of 100 ns.

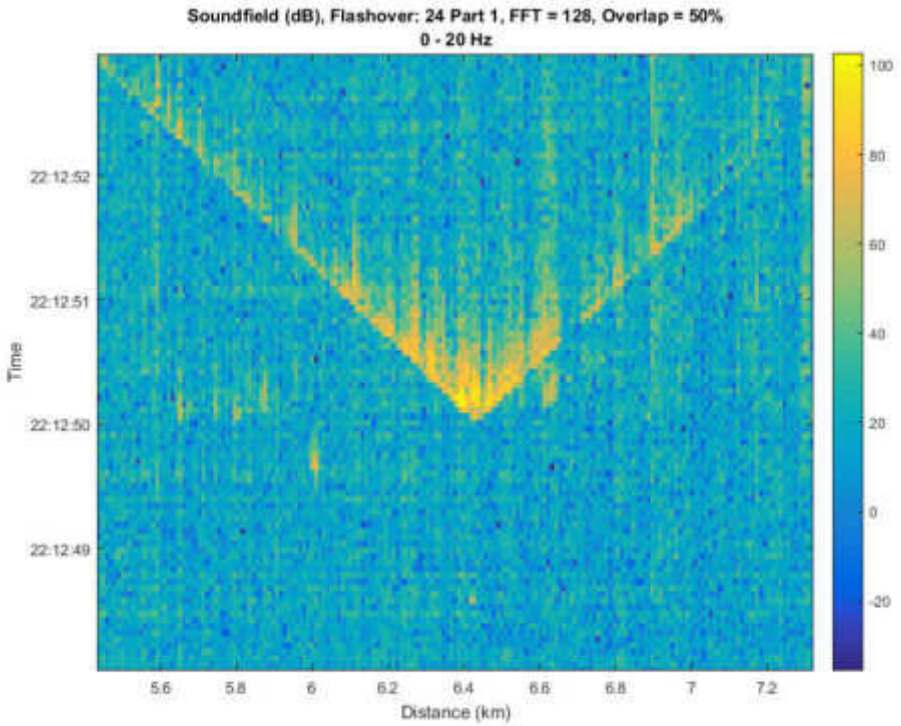

Abbildung 37: **Measurement 24, 0-20 Hz. Optical distance = 6400 m.**

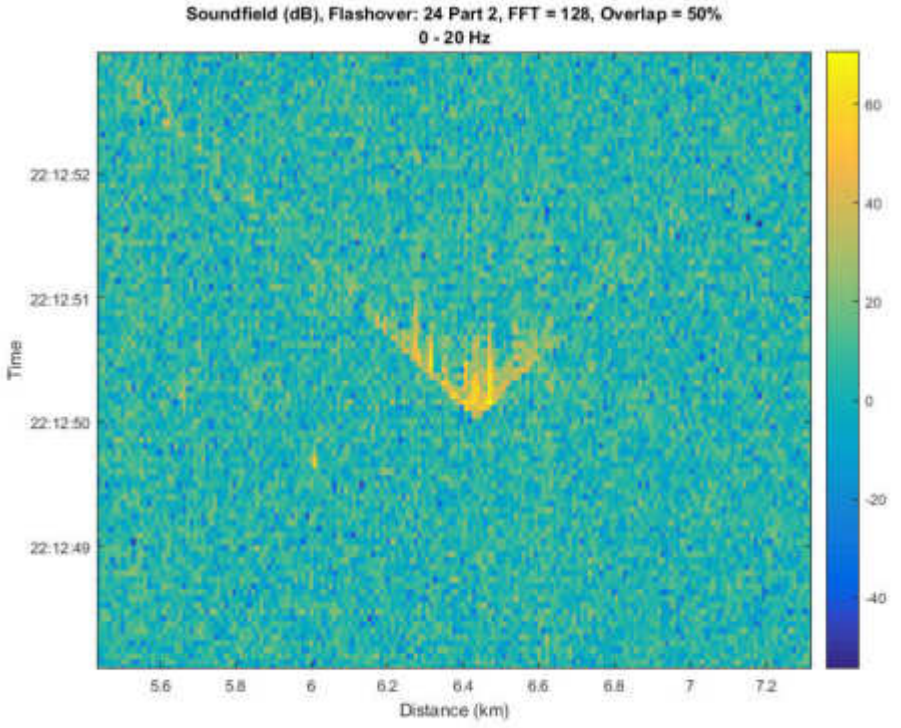

Abbildung 38: **Measurement 24, 0-20 Hz. Optical distance = 30200 m.**

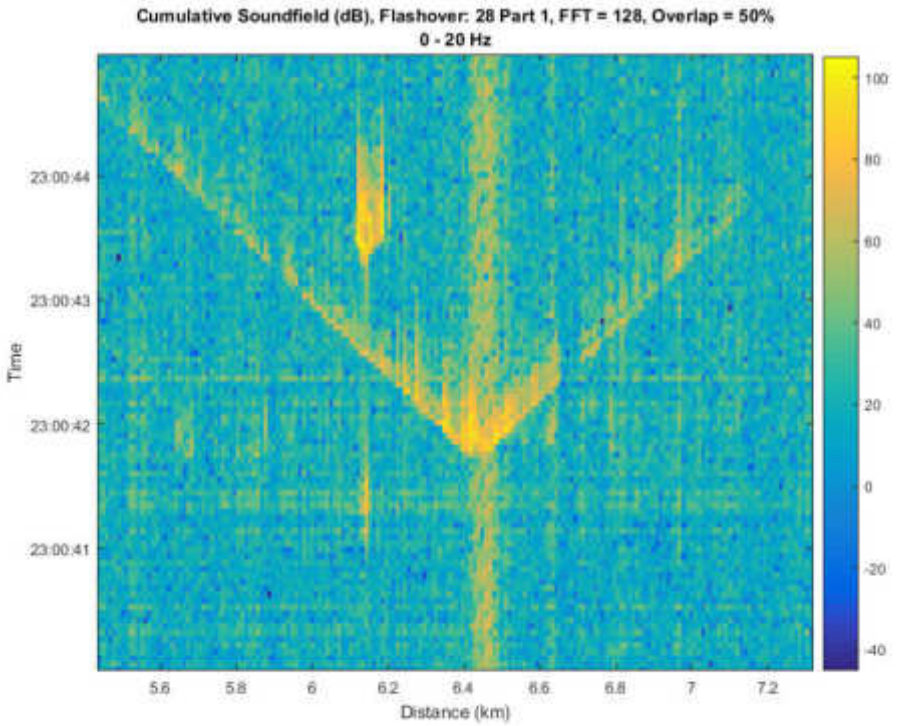

Abbildung 39: **Measurement 28, 0-20 Hz. Optical distance = 6400 m.**

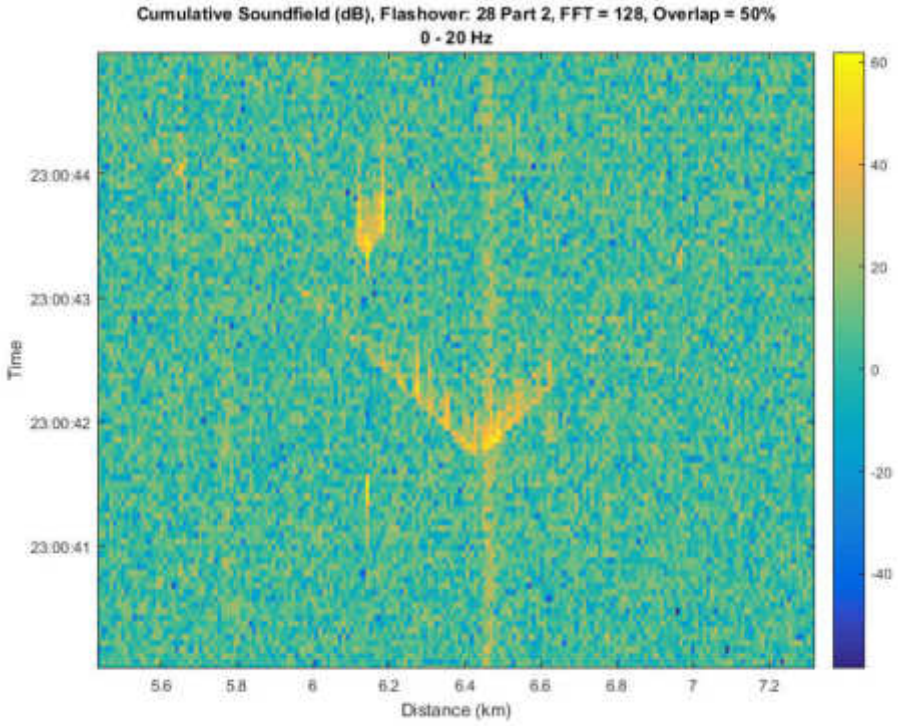

Abbildung 40: **Measurement 28, 0-20 Hz. Optical distance = 30200 m.**

Identifying the channels at which the flashover occurs (i.e. ~6.45 km) and plotting these for both optical distances, the decrease in signal amplitude can be better visualized. Two such plots for Measurements 24 and 28 are shown in Abbildung 41 and Abbildung 42 respectively.

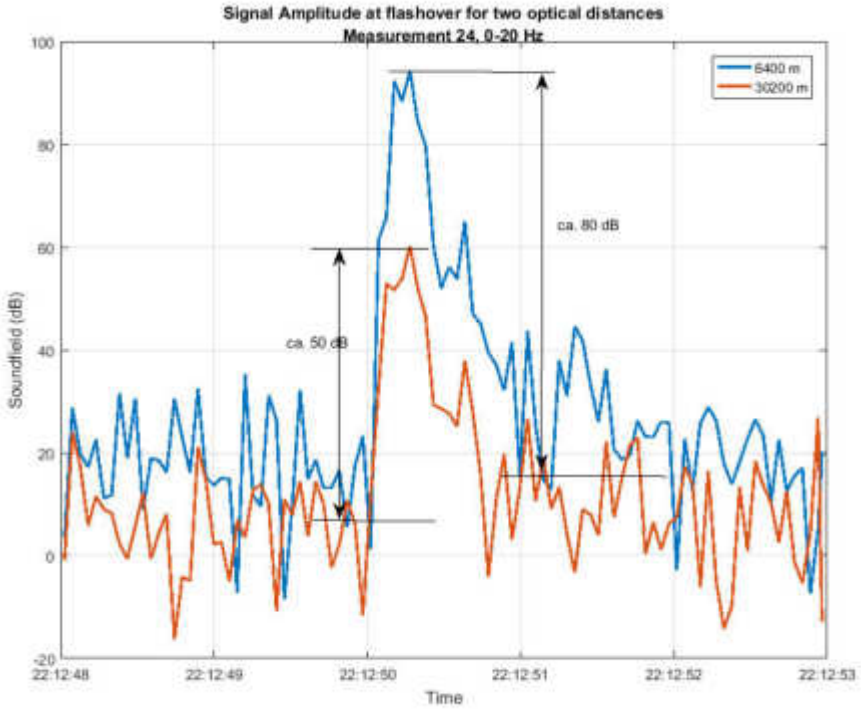

Abbildung 41: **Time evolution for Measurement 24 at two different optical distances.**

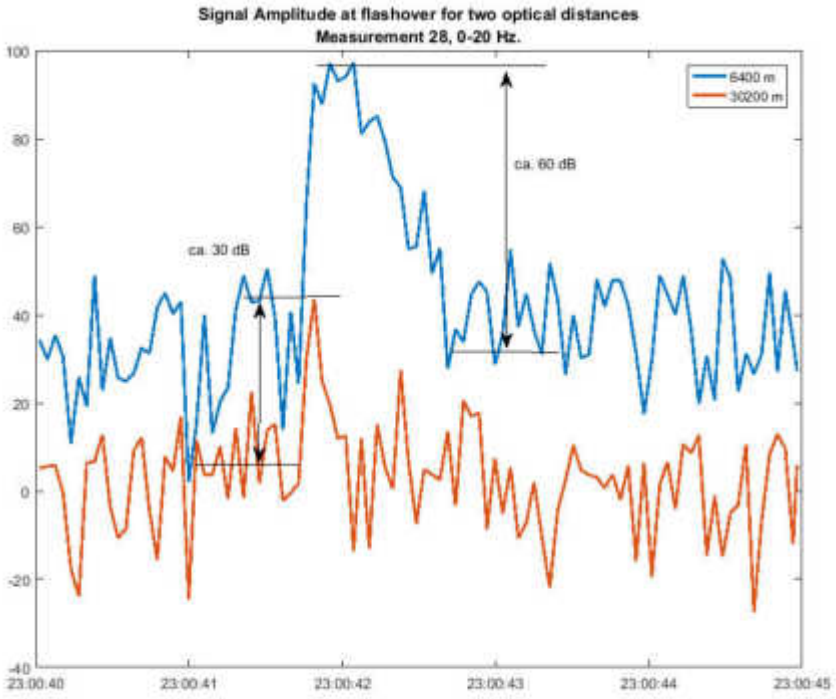

Abbildung 42: **Time evolution for Measurement 28 at two different optical distances.**

It can be observed for both measurements that the difference in maximum signal to the surrounding background at the location of the flashover is approximately 30 dB. This is a very preliminary statement as only two example files have been analysed but this work will be extended for all files and, in the future, for several optical distance in order to determine an optical limit for which any

signal could be detected. Nevertheless, it can be tentatively concluded that flashovers are detectable over an optical distance of 30 km, possibly up to 40 km, for at least larger flashovers which generate chevrons.

Pulse Width

The pulse width on the DAS measurement system can be set between 6 and 200 ns although 100 ns is typical for many applications and defines a spatial resolution of 10 m. By increasing the width of the laser pulse the signal response can be increased at the expense of spatial resolution. For example, increasing the pulse width to 200 ns increases the spatial resolution to 20 m which is absolutely acceptable when trying to locate a flashover within approximately 100 m.

As near to identical flashovers as possible were created at identical locations along the fibre while recording the event once with a pulse width of 100 ns and once with a pulse width of 200 ns. All other parameters were left unchanged. The cumulative soundfield at all signal frequencies for two such measurements (Measurements 49 and 51) are shown in Abbildung 43 and Abbildung 44.

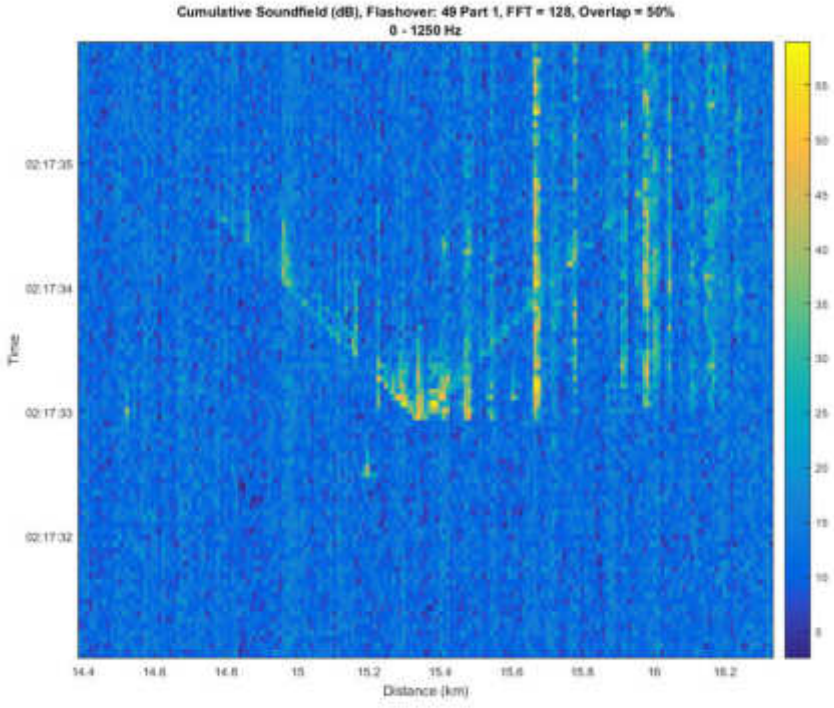

Abbildung 43: **Soundfield of all frequency components with the laser pulse width = 100 ns.**

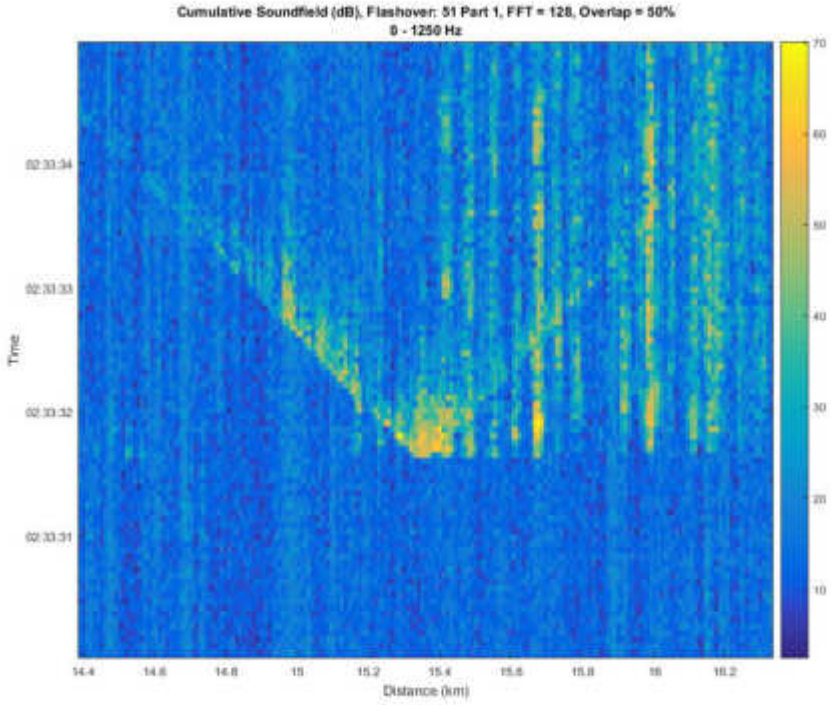

Abbildung 44: **Soundfield of all frequency components with the laser pulse width = 200 ns.**

Flashovers 49 and 51 are physically very similar as seen by comparing their measured currents of 16.4 kA and 15.5 kA respectively, and it can therefore be concluded that the increase in signal is a direct result of the increased pulse width. Comparing Abbildung 43 and Abbildung 44 it could be tentatively concluded that by increasing the pulse width from 100 to 200 ns improves the maximum signal by approximately 10 dB. Furthermore, on a qualitative basis, the chevron is considerably more visible and extends over a larger range which would ease any future algorithm trained to look for this pattern. The instantaneous excitation of neighbouring masts, visible as vertical lines stretching upwards from the time of the flashover, is also more prominent.
Much of the data for identical flashover parameters measured with differing pulse widths has yet to be analysed but it seems promising that an increased pulse width can, as expected, improve the detection ability of flashovers at greater optical distances as well as for smaller, less powerful flashovers.

Passing Train

A number of measurements were intentionally triggered as a freight train was passing the flashover location on the neighbouring track. This allows insight into the question of whether a flashover would be detectable while a moving train was present at this location. Octave analysis for two example measurements is presented in Abbildung 45 and Abbildung 46. In Abbildung 45 one side of a chevron is partially visible in the second lowest frequency band (39 – 50 Hz) while in Abbildung 46 no visual cue can be seen to infer the presence of a flashover. Both measurements have distinctly

different peak powers (139 and 84 MW respectively) and pulse energies (3.3 and 1.2 MJ respectively) which may explain why the one can be observed and the other not. The passing train occupies a considerable bandwidth with only the upper octave appearing free of any energy. For a robust detection it would therefore be necessary that the flashover is either strong enough to create signal at these high frequencies or that any chevrons produced lie out with the path of the travelling train.

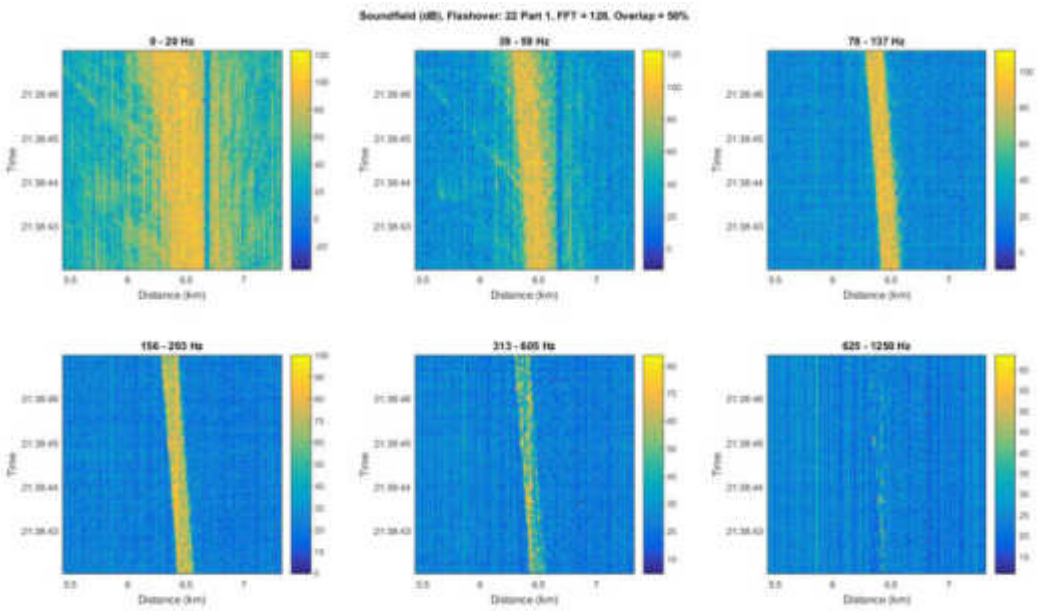

Abbildung 45: **Octave soundfields for a flashover while a train passes for Measurement 22.**

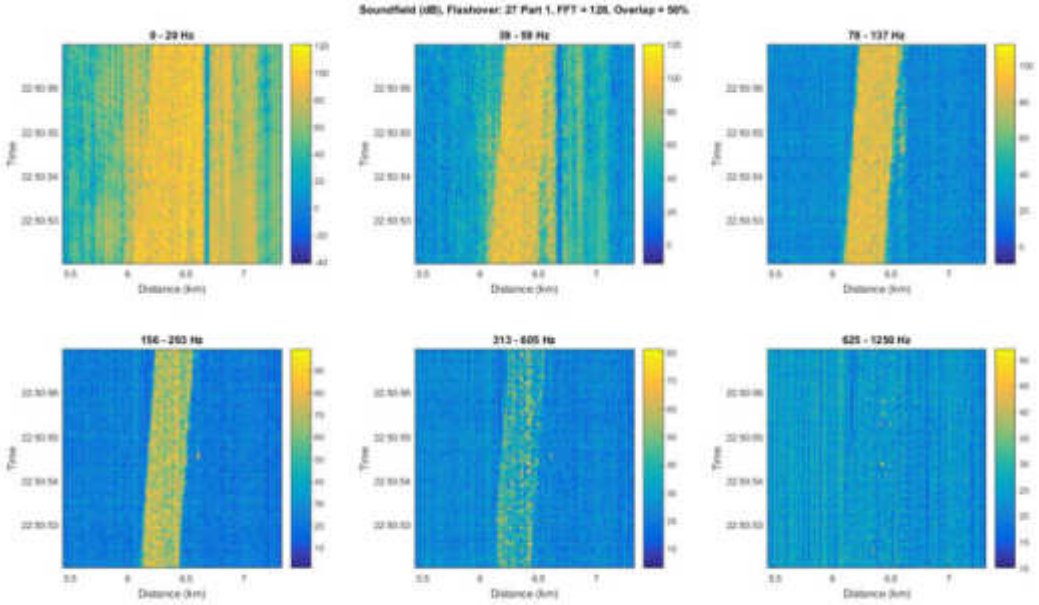

Abbildung 46: **Octave soundfields for a flashover while a train passes for Measurement 27.**

Unexpected signal sources

During the experiments, and also during the subsequent signal analysis, it was observed that not only was excitation of the fibre visible at the flashover location but at several other locations along

the railway track. These excitations do not emanate from the flashover location and travel to other locations at a given velocity, such as is seen with the chevron patterns, but rather occurred precisely at the flashover, see Abbildung 47. Many such locations could be identified within a few hundred meters of the flashover and could be attributed to the neighbouring masts. The near instantaneous transfer of energy from the flashover to these nearby locations is probably due to the strong coupling of one mast to its neighbour over the catenary (speed of sound in aluminium = 4600 m/s). However, many locations were excited instantaneously a number of kilometres away from the flashover location. After analysing the positions of these excitations it transpired that particular infrastructure along the side of the rail was responsible. For example, in Abbildung 48 the chevron pattern of the induced flashover near 6.5 km can be clearly observed. At a number of other locations a signal can be seen, particularly at 14 km, 16 km and 18.5 km. The signal at 14 km was found to be located at a crossover section in the track where a number of points were positioned close to one another. Additionally, and this was found to be responsible for the signal, there are a number of switchgears where power is fed to and removed from the separate catenaries. Two parallel copper cables, hanging freely in the air approximately 30 cm apart, are led from the switchgear up the mast. These are then joined together to feed the catenary. Current flows in the same direction in these cables and therefore when a flashover occurs, the sharp increase in current causes both cables to be attracted to one another through the Lorenz force. This theory could explain why mechanical energy could be detected several kilometres from the flashover location and was proven by observing this area during several of the flashovers. It could be observed that the cables violently crashed into one another before proceeding to oscillate, dissipating their energy into the surrounding masts and infrastructure, which also explains why these signals can be observed using DAS for up a couple of minutes after the flashover has occurred.

The signal at 18.5 km can be attributed to the switchgear at the substation in Riedau which powers the section of line used for the measurements. Indeed it could be observed that in some cases a signal could be detected at locations further away from the flashover before the flashover occurred, see Abbildung 48.

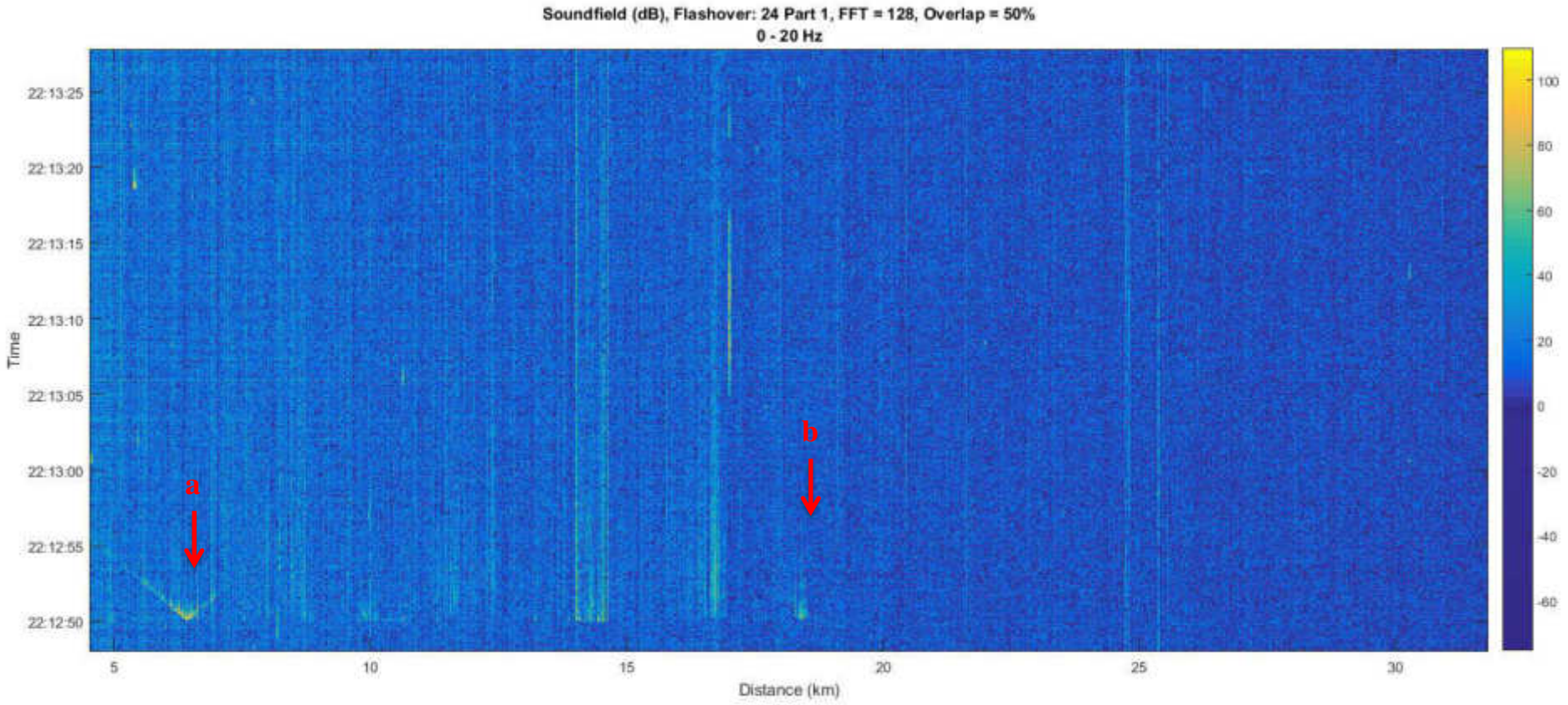

Abbildung 47 : Approximately 30 km of observed track from Allerding to Neumarkt. The typical chevron pattern of a flashover can be clearly seen at 6.5 km (a). Other sources of energy can be observed between the location of the flashover and the substation (~18.5 km) (b) which can be attributed to tethering of the catenaries. See text for further details.

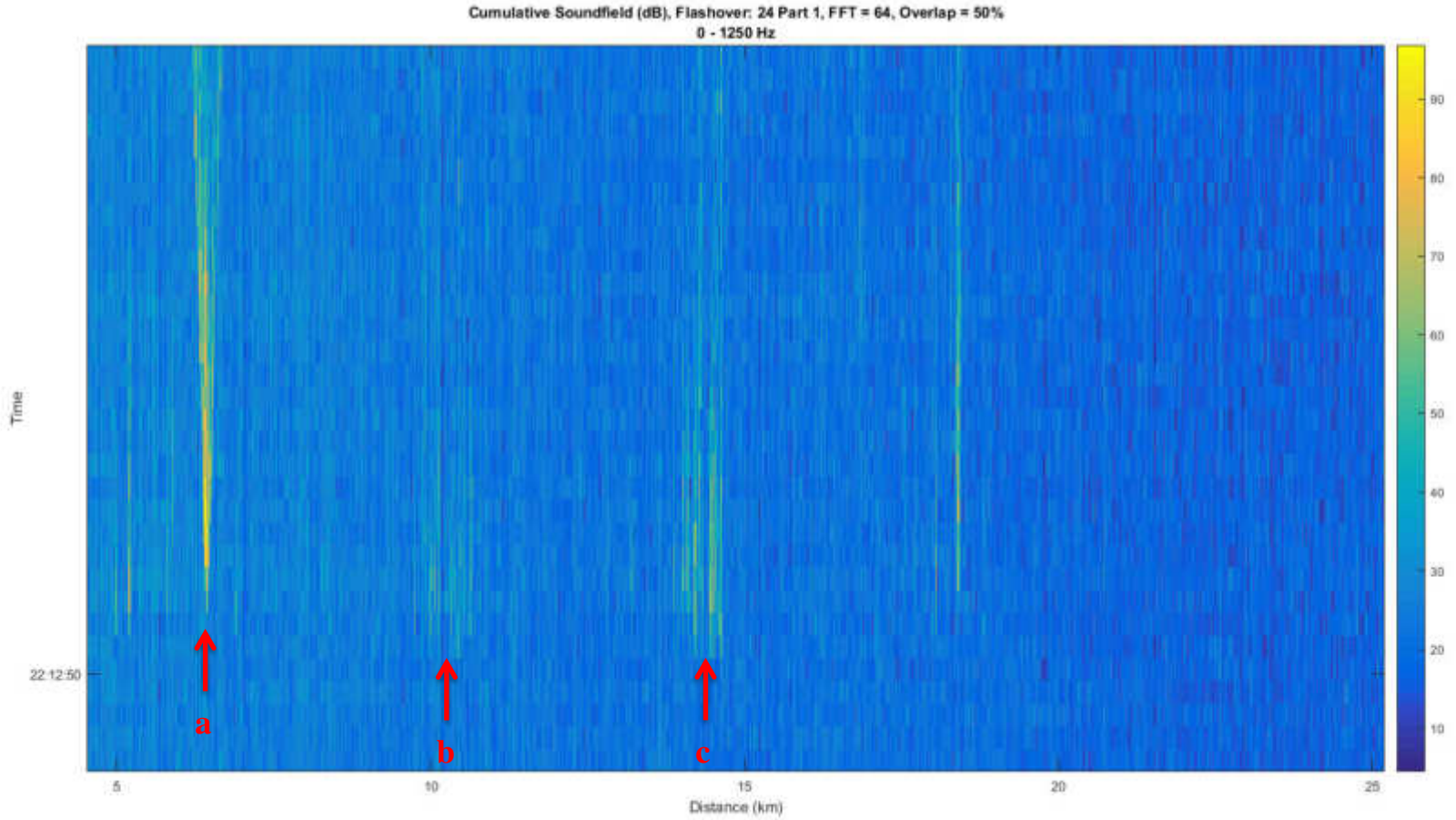

Abbildung 48: Cumulative soundfield for all frequencies showing excitation at 11 km (b) and 14 km (c) occurring ca. 50 ms BEFORE the flashover at 7 km (a). The FFT size has been reduced to 64 to highlight this effect

Spectrogram

As well as investigating the general frequency content of the signals using octaves, it is possible to plot the frequency content per FFT time step and generate what is known as a spectrogram. This has been done for one example data file, Measurement 24, see Abbildung 49. Three separate locations have been chosen from this file for analysis and are indicated with letters: the flashover location (a), the switchgear location near 14 km (b) and where the substation connects to the catenary at 18 km (c). The red horizontal line indicates the point in time at which the spectrogram for all channels is calculated. For each location and time interval the frequency spectrum is calculated and plotted as shown in Abbildung 50 for position (a), Abbildung 51 for position (b) and Abbildung 52 for position (c).

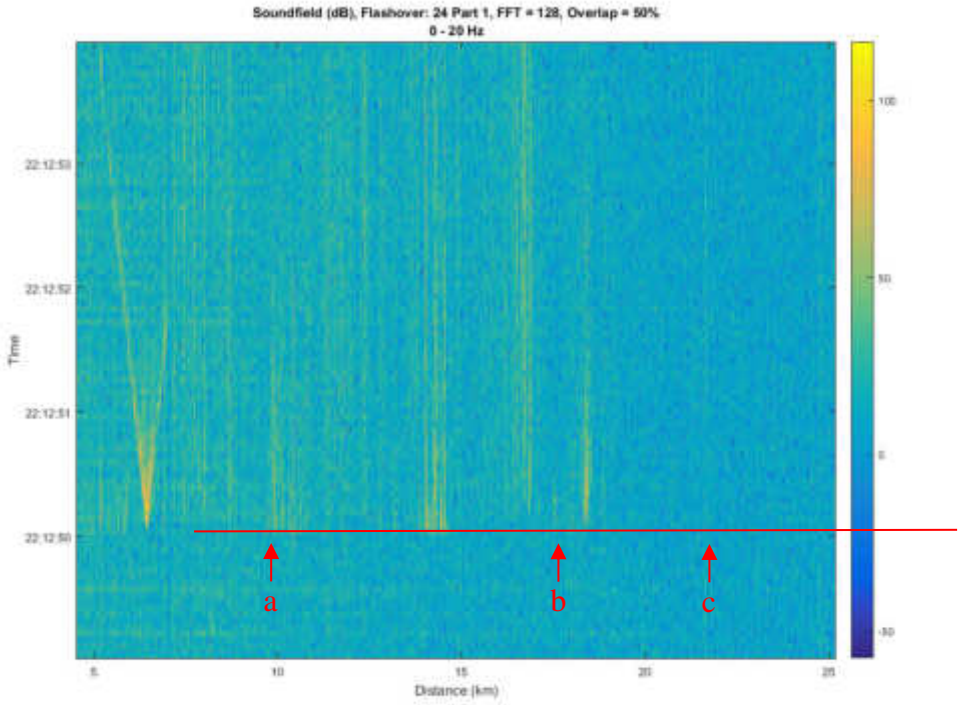

Abbildung 49: Soundfield for Measurement 24 between Allerding and Neumarkt. The red line marks the axes along which the data for the distance spectrogram have been extracted. The arrows indicate locations of signal generation: a) flashover location, b) switchgear,and c) substation.

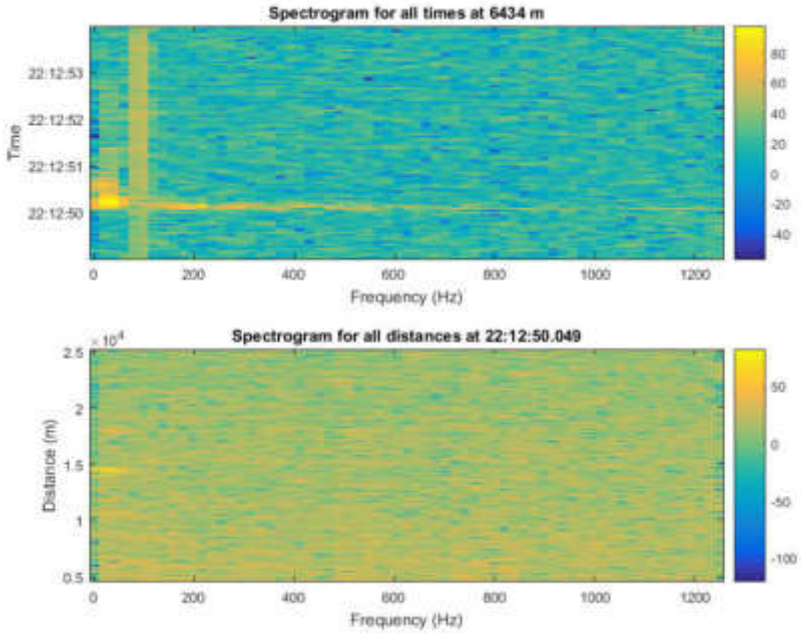

Abbildung 50: **The upper plot shows the spectrogram of the time evolution at the flashover location (a). It can be seen that at the time of the event (shortly after 22:12:50), the majority of the detection bandwidth has been excited. The lower plot shows the spectrogram of the distance evolution at the time of the flashover.**

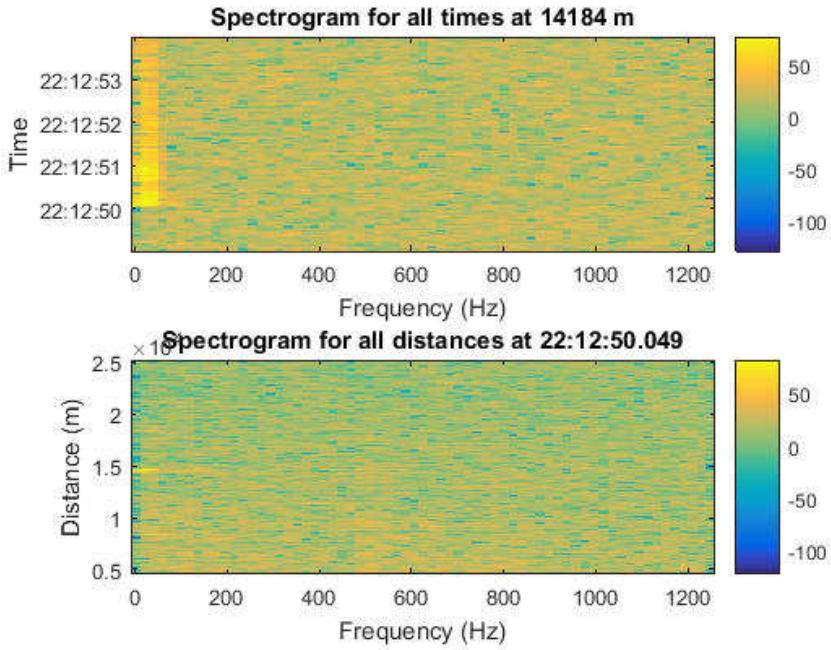

Abbildung 51: **The upper plot shows the spectrogram of the time evolution at the switchgear location (b). Only the low frequencies have been excited by the flashover. The lower plot shows the spectrogram of the distance evolution at the time of the flashover.**

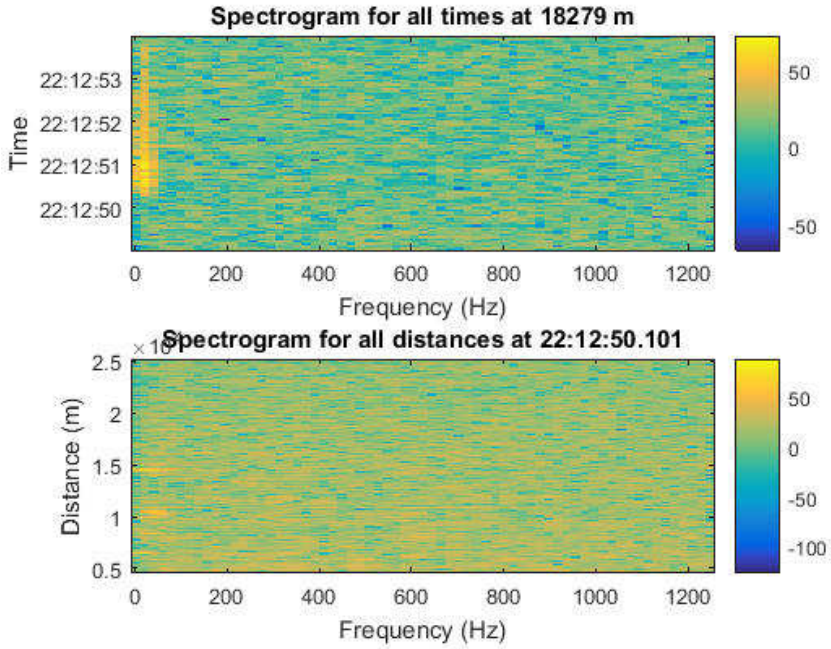

Abbildung 52: The upper plot shows the spectrogram of the time evolution at the sub-station location (c). Only the low frequencies have been excited by the flashover. The lower plot shows the spectrogram of the distance evolution at the time of the flashover.

It is interesting to note that only the spectral content at the location of the flashover contains higher frequencies. This is potentially a feature that could be used to help locate the flashover when multiple excitations due to the infrastructure are observed although it should be noted that the spectrogram analysis has only been done on one example flashover showing chevrons. Additional work is necessary to validate this hypothesis.

Current – Voltage

Characteristically, there were two types of flashovers observed. One in which the circuit breaker tripped after one half cycle of the supply voltage, as seen in Abbildung 53, the other after one complete cycle, Abbildung 54. This behaviour could not be actively influenced during the experiments with the circuit breaker intervening of its own accord leading to some measurements having a single pulse flashover while others having a double pulse. The vast majority of the flashovers to date were of the single pulse type.

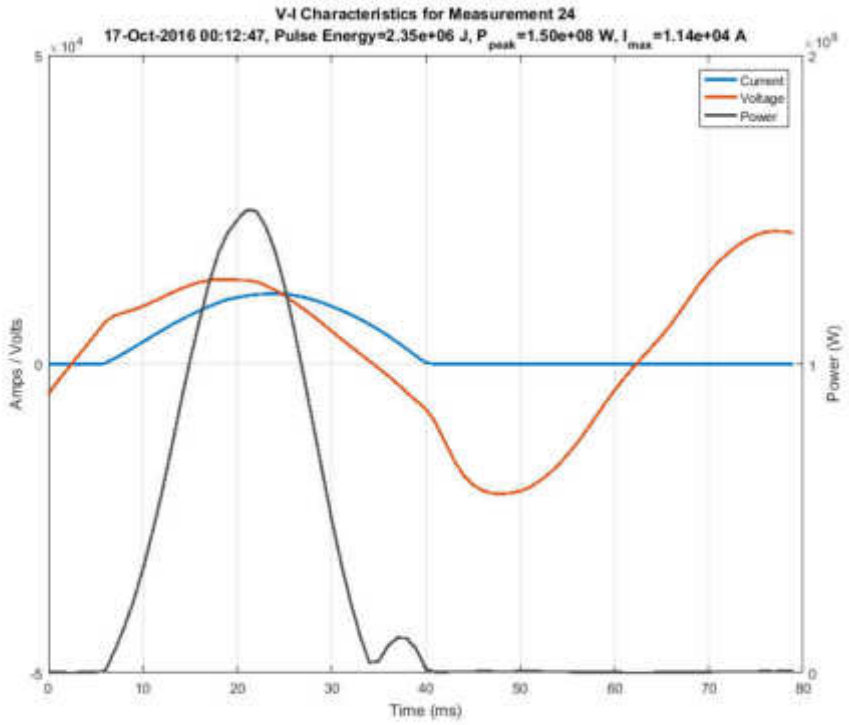

Abbildung 53: **Typical single pulse current, voltage and power evolution during a flashover.**

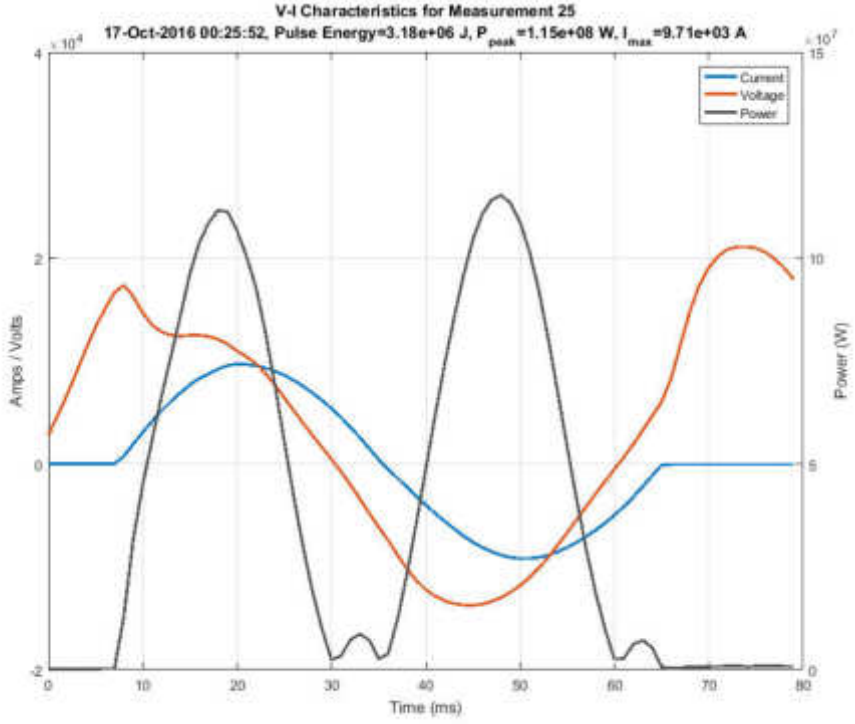

Abbildung 54: **Typical double pulse current, voltage and power evolution during a flashover.**

In Abbildung 53 and Abbildung 54 the power is calculated simply from the instantaneous current and voltage values at any period in time. The flashover energy content can then be

calculated from the integral of the pulse power over the duration of the pulse and is included in the title of each figure.
It was observed that many of the current measurements from the experiments conducted in November 2016 exceeded the input range of the ADC and were therefore saturated.

Calculating and plotting the peak power achieved during the flashover and the pulse energy for all events we attain Abbildung 55. This shows a near linear response of the pulse energy with respect to the peak power, which is to be expected as a higher peak power should lead to a linear increase in the pulse energy, assuming the pulse form and width remain approximately unchanged. Several flashovers, particularly during the November measurement campaign, induced a current high enough to saturate the ADC of the measurement apparatus. The input range of the Dewetron ADC should therefore be increased to account for this in future measurements. The saturation causes an under-estimation in both the peak power and pulse energy calculations but have been included nevertheless for completeness. Abbildung 55highlights these incorrect values as red.

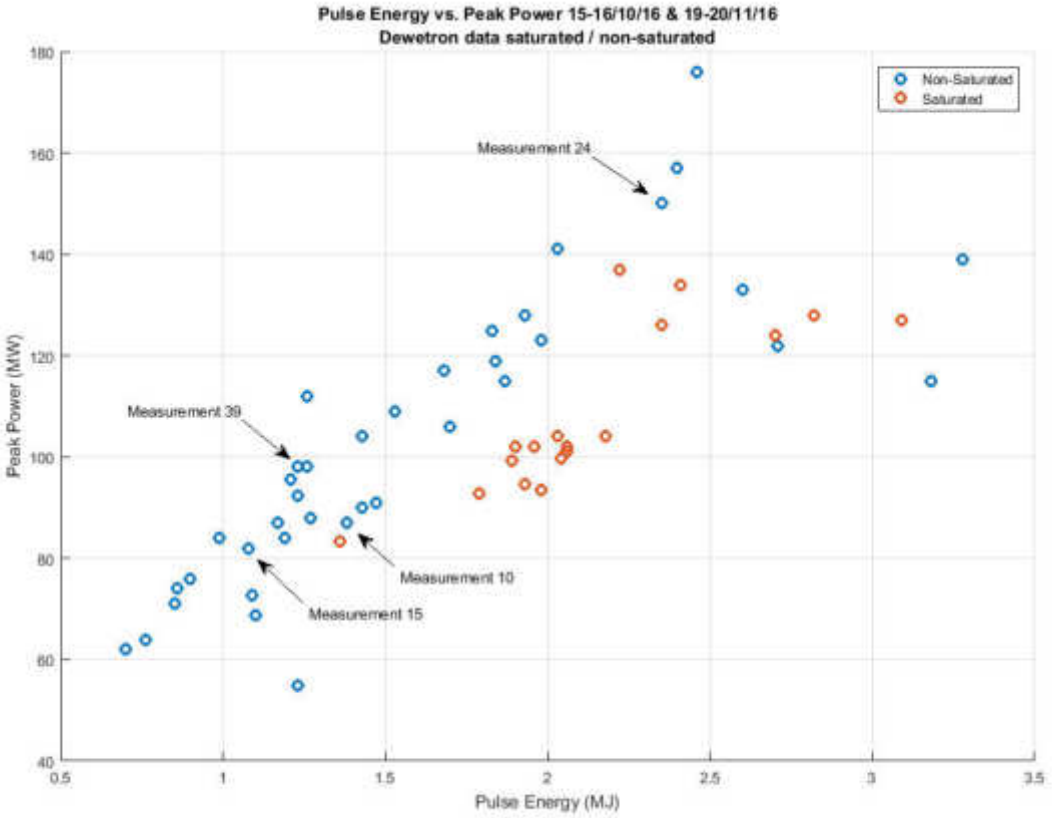

Abbildung 55: A plot showing the linearity of peak power against pulse energy for all measured flashovers. A number of chosen measurements based on a visual classification have been identified. The red circles signify that the current signal was saturated and are therefore incorrect. Assuming these measurements were correct then the points would be shifted upwards and to the right. The few measurements lying below the linear trend line (those in the far right of the figure) are double pulse flashovers.

Accelerometer

A typical time series plot of a flashover is shown in Abbildung 56. This data was taken for Measurement 40 on Mast M47/13. The accelerometer was mounted at a height of approximately X m above ground.

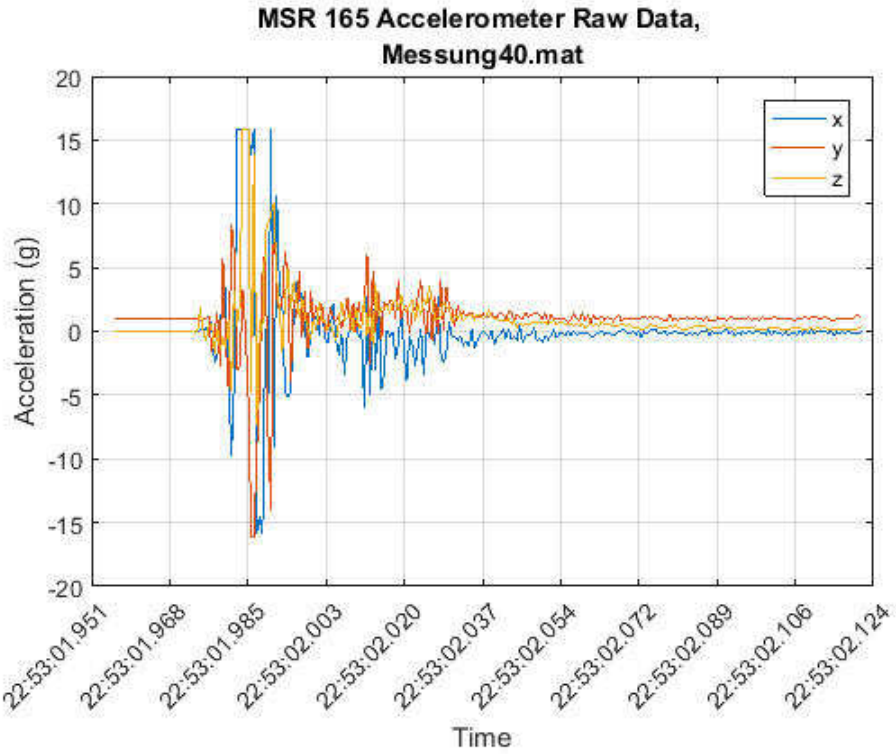

Abbildung 56: **A typical time series plot of all 3 axes, in this case for measurement 40.**

TODO
Investigate resulting vector evolution over time from combining x, y, and z.
TODO_END

By applying an FFT over the entire signal we obtain Abbildung 57 which tends to spread the frequency content of the event over the entire measurement time. This is not the optimal analysis toll due the flashover being impulsive in nature. Abbildung 58 shows an improvement over the FFT by calculating a spectrogram which investigates smaller sections of data from the signal to better isolate the event in time. From Abbildung 58 it is evident that at the time of the flashover there is energy within all frequency bands. This reinforces the fact that this event is impulsive. It can also be observed that the low frequency content remains for almost the duration of the measurement in the y-axis and the z-axis. The y-axis content endures simply because gravity is acting on the sensor in this direction. Further analysis of all data sets is required to be able to reach any conclusions on why the z-axis damping is less. Possible explanations could include asymmetries in the mast geometry or the method used to mount the accelerometer to the mast.

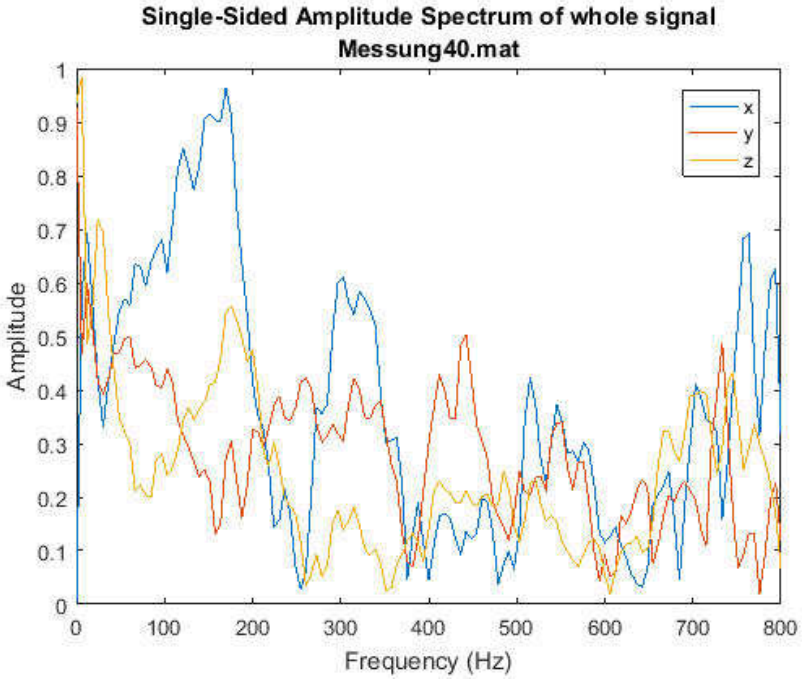

Abbildung 57: FFT analysis of Measurement 40. The entire signal is used to calculate the frequency content.

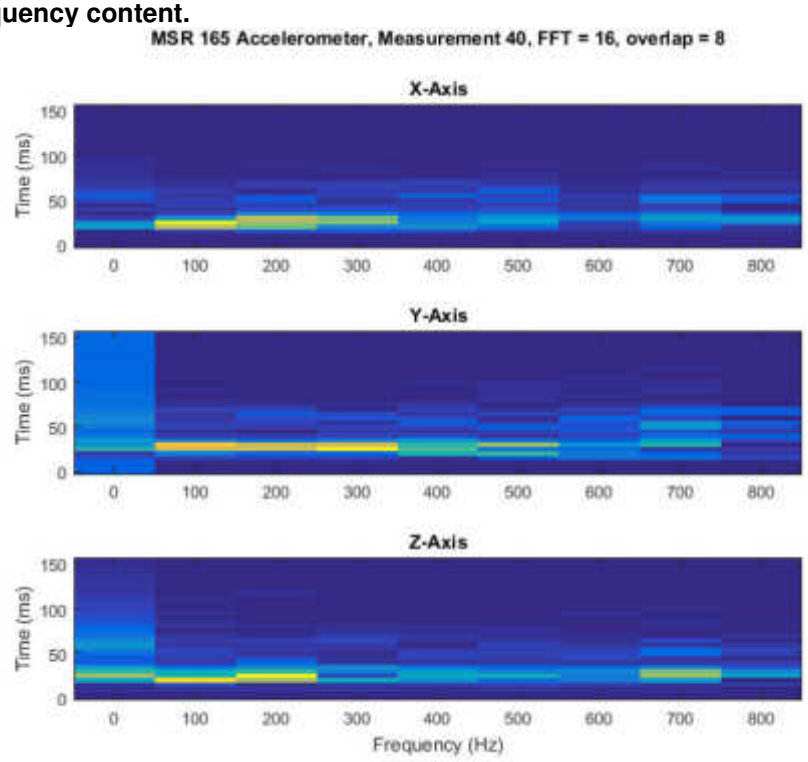

Abbildung 58: Spectrogram of Measurement 40 with FFT length of 16 and an overlap of 50%. Blue indicates low signal while yellow indicates high signal. Time increases upwards.

4.5 Next Steps

A number of data processing steps remain unfinished to date and these should be completed to gain the maximum insight in preparation for further tests planned for May 2017. These steps include:

- Complete visual classification of all flashovers.
- Complete analysis for all measurements with laser pulse widths of 100 ns and 200 ns.
- Complete analysis for all measurements with varying short circuit wire length.
- Complete investigation of frequency content at the location of flashover and at infrastructure related sources (switchgears, etc.).
- Interpolate saturated Dewetron data to better estimate the peak powers and pulse energies.
- Create a cross correlation matrix for all recorded parameters particularly noting any correlations to the visual classification.
- Investigate in particular the correlation between the distance between the flashover and the optical fibre.
- Optimise pre-processing to maximize signal to noise ratio, possibly incorporating wavelet analysis due to the impulsive nature of the events (Optional).

4.6 Conclusions

A number of short circuits, or flashovers, between the high voltage catenary and ground have been induced at several locations on a section of main line railway in Austria between Schärding and Wels. All parameters which were thought could possibly influence the creation, propagation or detection of the event were recorded. Several different measurements were taken during the flashovers including DAS, physical movement of the mast at the flashover location and the electrical surge pulse characteristics.

The vast majority of the flashovers could be visually observed from the DAS data after a number of simple pre-processing steps. In some cases a clear chevron identified the time and location of the flashover while in others no distinct signal unique to the event could be observed. A clear correlation between energy content of the electrical pulse and visibility in the DAS signal was seen with higher energy flashovers creating highly distinct and visible chevron patterns.

By using two separate optical fibres connected to the same DAS measurement system the same event could be simultaneously recorded at two different optical distances. It was found from the limited analysis to date that an optical distance difference of approximately 25 km reduced the signal to noise ratio by ca. 30 dB.

One known method of increasing signal at the expense of spatial resolution is to increase the laser pulse width. This was experimentally verified by inducing as near to identical flashovers at the same location and recording a DAS signal with two different pulse widths. As expected the increased pulse width would increase the detectability of flashovers at greater optical distances or smaller events at shorter optical distances. The higher energy flashovers could be detected at 30 km using a pulse width of 100 ns and it is therefore plausible that similar events could be detected at 40 km with a pulse of width 200 ns although this has yet to be experimentally verified.

A number of events were timed to coincide with the passing of a train. The goal was to verify if a detectable signal could be identified when masked by the broadband signal generated by the passing train. It was observed that if part of the chevron pattern propagated past the physical ends of the moving train then the flashover location could be identified. For less energetic events no distinguishable signal at the flashover location with the current signal processing could be observed. However, it could be noted that flashovers regularly excited not only locations in the DAS signal that were local to the flashover location but also many other locations, as detailed below, and therefore it would seem possible to harness this information to help identify the event.

One of the most unexpected results from the measurement campaign so far was that for nearly all of the induced flashovers, acoustic excitation could not only be measured at the location of the flashover but also *simultaneously* at a number of other locations, sometimes kilometres away. These acoustic sources were identified as being linked to particular equipment placed alongside the track. Signals could be observed emanating from masts, switchgears and parallel cable feeds and are particular to this installation, however it is to be expected that on all electrified routes similar equipment will be present. Such signals ease the detection of a flashover but complicate the localization in the cases where no distinct chevron is visible.

In conclusion, the measurement campaign has been successful in inducing and recording a large number of distinctly different flashovers. A number of preliminary findings and correlations have been identified and these will help in defining the measurement goals for the next campaign planned for May 2017.

5 BESCHREIBUNG ZWEITE VERSUCHSREIHE – ST. PÖLTEN

5.1 Introduction

This document provides interim results on experiments carried out in cooperation with ÖBB to assess the performance of a Frauscher Tracking Solutions (FTS) system using Distributed

Acoustic Sensing (DAS) on the detection and location of a catenary flashover. The experiments were conducted in Austria, St. Pölten, on the Güterzugumfahrung (GZU) at a number of locations in May 2017. A total of over 40 flashovers and additional tests with gun powder and physical shaking were induced over a period of 4 days, resulting in about 70 new recordings. This work is currently ongoing with the results to date being summarised in this document.

Catenary flashovers are electrical short circuits between the high voltage (15 kV) catenary and ground typically causing an electrical spark and associated acoustic bang. These can occur for a number of reasons: faults within the locomotive, driver error, wildlife or natural occurrences such as a branch falling off a nearby tree, to name but a few. Circuit breakers in the respective substation cut the supply within a few milliseconds but in order to be able to reapply the electrical supply and resume operation, the cause of the flashover must be found and repaired if required. In certain cases, the exact position of the flashover is not known and a considerable amount of time and effort is required to locate it. It is hoped FTS and DAS technology can help determine the source of a flashover event to within a few tens of metres which would be a vast improvement over the current accuracy. DAS operates by injecting pulses of laser light into an optical fibre which typical lies parallel to, and a few meters from, the railway track in a cable duct. Any acoustic disturbance of the fibre is detected and converted to an electrical signal which can be analysed using digital signal processing techniques. It is the acoustic bang caused by the flashover together with any induced mechanical vibrations which can be measured using DAS.

The technical goal of this research is to determine the physical parameters which influence the creation, propagation and detectability of such flashovers and to quantify these thereby allowing limits on the usability of DAS technology to be determined. A small number of the numerous influencing parameters which can affect the signal strength detected at the optical fibre have been isolated for investigation in these initial experiments.

5.2 Measurement Time and Locations

The flashovers were conducted at a number of catenary support masts on the GZU in St. Pölten on the days between 15th and 18th May 2017. Detailed information on the masts where the flashovers occurred is shown in Tabelle 7.

Mastnumber	**Position (ÖBB km)**	**Distance between flashover and fibre (cm)**
M 14/67	14.300	830

M 14/91	14.550	not measurable
M 14/92	14.550	not measurable
M 14/93	14.600	850
M 20/21	20.550	851
M 20/37	20.950	850
M 22/146	-	800
M 22/33	22.300	600
M 22/53	22.500	600
M 23/01	23.000	600

Tabelle 7: **Mast details of where flashovers were induced.**

5.3 Experimental Setup

Short Circuit

The short circuit setup was the same as in the tests in Allerding. Further information on the setup can be found in chapter 4.

Current – Voltage

The energy of the induced flashover is calculated from measuring the current and voltage at the substation used to supply the catenary. The supply voltage was directly measured using an ÖBB voltage transformer with the ratio 165:1. The current was measured using an ÖBB current transformer with ratio 150:1 and current clamp with conversion factor 1A = 10V.

Accelerometer

To assess the physical movement of the mast during and after a flashover is induced, two accelerometers of type MSR-165, see Abbildung 59, were mounted to the mast. This allowed acceleration in 3 mutually perpendicular axes at a maximum sample rate of 1600 Hz to be recorded. The sensors were physically mounted to the mas and set to be triggered to record when one of the axes measured acceleration greater than 1.5g.

Abbildung 59: **MSR-165 accelerometer. Dimensions are 39 x 23 x 72 mm.**

Abbildung 60: **MSR-165 accelerometer mounted to the mast. The measurement axes are defined as indicated.**

DAS

The DAS measurement system is housed in a small service hut at km 55.675 directly beside the track and is built up of several constituent parts, see Abbildung 61. Up to two single mode optical fibres (Channel A and Channel B) with a maximum length of 40 km each can be connected to the optical unit. The optical unit generates and orchestrates the timing of the laser pulses and detects the reflected single from the fibres. The analogue signal is then fed to the processing unit which digitizes and saves the data (up to 600MB/s) to the RAID. Additionally,

it processes the data and forwards the results onto the display unit where it can be observed in real time via a web browser interface.

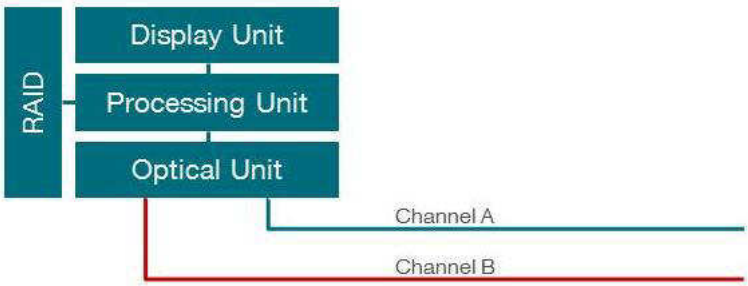

Abbildung 61: **The component parts of the DAS measurement system.**

For these experiments, two single mode optical fibres were utilized for detection whereby a fibre spool was connected in series to one of the fibres prior to it exiting the service hut. This enabled the same flashover to be simultaneously recorded at different optical distances. A schematics for the measurement setup is shown in Abbildung 62. Both channel A and channel B were terminated in Rohr (~ OEBB km 74, approximately 18 km from the service hut). The fibre spool length for the measurements was 10 km. The laser operates at 1550 nm while the pulse repetition rate was 2500 Hz and remained unaltered throughout the experiments. Contrary to the tests in Allerding, the pulse width was constant at 100 ns.

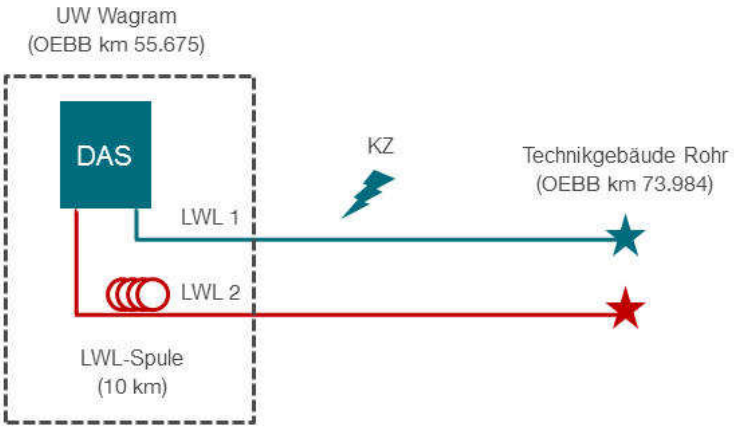

Abbildung 62: **Schematic setup for the measurement period between 15th and 18th May 2017.**

Additional to the two fibres for the HSi system, there was a third one for the Theta unit. The results of the Theta recordings are not discussed in this report.

5.4 Results

A number of tendencies can be identified which could be utilized in determining which flashovers can be detected and/or located and those which cannot. Any algorithm written to detect and precisely locate a flashover in the future will be based on recognizing a characteristic pattern associated with such an event. This pattern should be distinct, unique and present in as many of the recorded signals as possible. It is therefore beneficial to visually determine if any patterns exist after a number of signal enhancement and pre-processing steps have been performed on the raw data and then isolate any parameters affecting these patterns. This qualitative analysis step was one of the first to be conducted allowing the multitude of flashovers to be grouped according to their visual characteristics. Tabelle 8 lists single measurements identified from each group for in depth analysis described in the following sections.

Measurement Number	Description	Ik (ÖBB) (kA)	Ppeak (MW)	Energy (MJ)
79	Chevrons	13.9	189.8	5.9
78	Small chevrons	12.2	161.8	4.3
76	Visible, no chevrons	13.5	178.4	5.8
74	Barely visible, no chevrons	13.9	187	5.9

Tabelle 8: **Details of example measurements from each of the visual classification groups.**

DAS

The sample rate of the raw DAS signal at each location is defined by the pulse repetition frequency of 2500 Hz. This limits the highest analysis frequency, or Nyquist frequency, to equal 1250 Hz. Some rudimentary signal processing steps are applied to each raw file to enhance the signal to noise ratio. The first step was to remove spatial data channels corresponding to any spools of fibre along the route which can cause optical artefacts. Additionally, a high-pass filter and a spatial decimator were applied to detrend the data and improve signal to noise ratio, respectively. Thereafter the frequency content was calculated using a Fast Fourier Transform (FFT) to allow a simplistic analysis of the frequency content of the flashover event. It is

assumed that the majority of the signal energy resides in the lower part of the frequency spectrum and this allows an estimation of the noise. All signal processing was carried out using Matlab.

Octave Analysis

By dividing the energy content of the signal calculated from the FFT in to octaves, a crude frequency analysis can be conducted. For example, the upper octave contains energies in the range 625 – 1250 Hz; the next lower octave contains frequencies in the range 312.5 – 625 Hz, the next again in the range 156.25 – 312.5 Hz, etc. By plotting these energies calculated with an FFT length of 128 and an overlap of 50% we obtain Abbildung 63 to Abbildung 66. Each figure presents six octave plots from 1 second before to 3 seconds after the flashover occurred. A distance of 2 km either side of the event is observed.

It can be seen that the frequency content differs substantially. Abbildung 63 shows a clear "V", or chevron, as a result of the acoustic signal, or pressure wave, leaving the flashover location and travelling in both directions along the fibre route. The gradient of the "V" determines the speed of propagation and is experimentally found to be 340 m/s from the data. This matches the speed of sound in air very well (~343 m/s @ 20°C) and it can therefore be deduced with a high certainty that this signal results from the acoustic bang accompanying the short circuit.

From Abbildung 63 it can also be seen that, unlike in Allerding where only the low frequency components travelled a substantial distance with the higher frequency components (150 Hz and upwards) remaining local to the short circuit, in St. Pölten a lot of the events were best seen in the frequency range of 78 – 137 Hz. There is also the fact to consider that the categorisation is subjective to the track. Category 1 short circuits in Allerding tend to be far greater in size, both in the distance and time dimension. A theory was formed that this depends on the differences of the troughs' structure. Further experiments must be conducted to assess this theory.

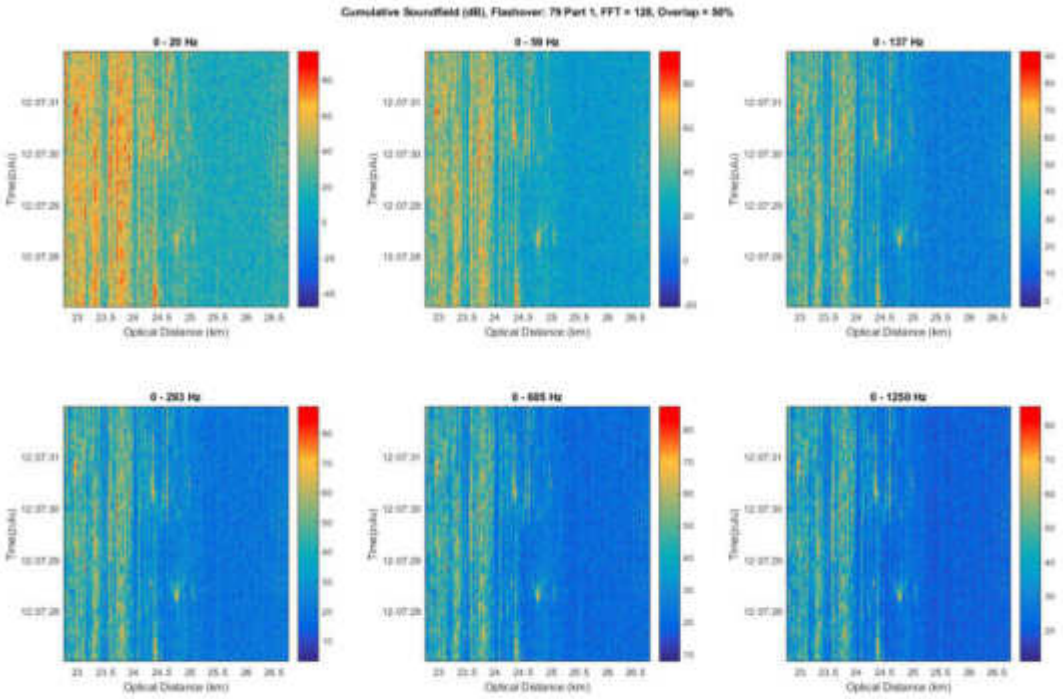

Abbildung 63: Octave plot of measurement 79 showing the typical "chevrons" of a powerful event. The event occurs between 24.5 – 25 km shortly after 12:07:28.

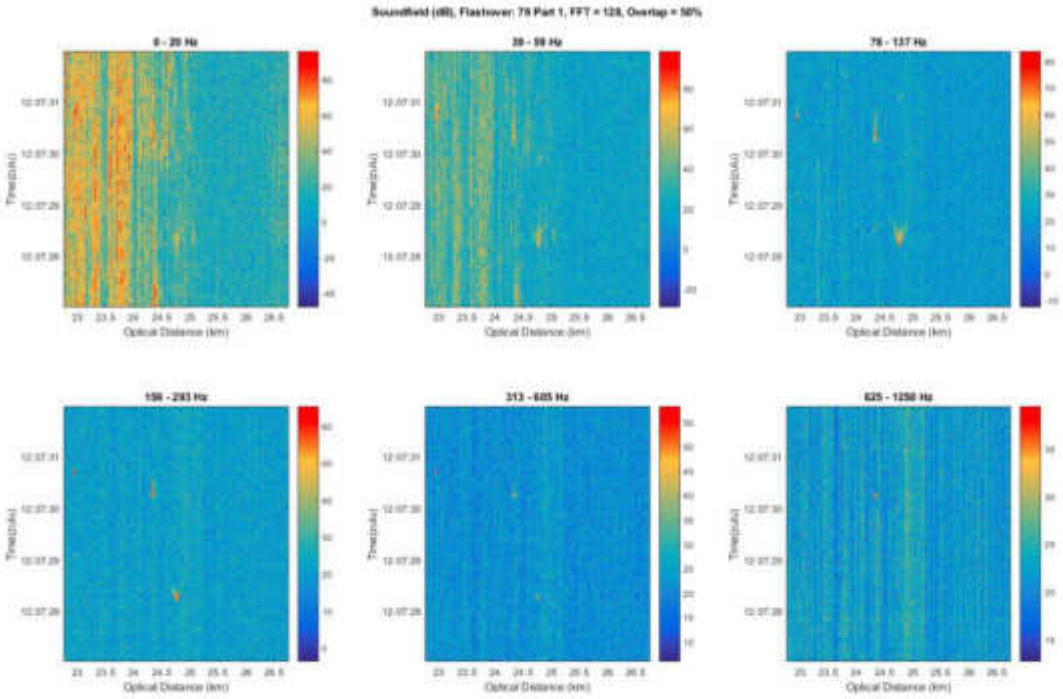

Abbildung 64: **Octave plot of Measurement 79. The event occurs between 24.5 – 25 km shortly after 12:07:28.**

As the energy content of the flashover is reduced the chevrons become less pronounced as can be seen for Measurement 79 in Abbildung 64. The high frequency content is still visible up to approximately the 4th octave after which it is swamped by the noise of the system.

The same effect as in Allerding could be seen for certain flashover events. They produced signal characteristics without any visible chevrons when applying the identical signal processing. These events caused a number of locations along the track to be excited simultaneously, particularly at low frequencies. After investigation those locations could be attributed to positions of other masts supporting the catenary along the track. Further information concerning these effects is detailed in chapter 4.

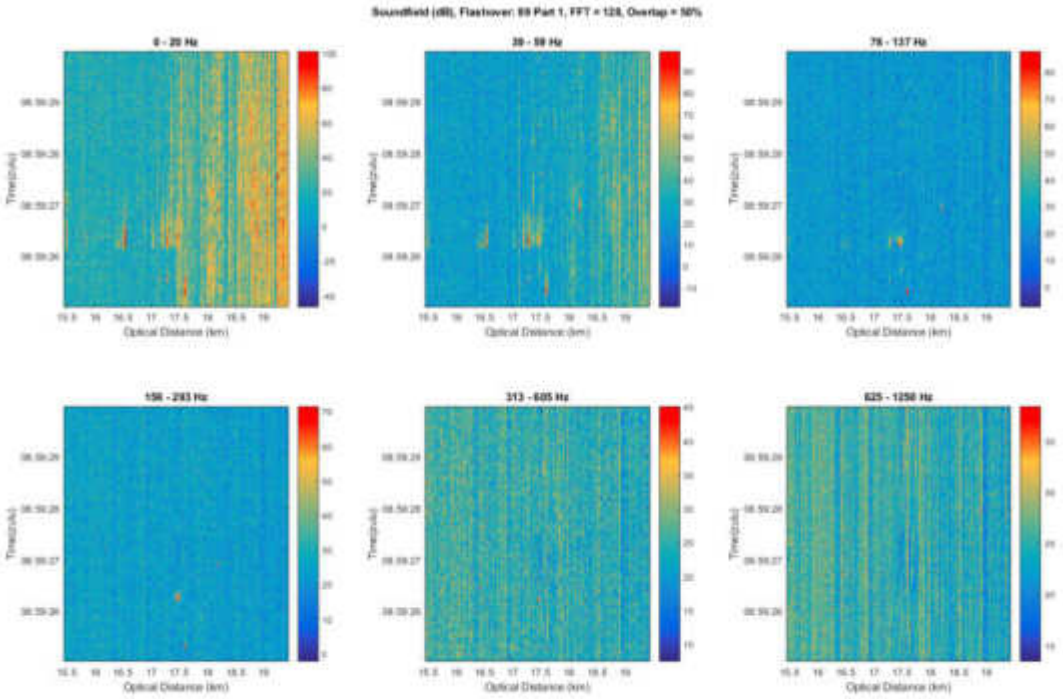

Abbildung 65: Octave plots for Measurement 89. Signals from the flashover are barely visible when visually assessing the plot.

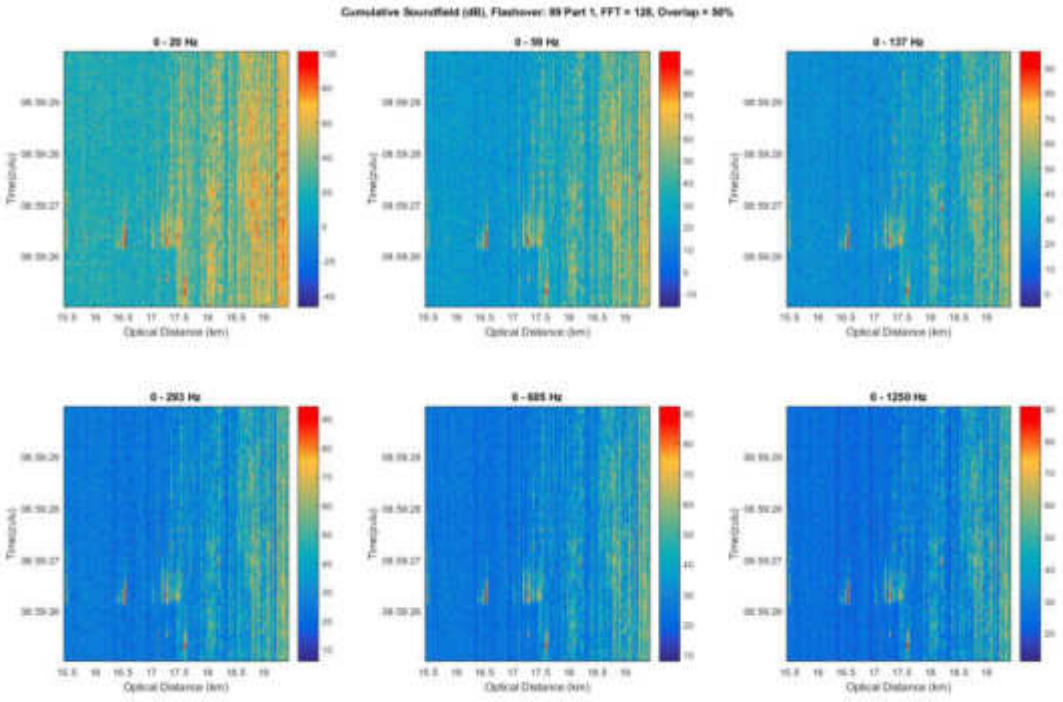

Abbildung 66: Octave plots for Measurement 89. Several signal sources are visible and it is therefore unclear where the flashover occurred.

5.5 Pranger shots

Additional to the self-induced flashovers, 19 shots were fired with a prangerstutzen (signal gun) as seen in Abbildung 67. Varying weights of gun powder (from 30 – 66 g) and compression (1- to 6-times) was used. The loud bang of the shots resulted in recorded data very similar to the induced flashovers. Abbildung 68 shows the example shot of measurement 130 with a clear chevron in it. All but two shots were classified into the categories “large chevron” and “small chevron”. In order to know if pranger shots can be seen as flashovers and may be used as a replacement for coming experiments, further analysis must be done on the differences between the parameters of self-induced flashovers and pranger shots.

Abbildung 67: A prangerstutzen

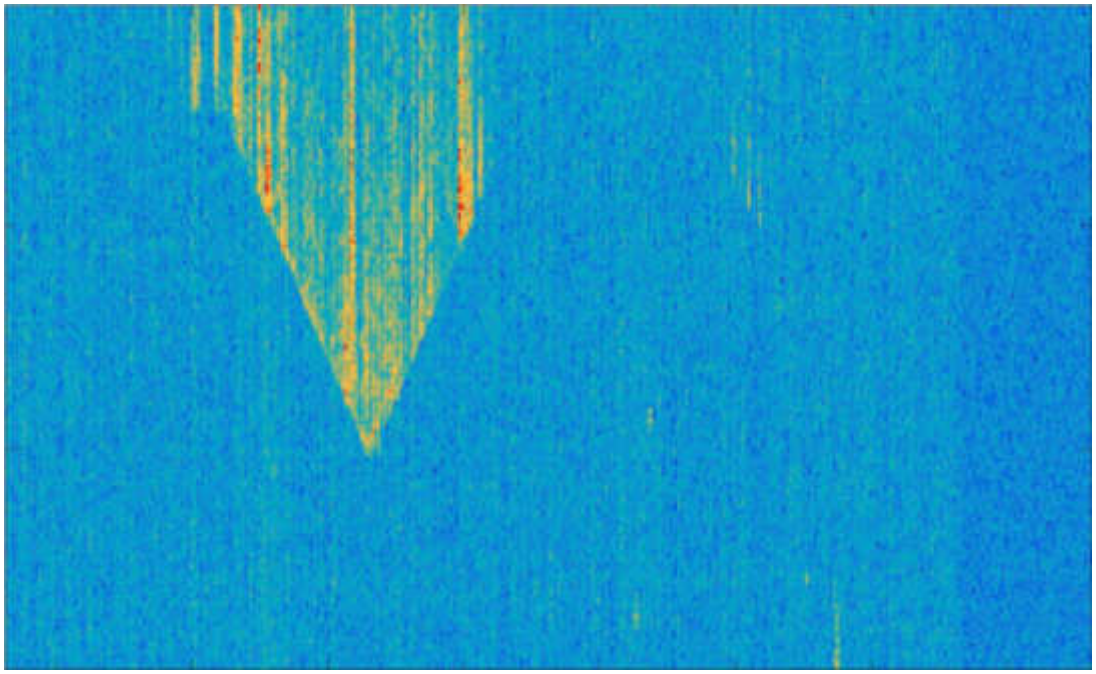

Abbildung 68: Example soundfield plot of a pranger shot; measurement 130.

Visual classification

From chapter 4 it is obvious that the pre-processed DAS signal patterns can vary substantially from the case in which a chevron is clearly visible at the flashover location to producing no visible signal at all. Determining which of the many parameters affect this signal response is important in determining any limitations of a detection algorithm. A sensible assumption could be, for example, that those signals containing chevrons were produced by higher energy events. To assess this correlation the pre-processed data from each measurement is visually classified and placed in one of the following groups describing the flashover as:

- having a large, clear chevron
- having small chevron
- being visible
- being barely visible
- being not visible

“Visible” was defined as being clearly able to see several locations of excitation which exactly coincide with the time of the flashover but with no other defining patterns. “Barely visible” is identical to “visible” but of less energy and a signal classified as being “not visible” contained no signal that could be visually detected with the current pre-processing steps. This is not to

say that with another analysis methodology an improved digital signal processing routine could not extract more useful signal. However, at this early stage in the project it was decided to concentrate on classifying the various measurements and their dependent parameters and not focus on extracting the very last signal from the data. By plotting the peak power and pulse energy together with the visual classification, any correlation between power, energy content and the visibility of the DAS signal can be determined, see Abbildung 69.

Each data point represents a flashover, pranger shots are not included. The colouring depends on the visual classification the flashover belongs to. It can be seen that most of the self-induced flashovers (pranger shots and shakes excluded) fall into the category *visible, no chevron*. As also seen in chapter 4, there seems to be a positive linear relationship between the pulse energy and peak power.

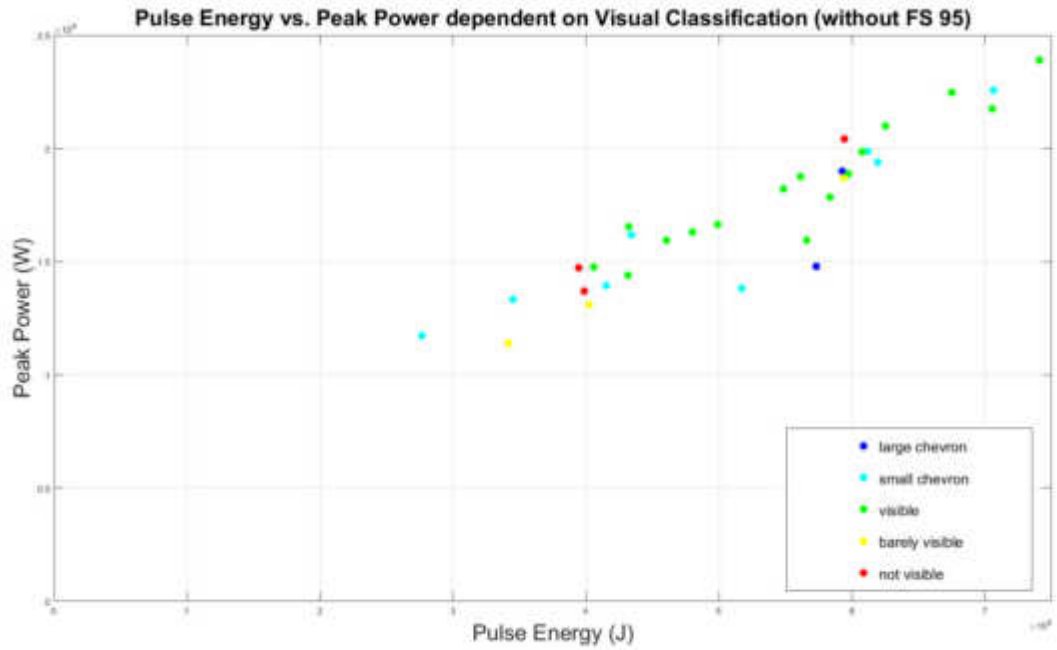

Abbildung 69: **Plot showing visual classification of the DAS signal plotted against peak power and energy.**

Optical Distance

The optical distance between the DAS system and the location of the flashover will also contribute to the amplitude of the measurable signal as the further the laser pulse has to travel in the fibre the weaker it becomes. This results in a decreased signal returning to the sensor.

Applying the identical pre-processing steps to a signal containing a clearly visible chevron pattern at two varying distances allow the attenuation of the signal to be determined. This

methodology was applied to Measurements 79 and 81 to generate Abbildung 70 and Abbildung 71 for an optical distance of 24.75 km and Abbildung 72 and Abbildung 73 for an optical distance of 34.77 km. These figures show example data taken from the highest accumulative frequency band, 0 – 1250 Hz, and the frequency band of 78 – 137 Hz respectively. Both measurements were recorded with a laser pulse width of 100 ns.

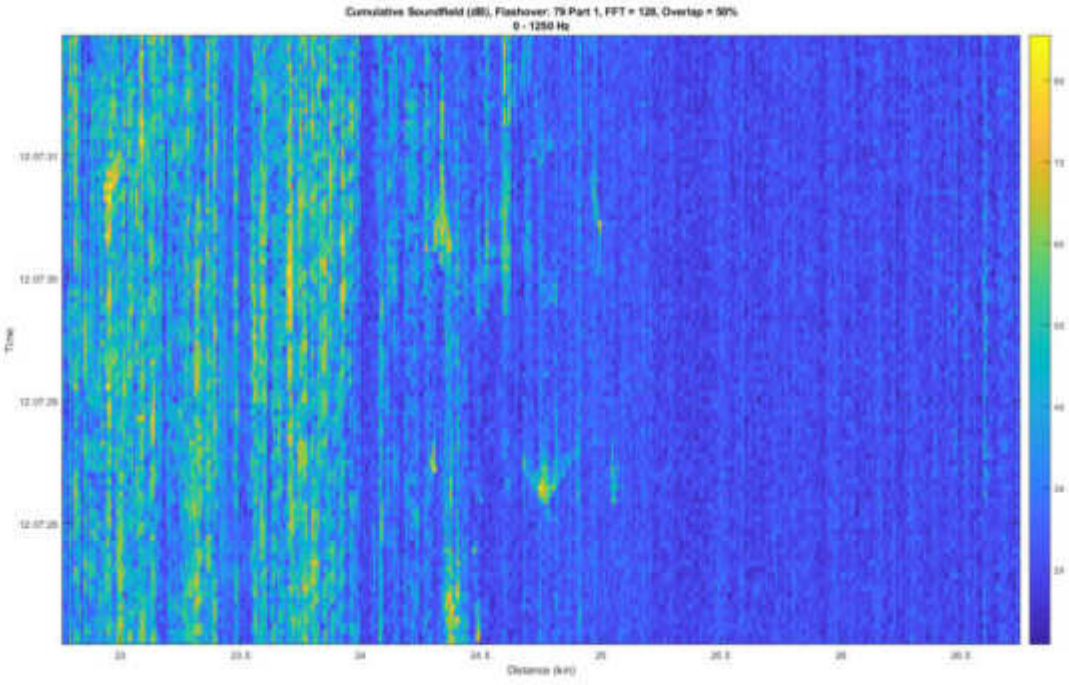

Abbildung 70: **Measurement 79, 0 - 1250 Hz. Optical distance = 24.75 km.**

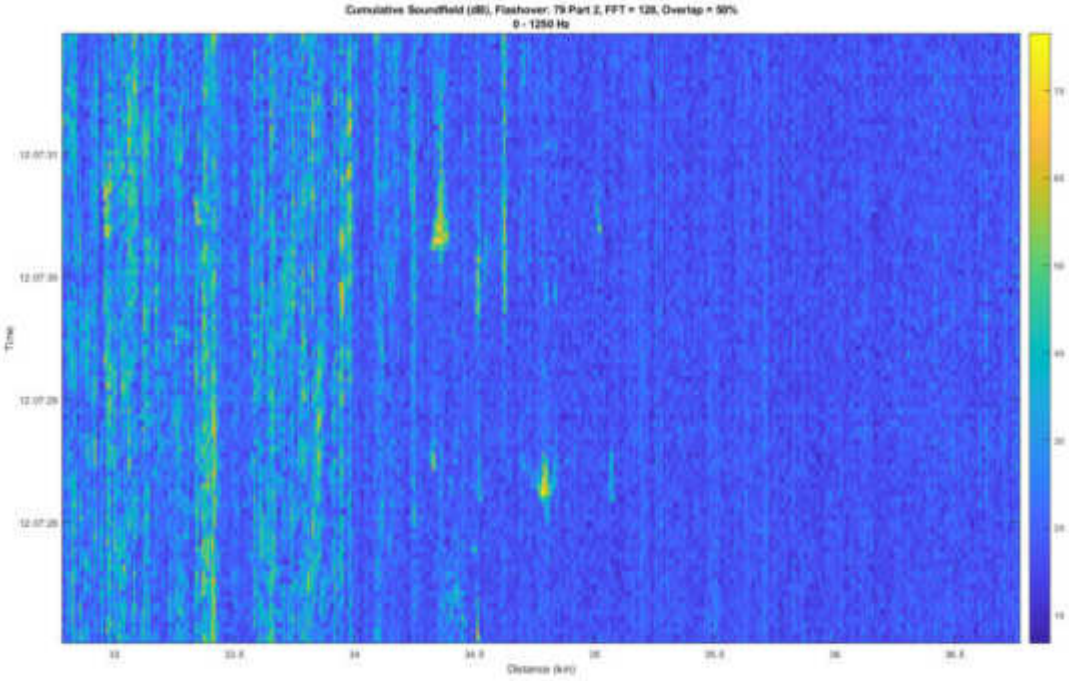

Abbildung 71: **Measurement 79, 0 - 1250 Hz. Optical distance = 24.75 km.**

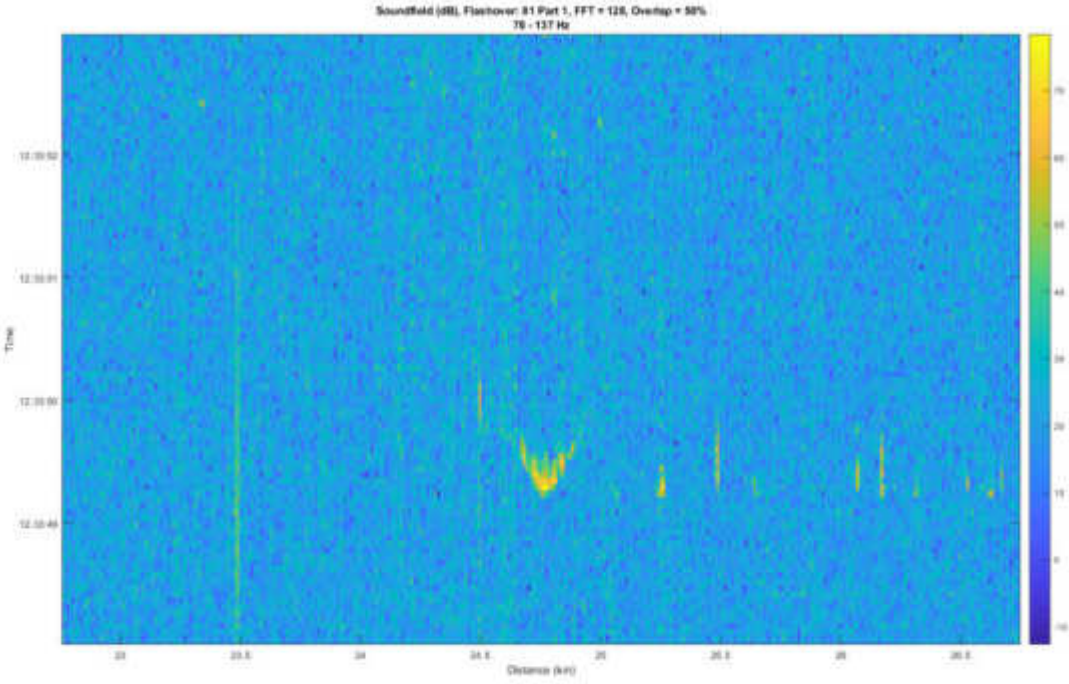

Abbildung 72: **Measurement 81, 78 - 137 Hz. Optical distance = 34.77 km.**

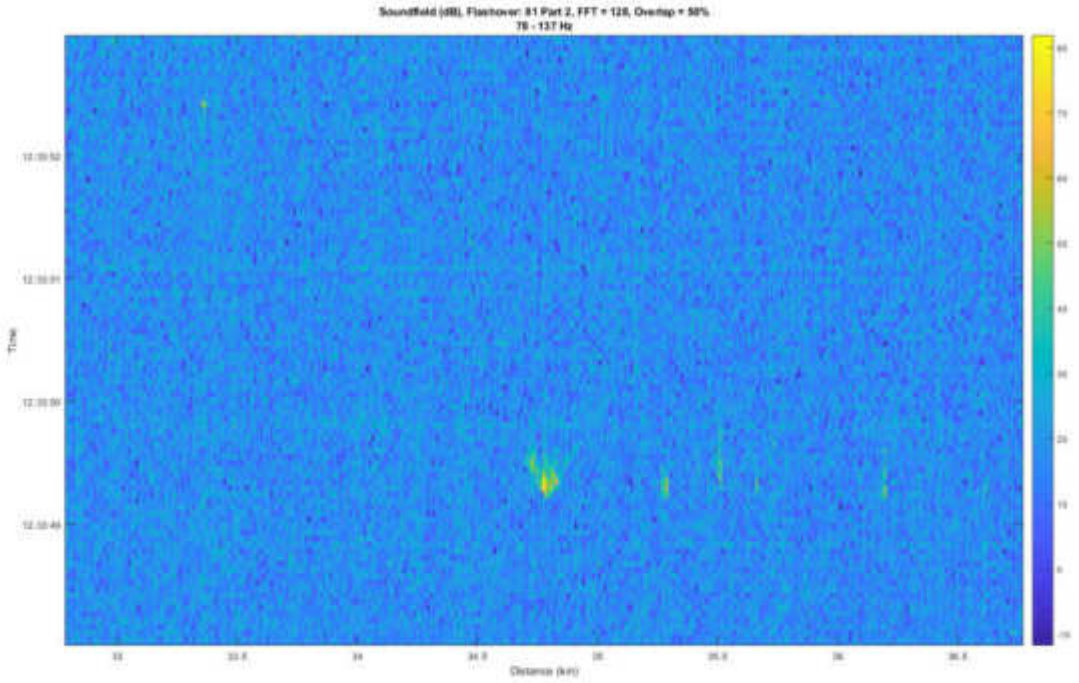

Abbildung 73: **Measurement 81, 78 - 137 Hz. Optical distance = 34.77 km.**

Identifying the channels at which the flashover occurs (i.e. ~ 20.95 km) and plotting these for both optical distances, the decrease in signal amplitude can be better visualized. Abbildung 74 shows the difference in the signal amplitude for measurement 81 at the frequency range 78 - 137.

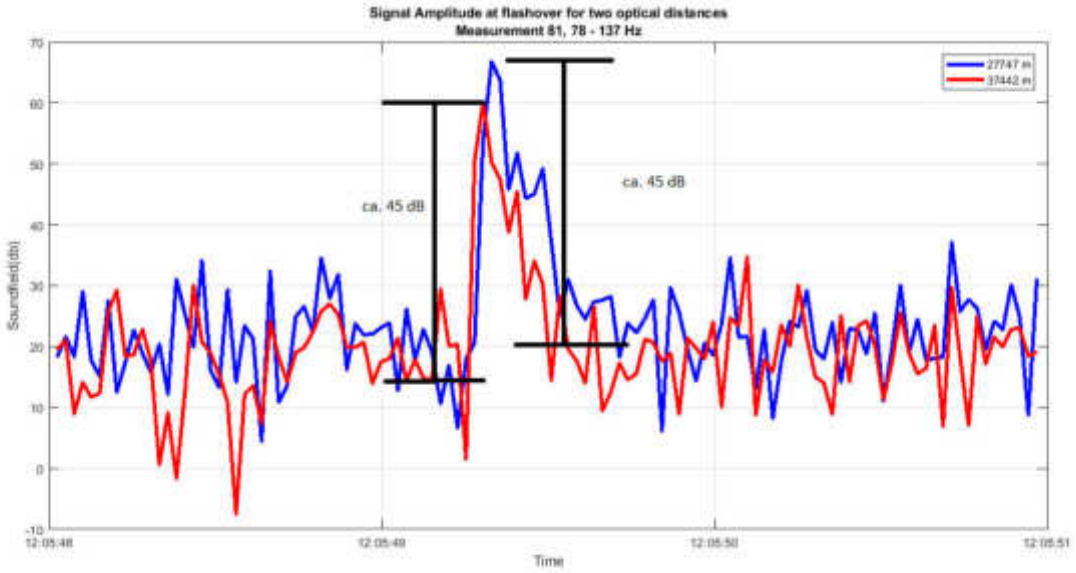

Abbildung 74: **Time evolution for Measurement 81 at two different optical distances.**

At both optical distances the difference in amplitude between the time of the flashover and the surrounding noise is about 45 dB. This stands in contrast to the findings in chapter 4, where there was a clear difference in dB between the optical distances. Further analysis has to be done on possible influences like ranges between the optical distances (~25 km in Riedau vs. ~10 km in St. Pölten) or locations. So there seems to be little difference between the two optical distances even though measurement 81 was visually categorised as class *large chevron* and class *small chevron* respectively. This could point to the fact that the visual classification should be done in a different way or that there should even be a completely different approach to classify the flashover data.

Unexpected signal sources

Just like in the 1st interim report, signal sources from other locations than the flashovers can be seen. For more information refer to chapter 4.

Spectrogram

As well as investigating the general frequency content of the signals using octaves, it is possible to plot the frequency content per FFT time step and generate what is known as a spectrogram. This has been done for one example data file, Measurement 24, see Abbildung 76. Two separate locations have been chosen from this file for analysis and are indicated with letters in Abbildung 75: the flashover location at 27.1 km (a), and one of the nine points

between 25 and 26.4 km (b). For each location and time interval the frequency spectrum is calculated and plotted as shown in Abbildung 76 for position (a) and Abbildung 77 for position (b).

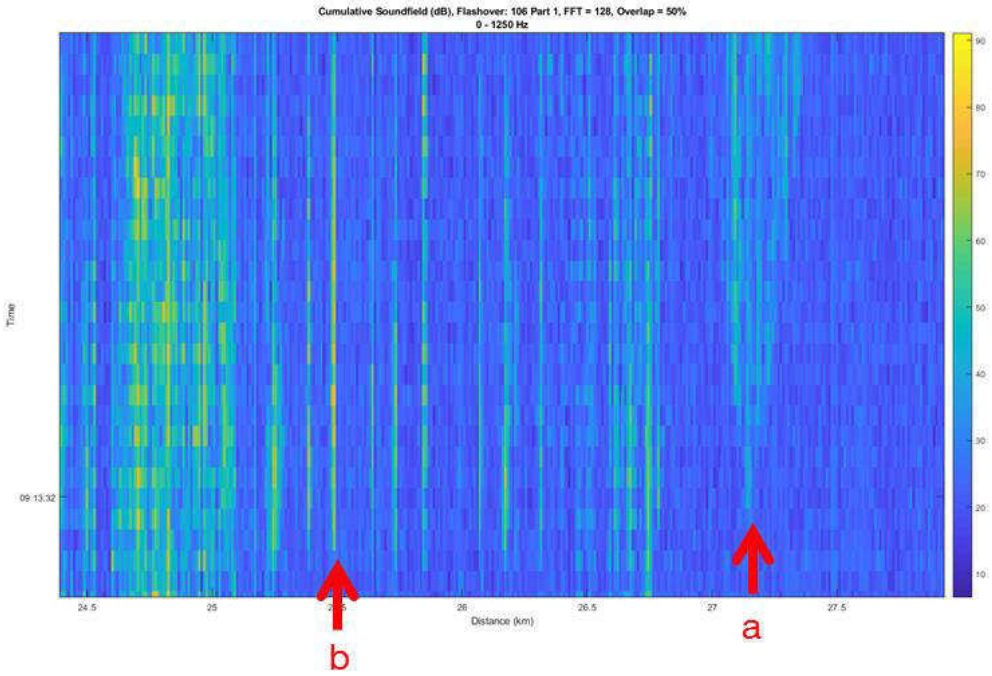

Abbildung 75: Cumulative soundfield for all frequencies showing excitation at kilometre 25 to 26.4. Point b, at 25.5 km, was chosen as a reference. The signals occurred ca. 50 ms BEFORE the flashover at 27.1 km (a).

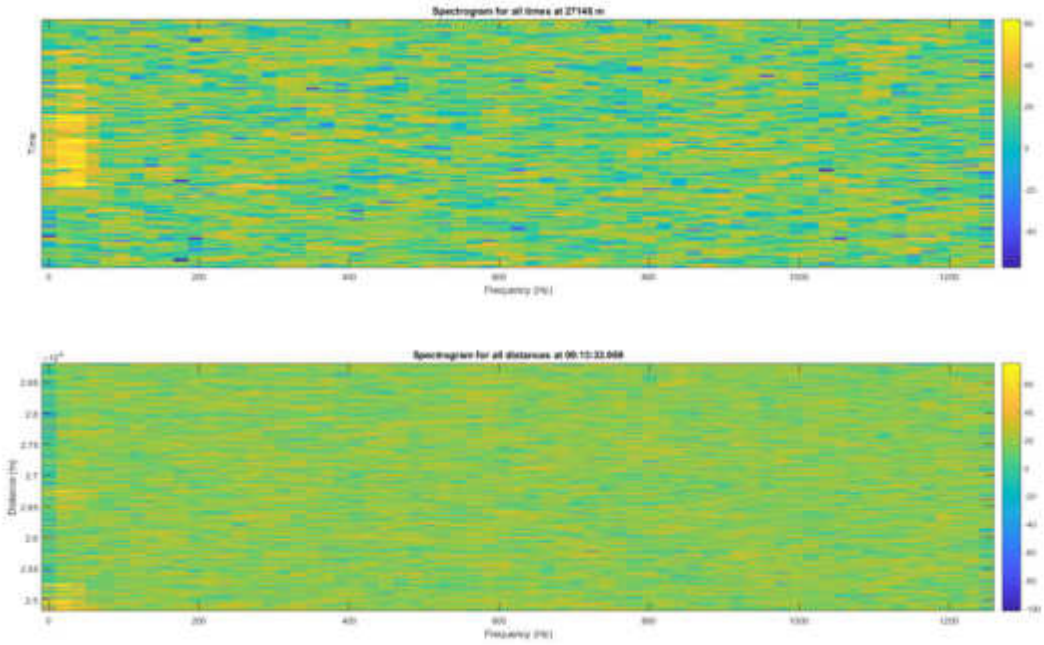

Abbildung 76: **The upper plot shows the spectrogram of the time evolution at the flashover location (a). It can be seen that at the time of the event (at about 11:13), the lower part of the detection bandwidth has been excited. The lower plot shows the spectrogram of the distance evolution at the time of the flashover.**

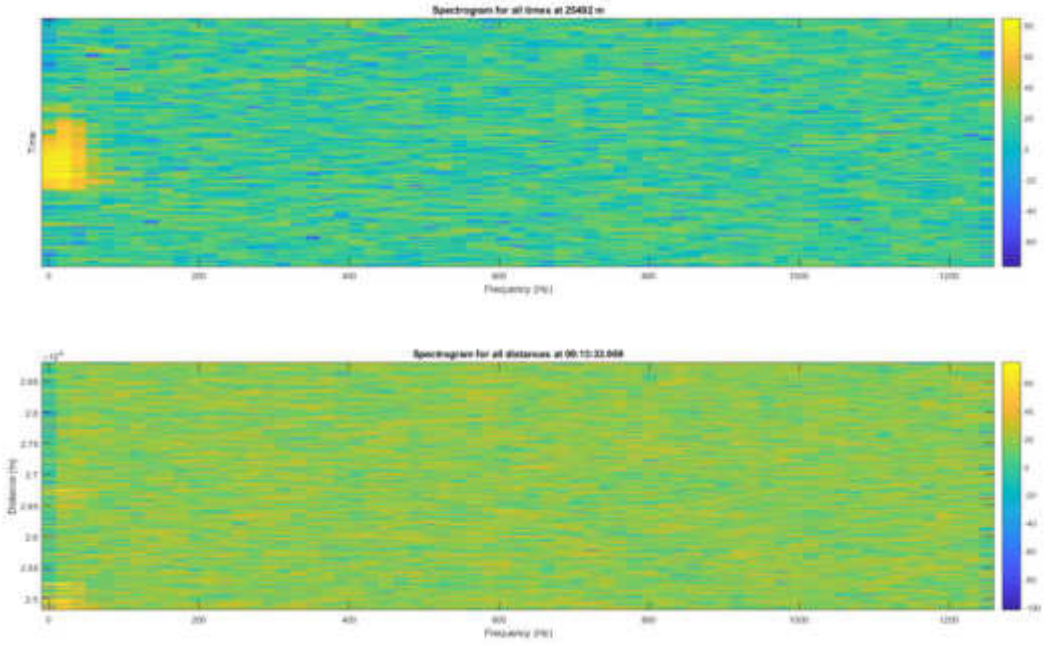

Abbildung 77: The upper plot shows the spectrogram of the time evolution at location (b). Only the low frequencies have been excited by the flashover. The lower plot shows the spectrogram of the distance evolution at the time of the flashover.

Current – Voltage

Despite the fact that at the experiment in Allerding the circuit breaker tripped after a complete cycle for some short circuits, this did not happen in St. Pölten. The short circuits were all of the single pulse type as seen in Abbildung 78.

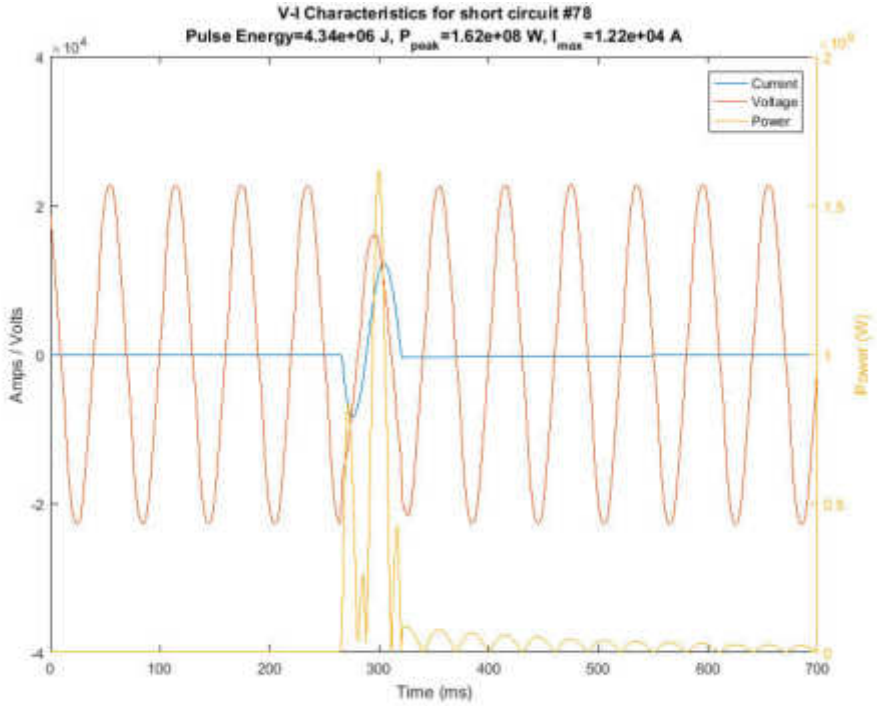

Abbildung 78: **Typical single pulse current, voltage and power evolution during a flashover.**

In Abbildung 78 the power is calculated simply from the instantaneous current and voltage values at any period in time. The flashover energy content can then be calculated from the integral of the pulse power over the duration of the pulse and is included in the title of the figure.

Calculating and plotting the peak power achieved during the flashover and the pulse energy for all events we attain Abbildung 79. This shows a near linear response of the pulse energy with respect to the peak power, which is to be expected as a higher peak power should lead to a linear increase in the pulse energy, assuming the pulse form and width remain approximately unchanged.

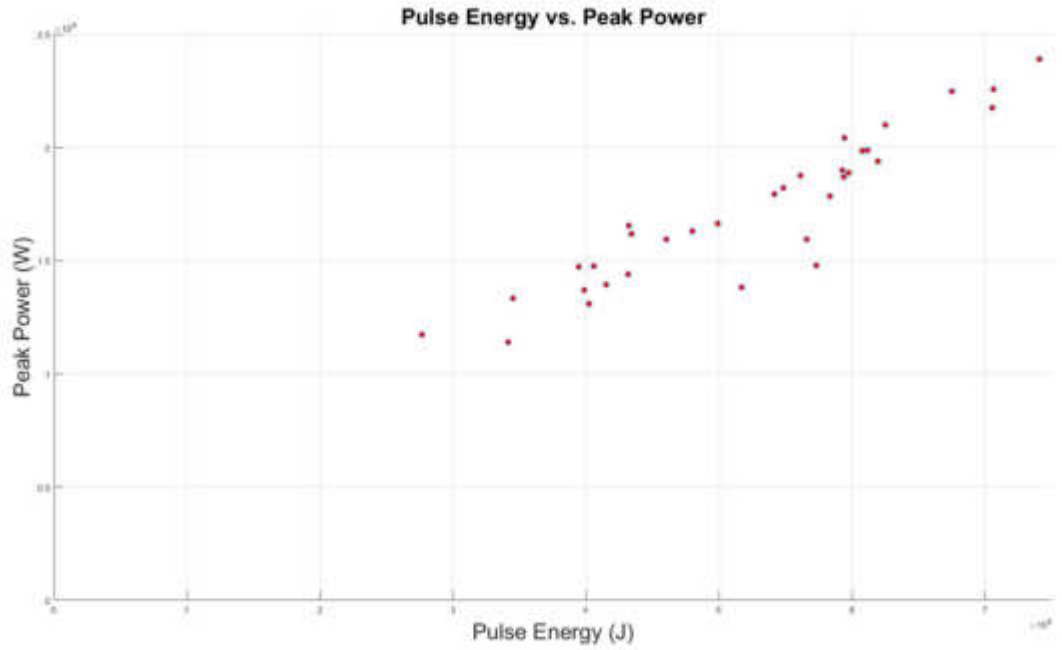

Abbildung 79: Peak Power vs. Pulse Energy for all measurements in St. Pölten.

Accelerometer

In contrast to the accelerometer data that was possible to derive from the experiments in Allerding, none of the recorded data in St. Pölten have any usable results to show for. Abbildung 80 shows the record of measurement #106. The short circuit occurred around 11:13 but the accelerometer clearly did not record any movement one minute before and after the event.

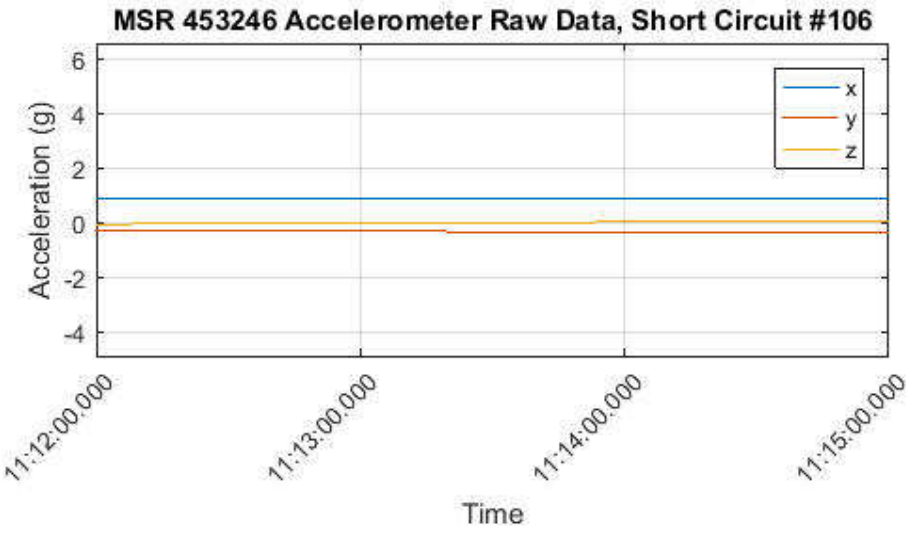

Abbildung 80: **A typical time series plot of all 3 axes, in this case for measurement 106.**

Even though no movement was recorded, the accelerometer was clearly working. Abbildung 81 shows forces around 100 g at the time the accelerometer was knocked three times for a controlled time offset. The reason why the accelerometer did not start recording us unclear.

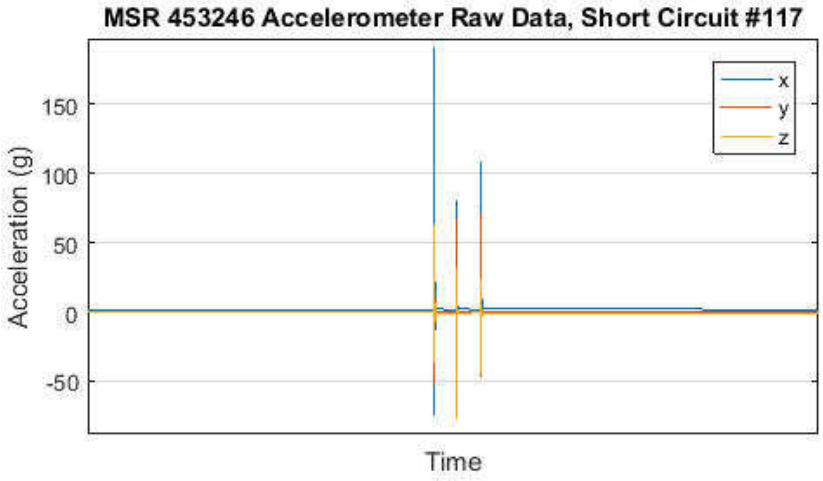

Abbildung 81: Controlled knocks of accelerometer.

5.6 Next Steps

- Complete analysis for all measurements with varying short circuit wire length.
- Create a cross correlation matrix for all recorded parameters particularly noting any correlations to the visual classification.
- Investigate in particular the correlation between the distance between the flashover and the optical fibre.
- Comparison of energy, mast type, short circuit wire length, visual classification and potential other important parameters between Allerding and St. Pölten.
- Optimise pre-processing to maximize signal to noise ratio, possibly incorporating wavelet analysis due to the impulsive nature of the events (Optional).

5.7 Conclusions

In addition to short circuits, or flashovers, between the high voltage catenary and ground, a number of pranger shots were induced at several locations on a section of the Güterzugumfahrung in St. Pölten. Several parameters affecting the creation, propagation or detection of the event were recorded. Several different measurements were taken during the

flashovers including DAS, physical movement of the mast at the flashover location and the electrical surge pulse characteristics.

The vast majority of the flashovers could be visually observed from the DAS data after a number of simple pre-processing steps. In some cases a clear chevron identified the time and location of the flashover while in others no distinct signal unique to the event could be observed. A clear correlation between energy content of the electrical pulse and visibility in the DAS signal was seen with higher energy flashovers creating highly distinct and visible chevron patterns.

By using two separate optical fibres connected to the same DAS measurement system the same event could be simultaneously recorded at two different optical distances. It was found from the limited analysis to date that an optical distance difference of approximately 10 km reduced the visual classification of the second fibre, but contrary to Allerding does not result in a worse signal to noise ratio.

For less energetic events no distinguishable signal at the flashover location with the current signal processing could be observed.

Similar to Allerding, acoustic excitation could not only be measured at the location of the flashover but also simultaneously at a number of other locations for nearly all of the induced flashovers. These acoustic sources were identified as being linked to particular equipment placed alongside the track. Signals could be observed emanating from masts, switchgears and parallel cable feeds and are particular to this installation, however it is to be expected that on all electrified routes similar equipment will be present. Such signals ease the detection of a flashover but complicate the localization in the cases where no distinct chevron is visible.

In conclusion, the measurement campaign has been successful in inducing and recording a large number of distinctly different flashovers.

6 BESCHREIBUNG DRITTE VERSUCHSREIHE – ALLERDING

6.1 Introduction

This document provides interim results on experiments carried out in cooperation with ÖBB to assess the performance of a Frauscher Tracking Solutions (FTS) system using Distributed Acoustic Sensing (DAS) on the detection and location of a catenary flashover. The experiments were conducted in Allerding, Austria, at three locations in March 2018. In total, 54 strikes with a sledgehammer against the catenary support masts as well as 33 pranger shots with gun

powder were recorded during the trial. This work is currently ongoing with the results to date being summarised in this document.

Catenary flashovers are electrical short circuits between the high voltage (15 kV) catenary and ground typically causing an electrical spark and associated acoustic bang. These can occur for a number of reasons: faults within the locomotive, driver error, wildlife or natural occurrences such as a branch falling off a nearby tree, to name but a few. Circuit breakers in the respective substation cut the supply within a few milliseconds but in order to be able to reapply the electrical supply and resume operation, the cause of the flashover must be found and repaired if required. In certain cases, the exact position of the flashover is not known and a considerable amount of time and effort is required to locate it. It is hoped FTS and DAS technology can help determine the source of a flashover event to within a few tens of metres which would be a vast improvement over the current accuracy. DAS operates by injecting pulses of laser light into an optical fibre which typical lies parallel to, and a few meters from, the railway track in a cable duct. Any acoustic disturbance of the fibre is detected and converted to an electrical signal which can be analysed using digital signal processing techniques. It is the acoustic bang caused by the flashover together with any induced mechanical vibrations which can be measured using DAS.

The technical goal of this research is to determine the physical parameters which influence the creation, propagation and detectability of such flashovers and to quantify these thereby allowing limits on the usability of DAS technology to be determined. A small number of the numerous influencing parameters which can affect the signal strength detected at the optical fibre have been isolated for investigation in these initial experiments.

Measurement Time and Locations

The strikes and shots were conducted at three different catenary support masts in Allerding on the 30th March 2018. Detailed information on the masts where the trials were done is shown in Tabelle 9.

Mastnumber	Position (ÖBB km)	Distance between pranger shot and fibre (cm)
M 45/27	45.828	1144
M 47/13	47.434	1202
M 45/26	45.763	1925

Tabelle 9: Mast details of where flashovers were induced.

6.2 Experimental Setup

Accelerometer

To assess the physical movement of the mast during and after the knock with the sledgehammer, an accelerometer of type MSR-165, see Abbildung 82, was mounted to the mast. This allowed acceleration in three mutually perpendicular axes at a maximum sample rate of 1600 Hz to be recorded. The sensor was physically mounted to the mast and was manually triggered to record by one of the persons present at the trial. Abbildung 83 shows how the sledgehammer and the accelerometer were mounted to the mast.

Abbildung 82: MSR-165 accelerometer. Dimensions are 39 x 23 x 72 mm.

Abbildung 83: Sledgehammer and MSR-165 accelerometer mounted to the mast.

DAS

The DAS measurement system is housed in a small service hut at km 60.656 directly beside the track and is built up of several constituent parts, see Abbildung 84. Up to two single mode optical fibres (Channel A and Channel B) with a maximum length of 40 km each can be connected to the optical unit. The optical unit generates and orchestrates the timing of the laser pulses and detects the reflected single from the fibres. The analogue signal is then fed to the processing unit which digitizes and saves the data (up to 600 MB/s) to the RAID. Additionally, it processes the data and forwards the results onto the display unit where it can be observed in real time via a web browser interface.

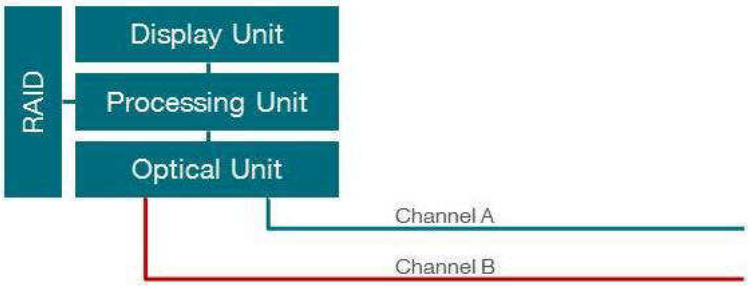

Abbildung 84: The component parts of the DAS measurement system.

For these experiments, only one single mode optical fibre was utilized for detection. A schematics for the measurement setup is shown in Abbildung 85. The laser operates at 1550 nm while the pulse repetition rate was 2500 Hz and remained unaltered throughout the experiments. The pulse width remained constant at 100 ns.

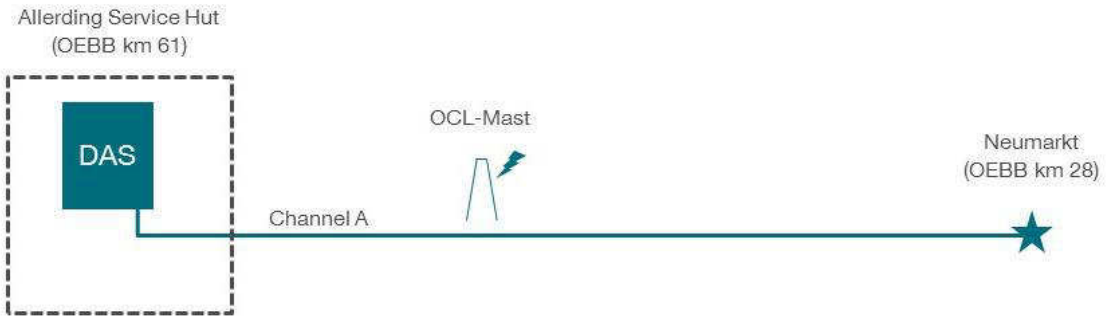

Abbildung 85: Schematic setup for the measurements on the 30th March 2018.

In addition to the fibre for the HSi system, a second one was utilised by a Theta unit (a prototype DAS system with a slightly different measurement method). The results of the Theta recordings are not discussed in this report.

6.3 Results

DAS

The sample rate of the raw DAS signal at each location is defined by the pulse repetition frequency of 2500 Hz. This limits the highest analysis frequency, or Nyquist frequency, to equal 1250 Hz. Some rudimentary signal processing steps are applied to each raw file to enhance

the signal to noise ratio. The first step was to remove spatial data channels corresponding to any spools of fibre along the route which can cause optical artefacts. Additionally, a high-pass filter and a spatial decimator were applied to detrend the data and improve signal to noise ratio, respectively. Thereafter the frequency content was calculated using a Fast Fourier Transform (FFT) to allow a simplistic analysis of the frequency content of the event. It is assumed that the majority of the signal energy resides in the lower part of the frequency spectrum and this allows an estimation of the noise. All signal processing was carried out using Matlab.

Octave Analysis

By dividing the energy content of the signal calculated from the FFT in to octaves, a crude frequency analysis can be conducted. For example, the upper octave contains energies in the range 625 – 1250 Hz; the next lower octave contains frequencies in the range 312.5 – 625 Hz, the next again in the range 156.25 – 312.5 Hz, etc. By plotting these energies calculated with an FFT length of 128 and an overlap of 50% we obtain Abbildung 86 to Abbildung 89. Each figure presents six octave plots from 1 second before to 2 seconds after the event occurred. A distance of 2 km either side of the event is observed.

It can be seen that the energy content within each octave differs substantially. Abbildung 89 shows a clear “V”, or chevron, as a result of the acoustic signal, or pressure wave, leaving the location of the shot and travelling in both directions along the fibre route. The chevron is clearly observable in the lower frequency spectrum and reduces in amplitude until it is not recognizable as a “V” in the range 313 – 605 Hz. The gradient of the “V” determines the speed of propagation and is experimentally found to be 340 m/s from the data. This matches the speed of sound in air very well (~343 m/s @ 20°C) and it can therefore be deduced with a high certainty that this signal results from the acoustic bang of the shot.

It can be seen in Abbildung 87 and Abbildung 89 that the events, both for the sledgehammer and the pranger shots, can be best observed in the lower frequency spectrum from 0 – 137 Hz.

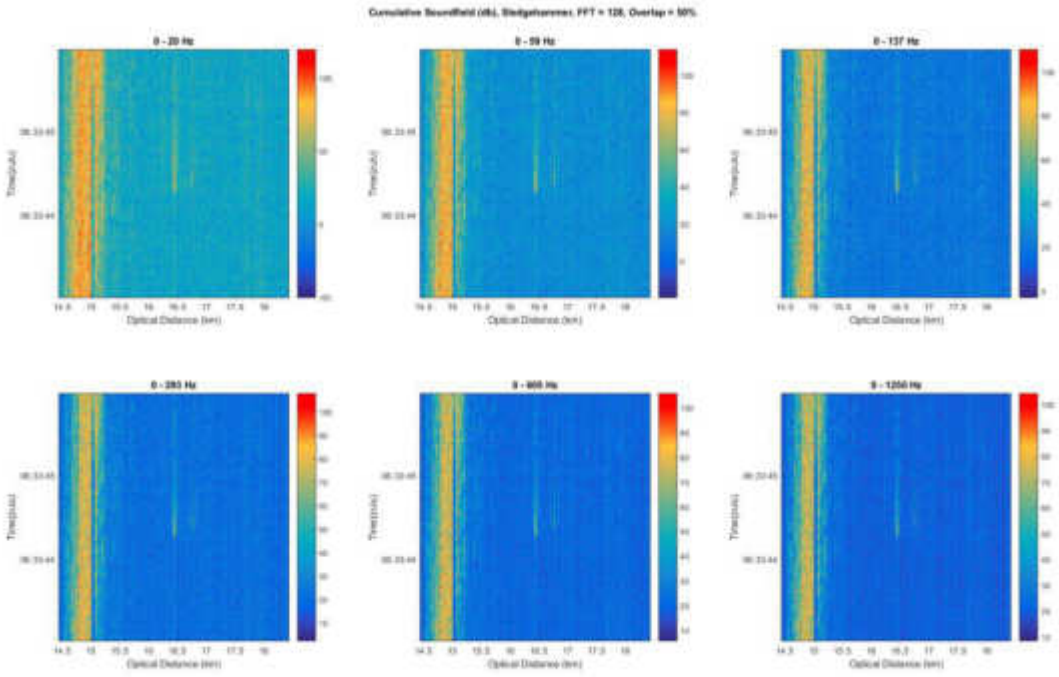

Abbildung 86: Cumulative octave plot of measurement 151.2, knocking the mast with a sledgehammer. The event occurs at 16.44 km shortly after 08:33:44.

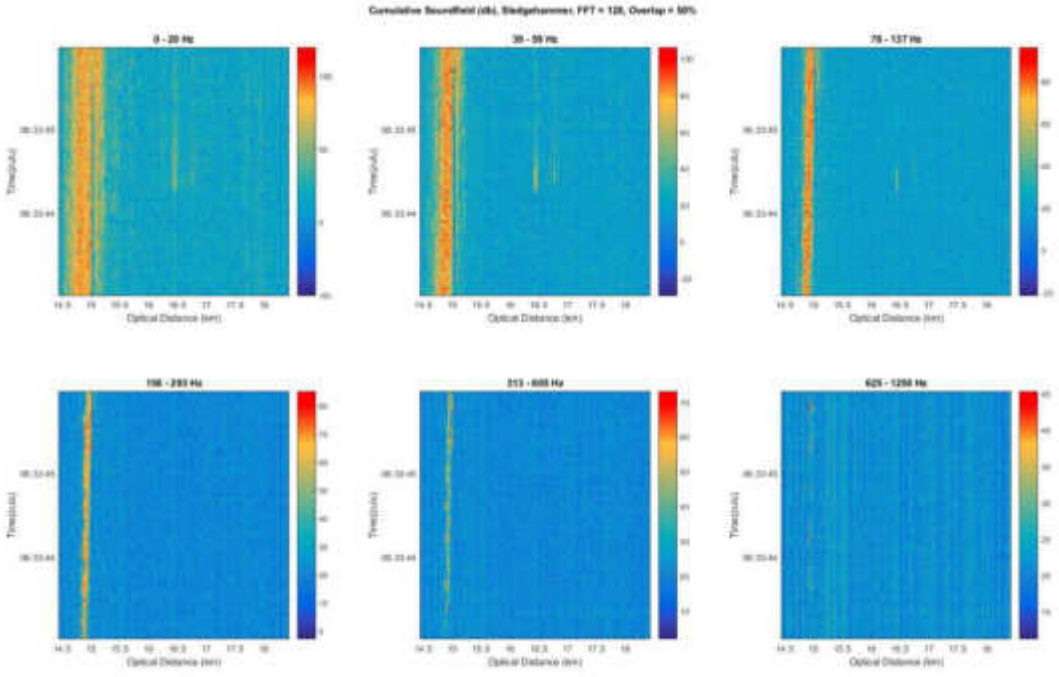

Abbildung 87: Octave plot of measurement 151.2, knocking the mast with a sledgehammer. The event occurs at 16.44 km shortly after 08:33:44.

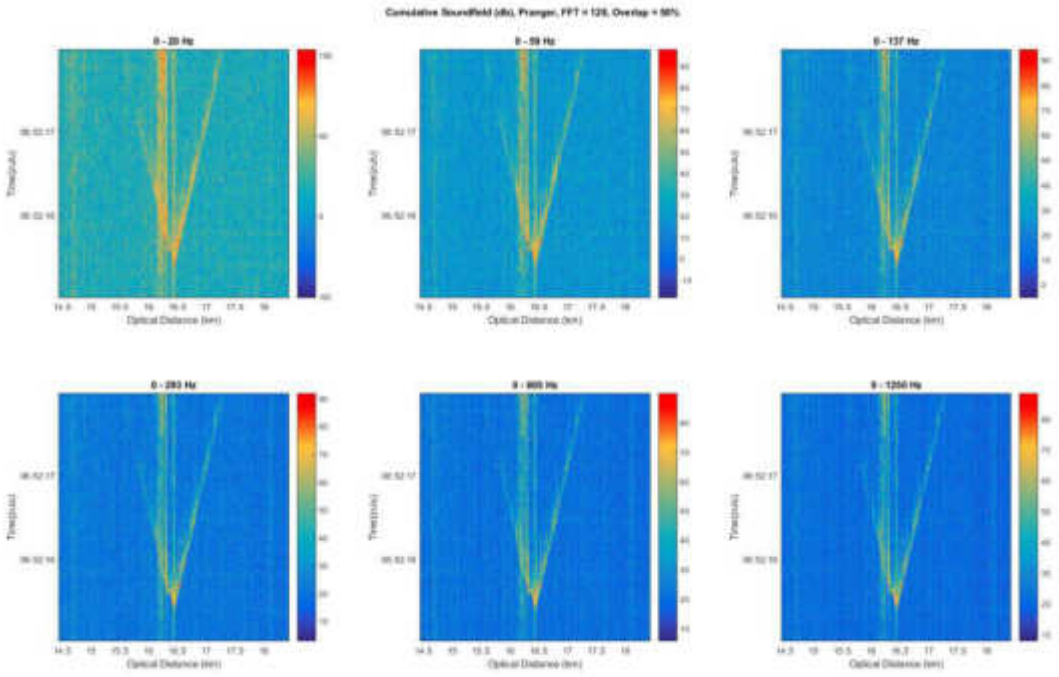

Abbildung 88: Cumulative octave plots for measurement 152, a pranger shot with 45g of gun powder.

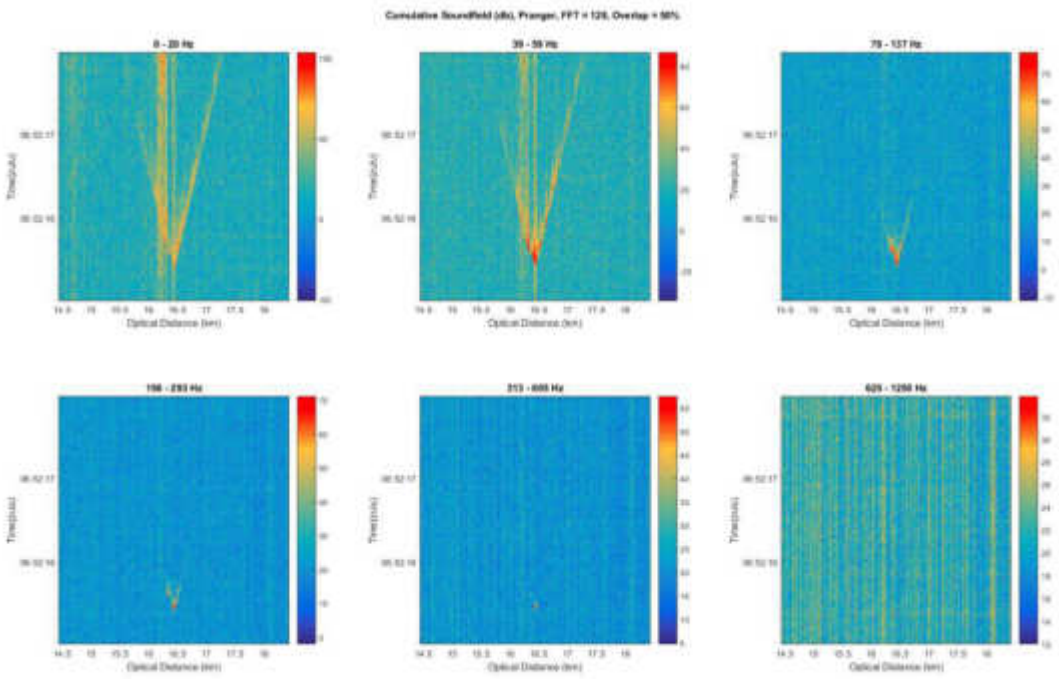

Abbildung 89: Octave plots for measurement 152, a pranger shot with 45g of gun powder.

Pranger shots and Sledgehammer

In contradiction to the first two trials in Allerding and St. Pölten, no self-induced flashovers, but only sledgehammer strikes and pranger shots were carried out in this trial. 33 shots were fired with a prangerstutzen (signal gun). Varying weights of gun powder (from 40 – 60 g) and compression (1- to 6-times) was used. The loud bang of the shots resulted in recorded data very similar to the induced flashovers that were recorded in Allerding and St. Pölten in previous measurement campaigns. Additionally 54 hits with a sledgehammer against the masts were carried out. 27 of them with a mounting device allowing similar impact energy for each strike. The other half was recorded while a person hammered against the mast with an undefined force.

Visual classification

The pre-processed DAS signal patterns can vary substantially from the case in which a chevron is clearly visible at the flashover location to producing no visible signal at all. Determining which of the many parameters affect this signal response is important in determining any limitations of a detection algorithm. A sensible assumption could be, for example, that those signals containing chevrons were produced by higher energy events. To assess this correlation the pre-processed data from each measurement is visually classified and placed in one of the following groups describing the flashover as:

having a large, clear chevron
having small chevron
being visible
being barely visible
being not visible

“Visible” was defined as being clearly able to see several locations of excitation which exactly coincide with the time of the flashover but with no other defining patterns. “Barely visible” is identical to “visible” but of less energy and a signal classified as being “not visible” contained no signal that could be visually detected with the current pre-processing steps. This is not to say that with another analysis methodology an improved digital signal processing routine could not extract more useful signal. However, at the beginning of the project it was decided to concentrate on classifying the various measurements and their dependent parameters and not

focus on extracting the very last signal from the data. All of the pranger shots show a large chevron that is easy to detect in the plots and are therefore categorised into group 1. The impact of the hammer connecting with the mast can be seen in all the recordings, but looking at signal results, the signal does not look like a chevron that was created by a pranger shot or flashover.

In order to assess potential differences in the recorded signal by how the sound and pressure wave of the shot travel until they excite the fibre, the shots were fired in different directions relative to the track. Every shot was repeatedly fired in the direction of Passau, normal to the track and in the direction of Wels. Abbildung 90 shows this from left to right. It can be seen that the signal travels further along the fibre and excites the fibre to a greater extent in the corresponding direction the shot was fired. A near symmetrical excitation of the shot fired normal to the track is clearly evident in the central plot. The shape of the chevron is independent from the firing direction.

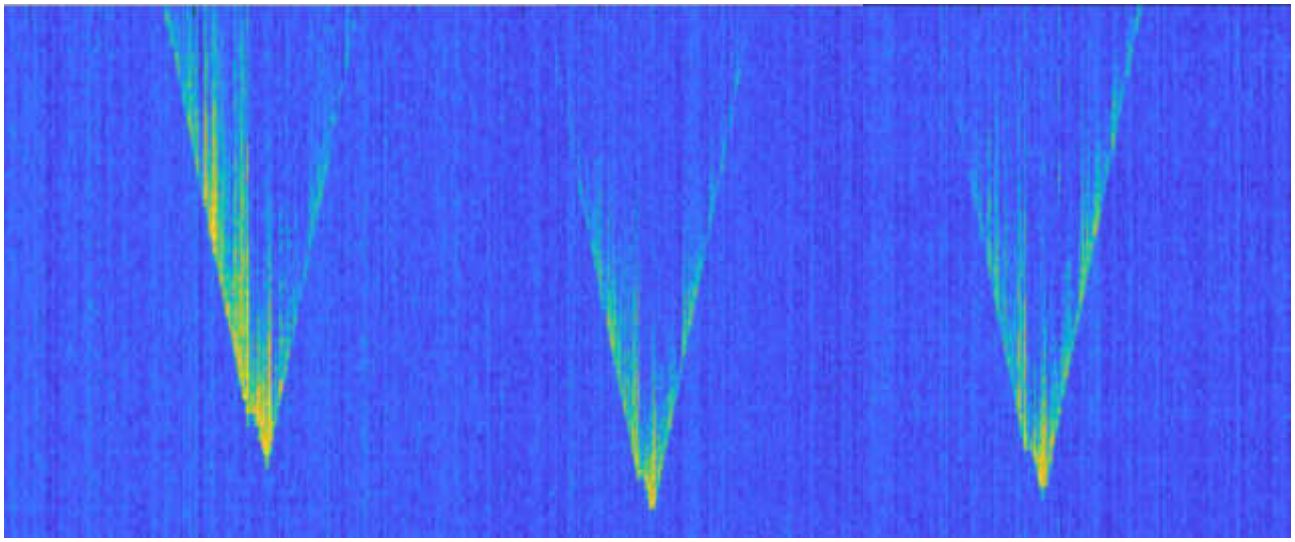

Abbildung 90: The signal of a shot (45 g gun powder) in the direction of Passau (left), normal to the track (centre) and Wels (right) at the location of mast M45/27.

Accelerometer

A typical time series plot of a hit with the sledgehammer is shown in Abbildung 91 and Abbildung 92. This data was taken for measurement 146.1 (named this way as recording 146 contains the first three hits) on mast M45/27. The accelerometer was mounted at a height of approximately 8.75 m above ground and saturated at approximately 15g.

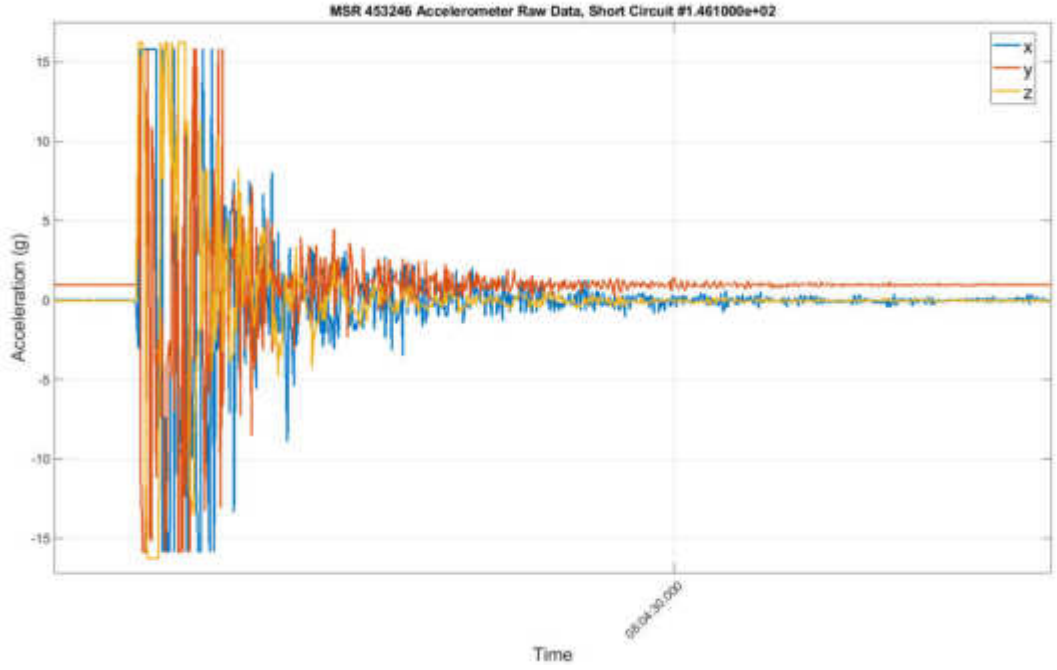

Abbildung 91: A typical time series plot of all three axes, in this case for measurement 146.1.

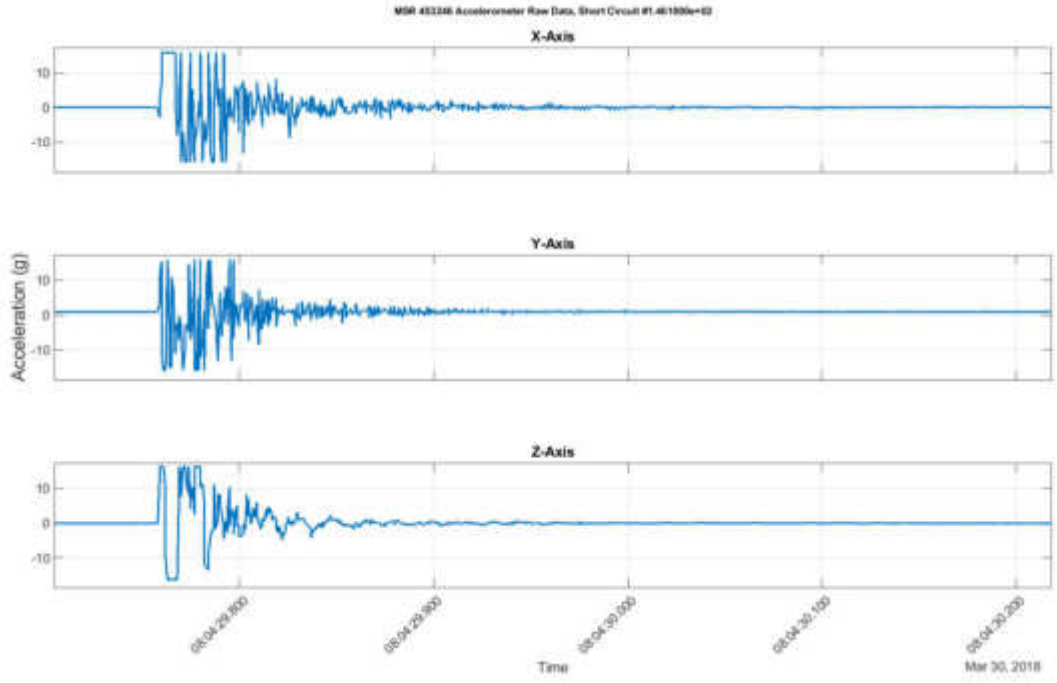

Abbildung 92: A typical time series plot of all three axes, in this case for measurement 146.1. The x-axis is horizontally normal, the y-axis vertically normal and the z-axis parallel to the track, as shown in Abbildung 83: Sledgehammer and MSR-165 accelerometer mounted to the mast.

By applying an FFT over the entire signal we obtain Abbildung 92 which averages the frequency content of the event over the entire measurement time. This is not the optimal

analysis due to the hit being impulsive in nature. Abbildung 93 shows an improvement over the FFT by calculating a spectrogram which investigates smaller sections of data from the signal to better isolate the event in time. From Abbildung 93 it is evident that at the time of impact there is energy within all frequency bands. This reinforces the fact that this event is impulsive. It can also be observed that the reverberations are most prominent on the x- and y-axis.

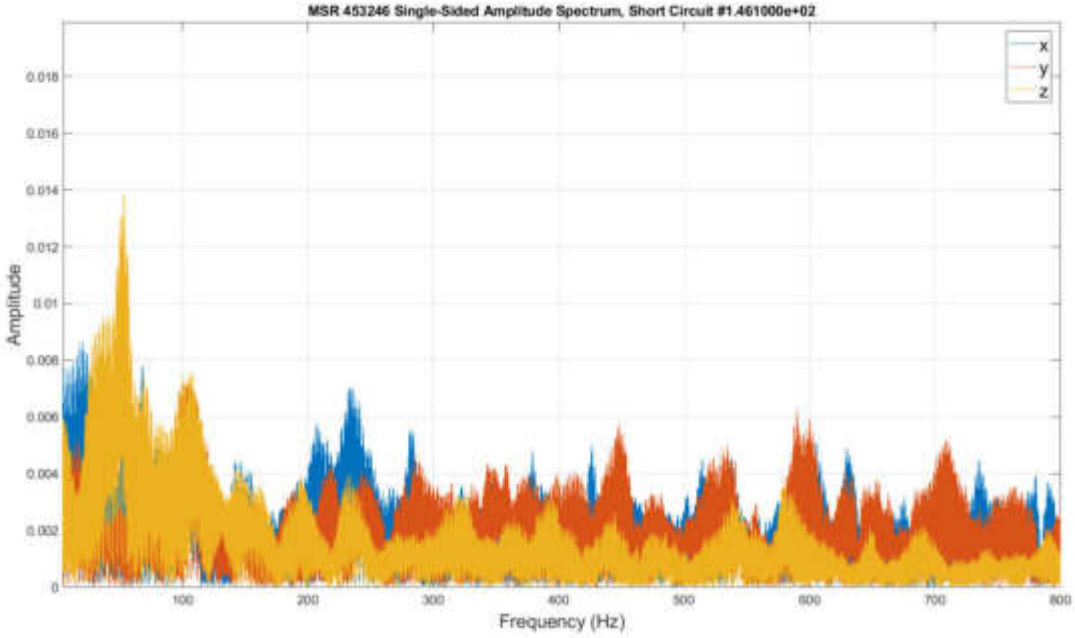

Abbildung 93: FFT analysis of measurement 146.1. The entire signal is used to calculate the frequency content.

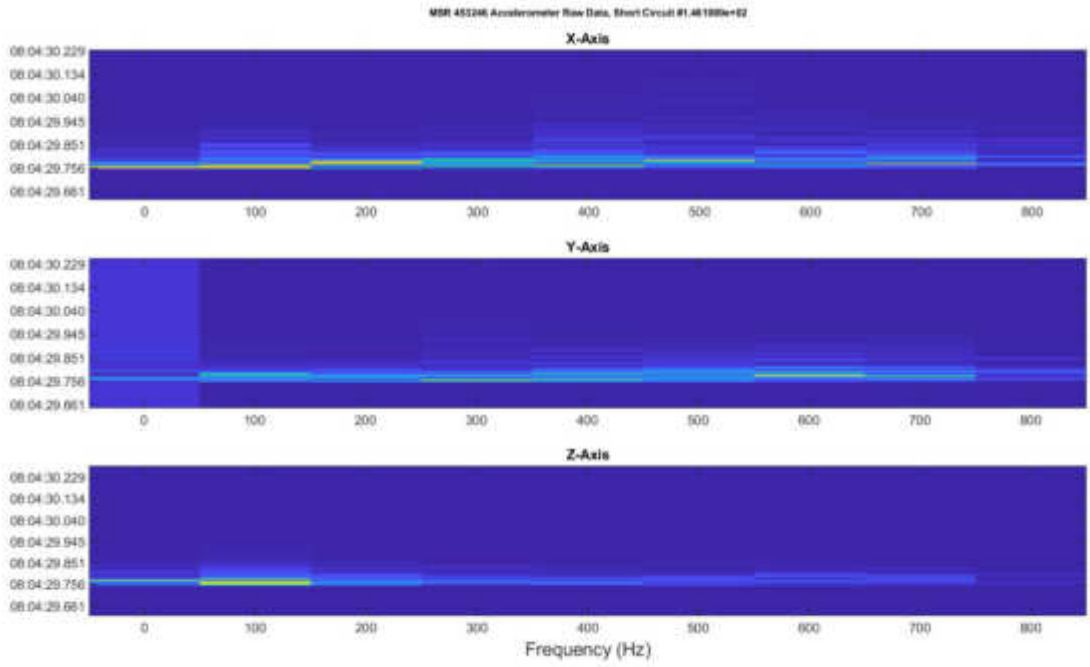

Abbildung 94: Spectrogram of measurement 146.1 with FFT length of 16 and an overlap of 50%. Blue indicates low signal while yellow indicates high signal. Time increases upwards.

6.4 Conclusions

In addition to short circuits, or flashovers, between the high voltage catenary and ground from previous experiments, a number of pranger shots and sledgehammer impacts have been induced at several locations on a section of main line railway in Austria between Schärding and Wels. Several parameters affecting the creation, propagation or detection of the event were recorded. Several different measurements were taken during the shots and strikes including DAS and the physical movement of the mast that was struck by the hammer.

All of the shots and strikes could be seen in the DAS data after a number of simple pre-processing steps. In the case of the pranger shots a clear chevron could be identified at the time and location of the event similar to the self-induced flashovers from the previously conducted experiments. The sledgehammer knocks were all observable in the data, but do not emit the typical chevron of pranger shots and flashovers, as expected.

In conclusion, the measurement campaign has been successful in recording a large number of pranger shots which can also be used for training the existing model for automatically finding flashovers.

7 BESCHREIBUNG VIERTE VERSUCHSREIHE – TESTAUFBAU FRAUSCHER

7.1 Introduction

This document provides interim results on experiments carried out in cooperation with ÖBB to assess the performance of a Frauscher Tracking Solutions (FTS) system using Distributed Acoustic Sensing (DAS) on the detection and location of a catenary flashover.

Catenary flashovers are electrical short circuits between the high voltage (15 kV) catenary and ground typically causing an electrical spark and associated acoustic bang. These can occur for a number of reasons: faults within the locomotive, driver error, wildlife or natural occurrences such as a branch falling off a nearby tree, to name but a few. Circuit breakers in the respective substation cut the supply within a few milliseconds but in order to be able to reapply the electrical supply and resume operation, the cause of the flashover must be found and repaired if required. In certain cases, the exact position of the flashover is not known and a considerable amount of time and effort is required to locate it. It is hoped FTS and DAS technology can help determine the source of a flashover event to within a few tens of metres which would be a vast improvement over the current accuracy. DAS operates by injecting pulses of laser light into an optical fibre which typical lies parallel to, and a few meters from, the railway track in a cable duct. Any acoustic disturbance of the fibre is detected and converted to an electrical signal which can be analysed using digital signal processing techniques. It is the acoustic bang caused by the flashover together with any induced mechanical vibrations which can be measured using DAS.

After a successful trial in October and November 2016 in Allerding, a second trial has been conducted on the Güterzugumfahrung in St. Pölten in May 2017. Even though most of the self-induced flashovers and pranger shots were visible on the FTS system, their markedness was reduced in St. Pölten compared to Allerding. After inspection of the troughs, it was found that a mat of compressed rubber granulate was present between asphalt and trough. Therefore two different trough installations exist in Allerding and St. Pölten: the troughs in Allerding are buried with no mats while the troughs in St. Pölten are not buried but stand on mats, as can be seen in Abbildung 95.

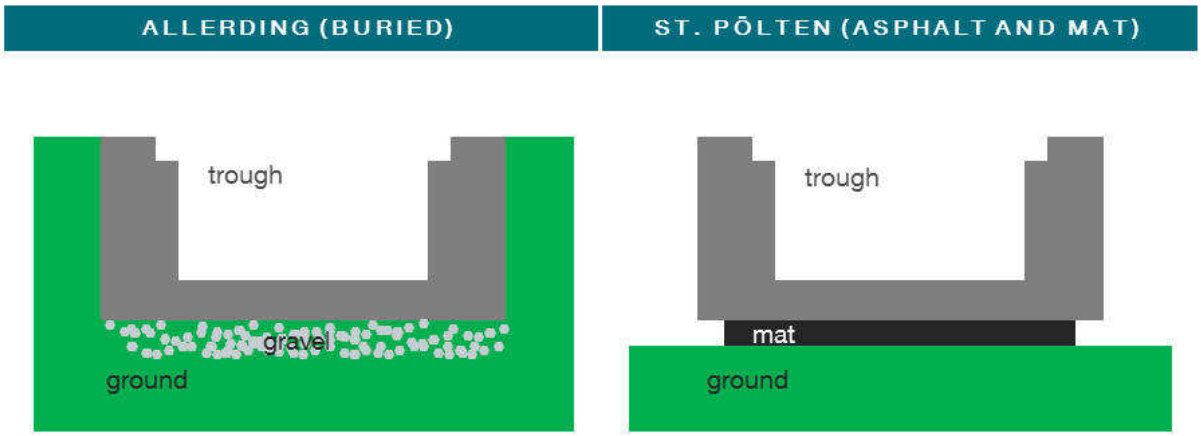

Abbildung 95: Difference in trough installation between Allerding (left) and St. Pölten (right).

In order to assess the dampening effects of this mat, which may lead to the smaller signal amplitudes, an experimental trial was planned. The experiments were conducted within the Frauscher company grounds, Austria, in April 2018. In total, 76 files were recorded during the trial. 66 files contain information on drop tests with a kettlebell, the remaining 10 are recordings of a signal horn, drops of a bolt and walking on the troughs.

The goal of this experiment was to support or reject the hypothesis that was formed after the second flashover trials at St. Pölten in March 2017, namely that rubber granulate mats between the ground and the troughs attenuate the recorded signal more than buried troughs, making it more difficult to locate a specific event.

7.2 Experimental Setup

To assess the potential difference in the setups, the experiment was planned in a way that the same event was recordable for both the buried trough (Allerding) and the trough on the rubber matting on asphalt (St. Pölten). Abbildung 96 shows this setup. The buried troughs (left in the figure) sit on a gravel bed at such a depth that the top edge is level with the ground. The asphalt troughs (right in the figure) sit on four rubber granule mats as seen inAbbildung 98. The lower red circle in the figure shows a polystyrene plates affixed with polyurethane (PU) foam to the open ends of the troughing. This was to dampen the signal reaching the fibre through the open ends of the troughing, thereby simulating a longer , continuous section as found in practice. The upper red circle shows a fibre spool of 33 metres, which was used to differentiate the troughs in the recordings. This was placed as far away as practicably possible from the kettlebell's point of impact so as not to be excited by the simulated acoustic events.. In retrospective, an even longer spool distance would have been better in easing the signal

differentiation. The acoustic event is produced approximately in the middle of the two trough setups (at the point in Abbildung 96 where the kettlebell is lying on the ground). Four troughs were provided by ÖBB consisting of two different sizes (named as size 3 and 4 by ÖBB). Normally, troughs of the same size would be incorporated beside the track, but as only these four were at hand, a combination of size 3 and size 4 was used for both “tracks”. By using the combination of sizes for both setups, identical conditions are given. Hence making it possible to compare the signals and state a conclusion even though different trough sizes could also affect the signal. At the time of testing, the troughs were closed with the provided lid. Abbildung 99 shows the dimensions of the trough types.

Abbildung 96: Setup for the measurement on April 24th 2018.

Abbildung 97: A 20 kg heavy kettlebell used for the droptests.

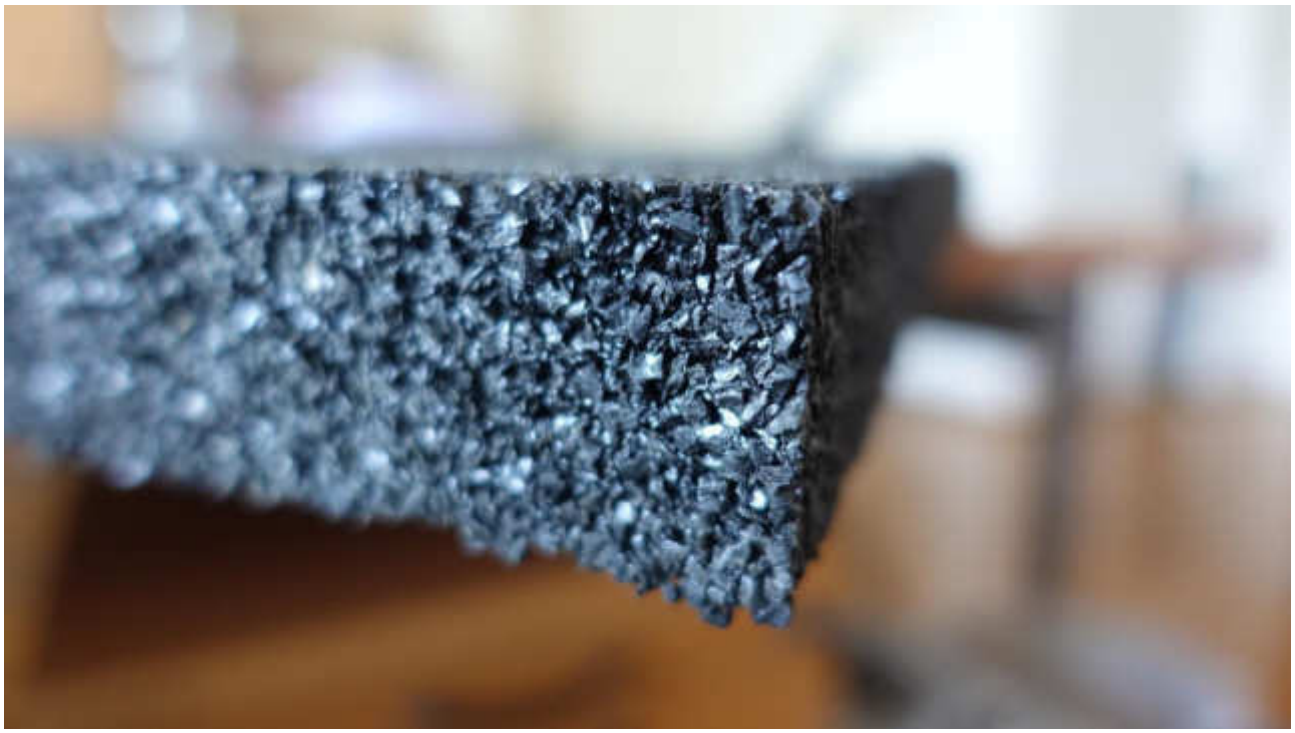

Abbildung 98: The troughs sit on these granule mats. Their specifications are 3 cm height x 20 cm width x 72.5 cm length for S4 troughs and 3 cm height x 20 cm width x 59.5 cm length for S3.

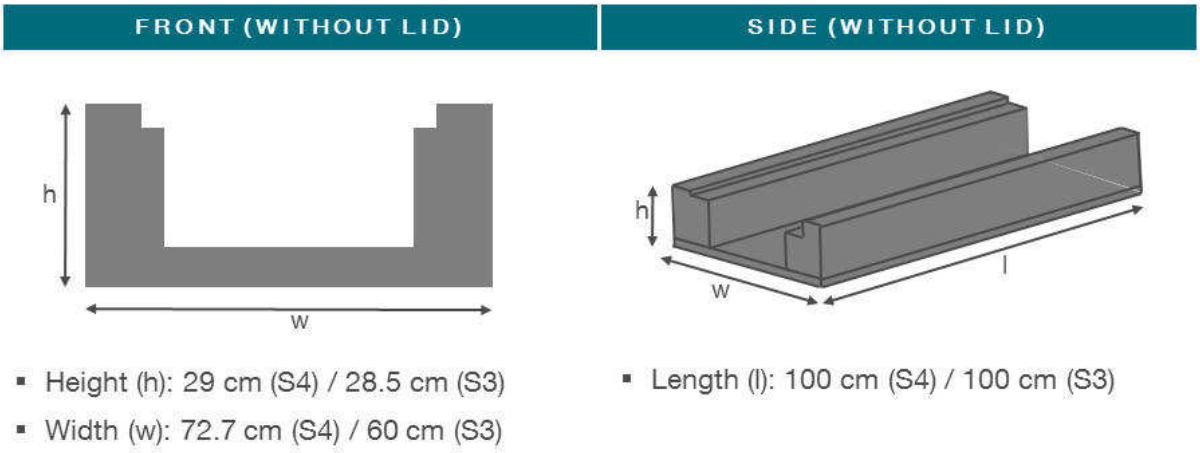

Abbildung 99: Measurements of troughs of size 4 (S4) and 3 (S3).

DAS

The DAS measurement system was housed in the laboratory in Frauscher's Innovation Centre and is built up of several constituent parts, see Abbildung 100. Up to two single mode optical fibres (Channel A and Channel B) with a maximum length of 40 km each can be connected to the optical unit. The optical unit generates and orchestrates the timing of the laser pulses and detects the reflected single from the fibres. The analogue signal is then fed to the processing unit which digitizes and saves the data (up to 600 MB/s) to the RAID. Additionally, it processes the data and forwards the results onto the display unit where it can be observed in real time via a web browser interface.

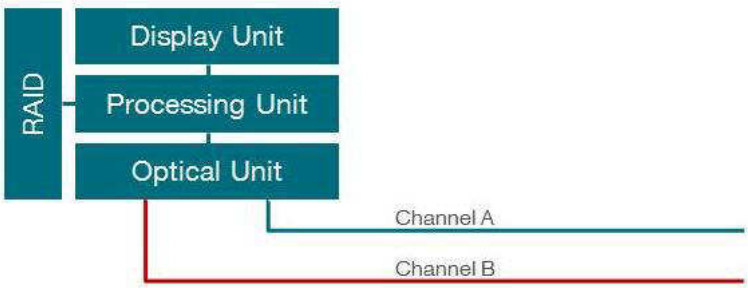

Abbildung 100: The component parts of the DAS measurement system.

For these experiments, one single mode optical fibre was utilized for detection. A schematics for the measurement setup is shown in Abbildung 101. In total, the fibre used is approximately 12.5 km long. A 10 km spool leads from the DAS system to the first troughs on the asphalt into which 33 m of fibre were coiled . After a small spool of 33 m, which served to separate the troughs' signals, another 33 m of fibre was placed inside the trough buried in the ground. The

fibre is terminated 2 km after exiting the second trough. The laser operates at 1550 nm while the pulse repetition rate was 2500 Hz and remained unaltered throughout the experiments. The pulse width was constant at 100 ns.

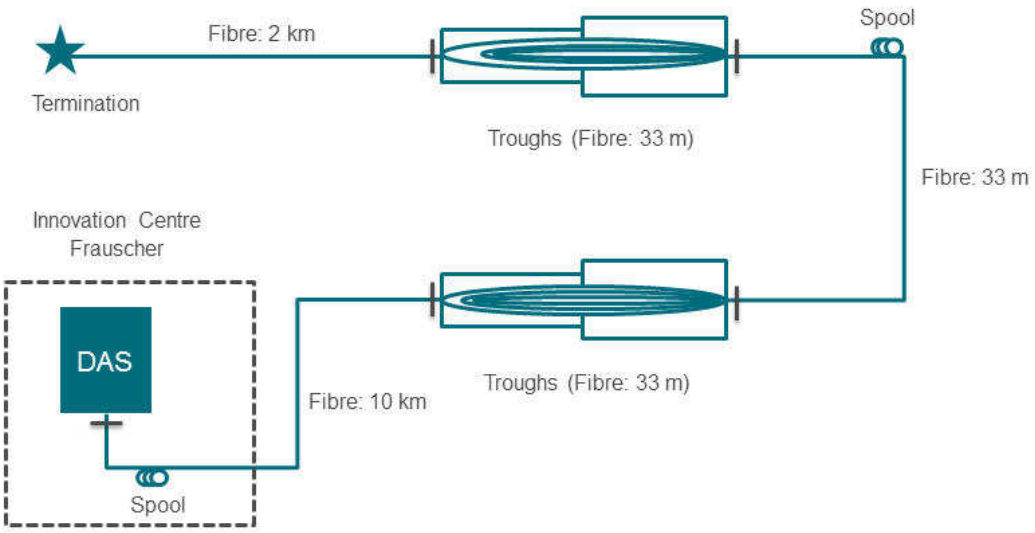

Abbildung 101: Schematic setup for the measurement on April 24th 2018.

Additional to the HSi system, there was also a Theta unit that recorded the same events. The results of the Theta recordings are not discussed in this report.

Results

The sample rate of the raw DAS signal at each location is defined by the pulse repetition frequency of 2500 Hz. This limits the highest analysis frequency, or Nyquist frequency, to equal 1250 Hz. Some rudimentary signal processing steps are applied to each raw file to enhance the signal to noise ratio. A high-pass filter and a spatial decimator were applied to detrend the data and improve signal to noise ratio, respectively. Thereafter the frequency content was calculated using a Fast Fourier Transform (FFT) to allow a simplistic analysis of the frequency content of the flashover event. All signal processing was carried out using Matlab.

Octave Analysis

By dividing the energy content of the signal calculated from the FFT in to octaves, a crude frequency analysis can be conducted. For example, the upper octave contains energies in the range 625 – 1250 Hz; the next lower octave contains frequencies in the range 313 – 625 Hz, the next again in the range 156 – 293 Hz, etc. The resulting figures present either a cumulative frequency plot or a plot of specific frequency ranges.

7.3 Kettlebell

66 of the files are recordings from dropping a 20 kg kettlebell as seen in Abbildung 97. The kettlebell fell on average from a 95 cm height defined by the height of a tripod. Hence the energy at the impact is approximately 186.4 Joule (E = m*g*h). The starting height was 91 cm (178.54 Joule), but as the ground and grit gave way over time due to the impact of the kettlebell, the last drops had a height of 98 cm (192.28 Joule). This leads to an increased impact energy of 7.7%. If the increased energy does also affect the recorded signal, will be discussed later in this chapter after explaining the metrics behind the value used to compare the trough setups. Abbildung 102 and Abbildung 103 show the octave plots of measurement 17.

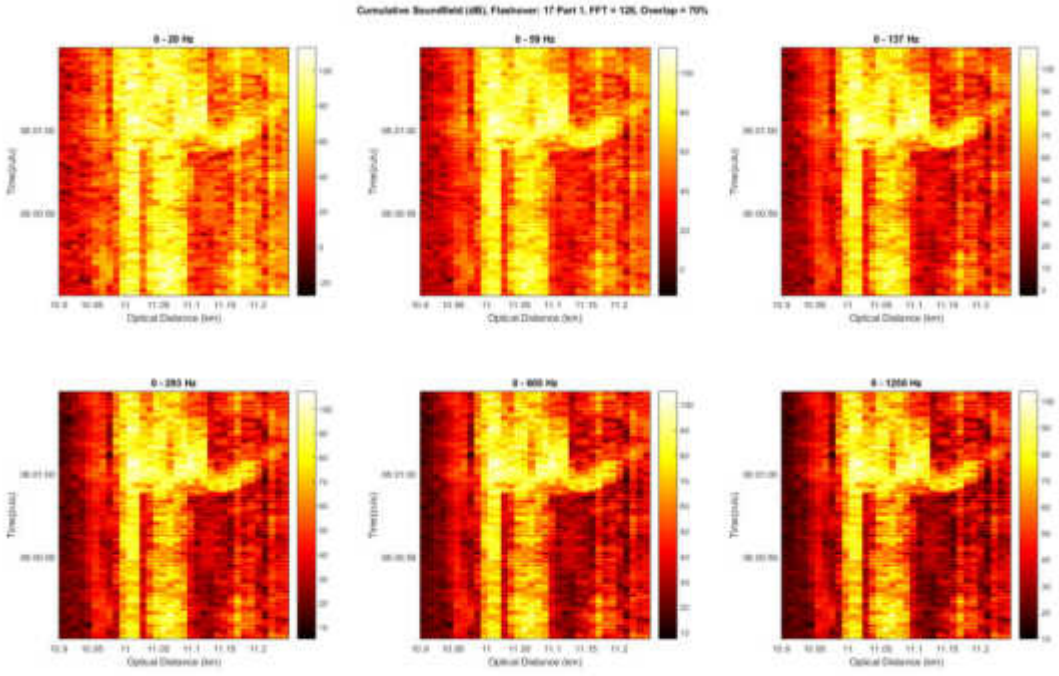

Abbildung 102: Octave plot of cumulative frequency ranges of kettlebell measurement 17. The impact occurred shortly before 10:01:00 CEST.

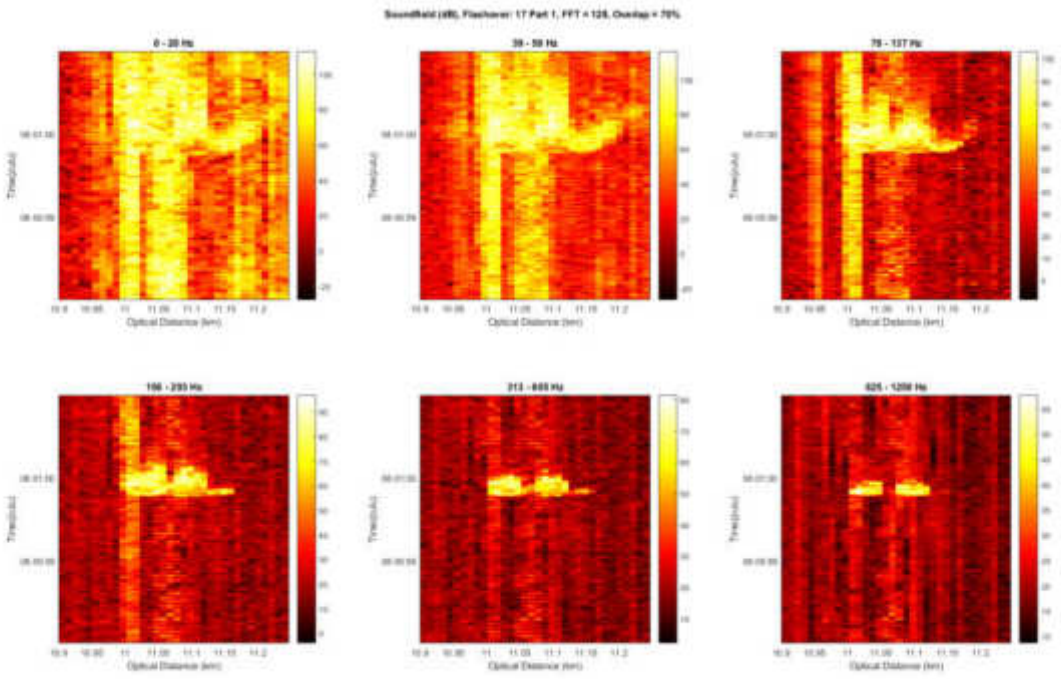

Abbildung 103: Octave plot of different frequency ranges of kettlebell measurement 17. The impact occurred shortly before 10:01:00 CEST.

In Abbildung 104 to Abbildung 105 the frequency ranges of 156 – 293 Hz, 313 – 605 Hz and 625 – 1250 Hz can be observed. The parts of the fibre that is inside either of the troughs is best visible in Abbildung 106; one bin represents roughly 10 m, hence the asphalt trough is expected to be approximately in the middle of the signal that reaches from 11000 m to 11050 m. The reason why the impact's signal is visible for 50 m even though the fibre inside the trough is only 33 m long, stems from the fact that despite the attempt to dampen the signal that excites the fibre outside of the troughs, this is not completely manageable. Furthermore, even if the measured signal's amplitude is only high at the start of a 10 m bin, the whole bin, on average, will obtain a higher value . After the 33 m loop between the troughs, the buried trough can be seen from about 11080 m to 11130 m. By analysing the plots of all 66 recordings visually, the lower frequency ranges are excited the most for both setups, and it seems that the asphalt's signal is more prominent. The higher the observed frequency range gets, the better the troughs' location can be seen. It also seems that the asphalt trough's signal gets relatively weaker with increasing frequencies in comparison to the buried one.

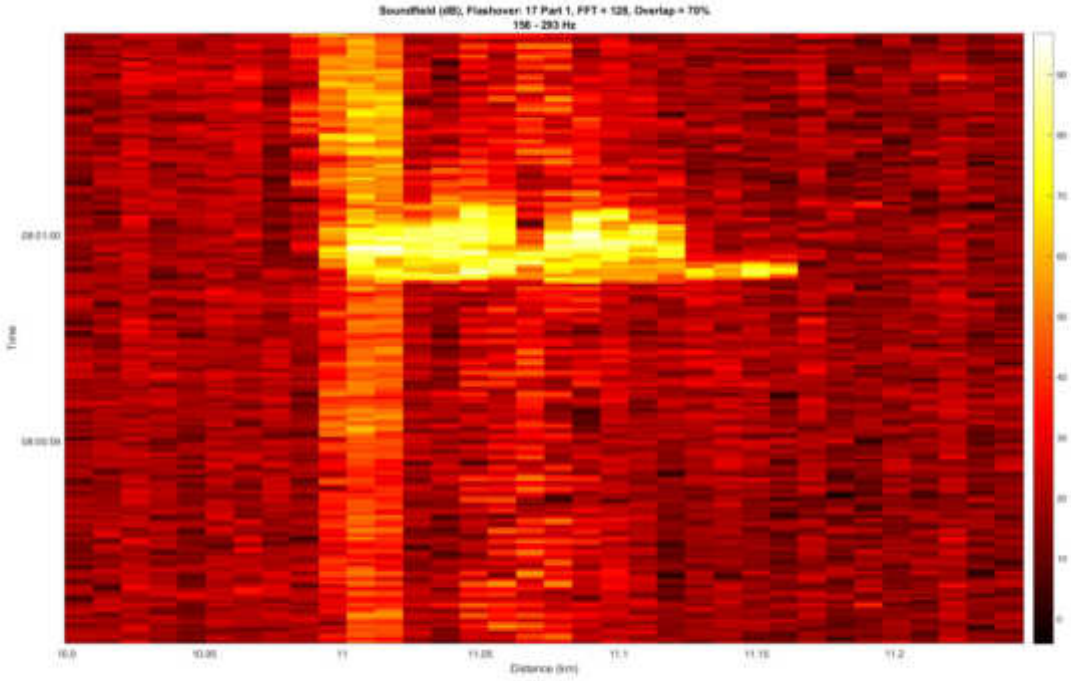

Abbildung 104: Frequency range of 156 Hz – 293 Hz for kettlebell measurement 17. The impact occurred shortly before 10:01:00 CEST.

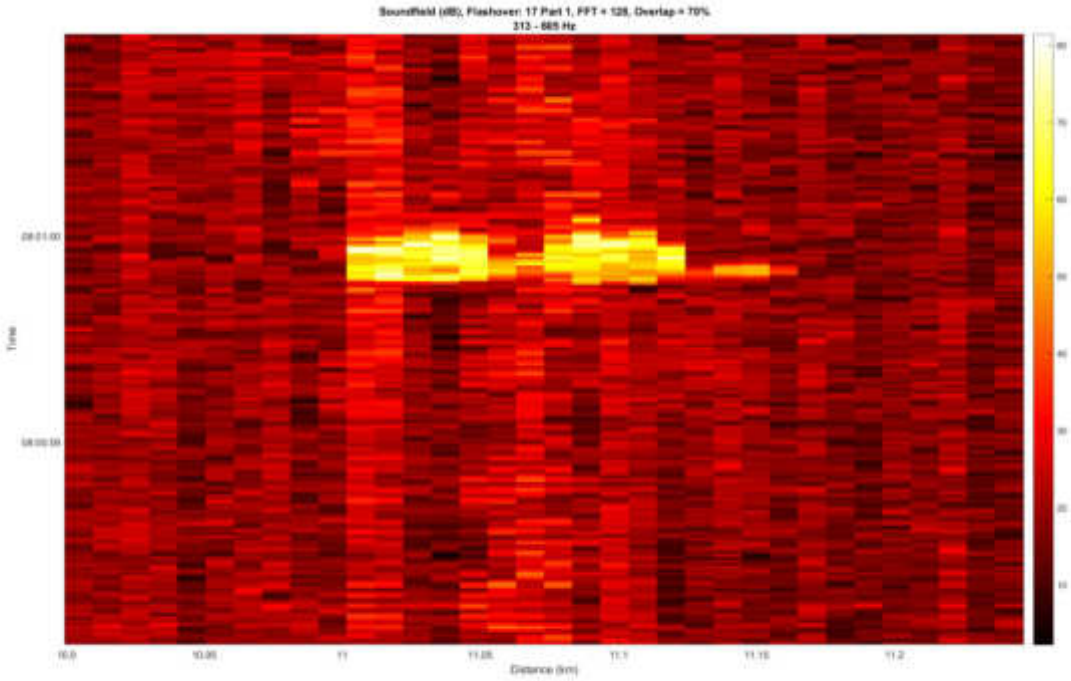

Abbildung 105: Frequency range of 313 Hz – 605 Hz for kettlebell measurement 17. The impact occurred shortly before 10:01:00 CEST.

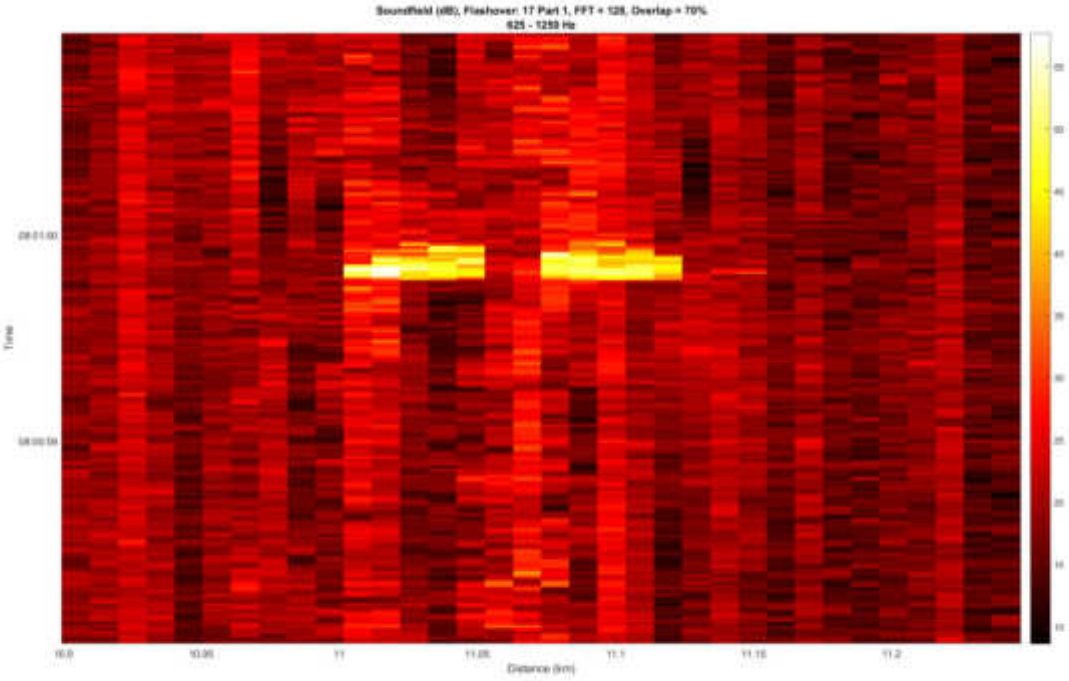

Abbildung 106: Frequency range of 625 Hz – 1250 Hz for kettlebell measurement 17. The impact occurred shortly before 10:01:00 CEST.

Normalization

In order to analyse the data not only from a visual perspective but also a statistical point of view, the data is prepared beforehand. A difference in the background noise could falsify the intensity of the signal. Hence, even though the recorded data is already normalized in the processing, in order to account for the different background noises for the asphalt trough's and buried trough's channels, the data is normalized again depending on these channels' dB values. By marking the lower-left and the upper-right bin of both troughs for every recording (the blue and grey markings in Abbildung 107), all the needed information can be gathered. The x coordinates of the marked bins tell which channels are interesting for each trough (the horizontal blue and grey arrows). This shows the length of the signal in the space dimension. The y coordinates specify the signal's length in the time dimension. This results in two matrices m1 and m2 of dimension 195 x 5 (195 entries in time per 5 entries in space), one for the asphalt trough and one for the buried. For each matrix the mean of the ten lowest and ten highest values are calculated. Taking this mean and not just the minimum and maximum values counters possible outliers. After this, the matrices' values are normalized by the formula:

$$normalized\_value_i = {value_i - \min(m_j)} \Big/ {\max(m_j) - \min(m_j)}$$

Depending on the coordinates, the biggest possible rectangle of the same size is placed over the troughs' bins and their normalized values are summed. This leads to one single value for both troughs that is comparable. The higher the number, the more intense the recorded signal was for the specific frequency range in the rectangle.

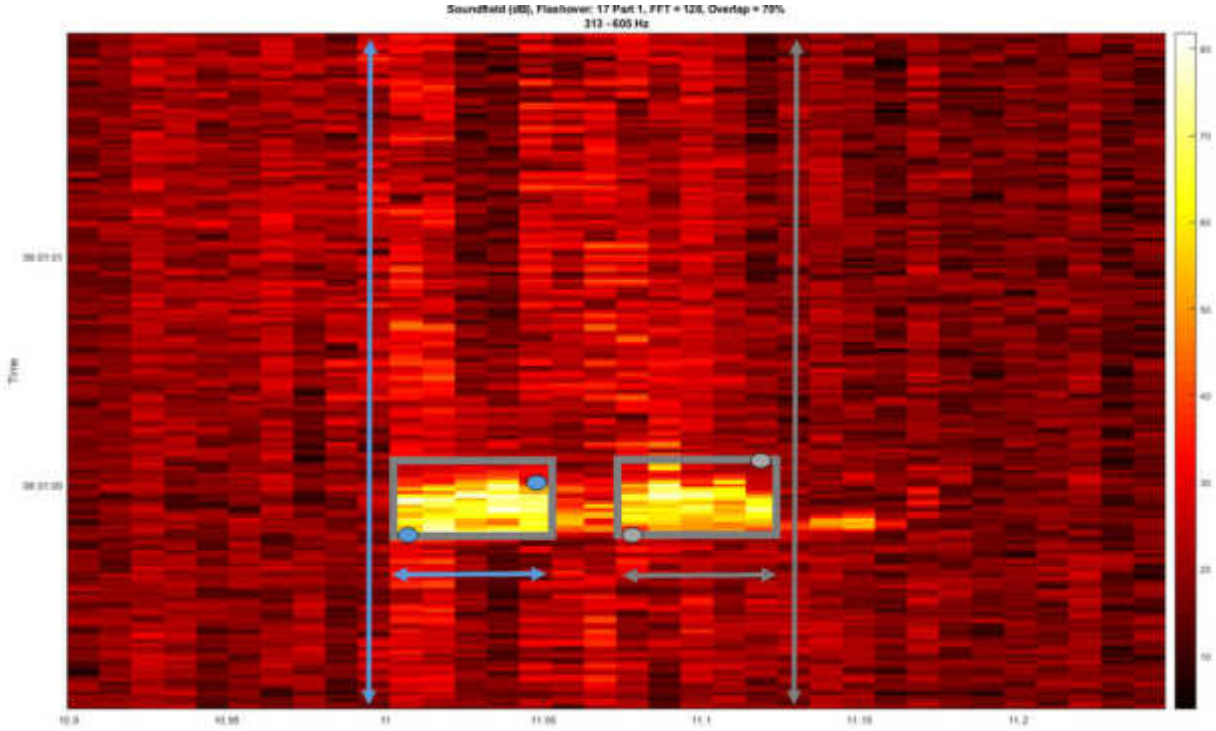

Abbildung 107: Example of marking the start and end bin of the troughs' signals for measurement 17.

Comparing Asphalt and Buried Tough Setup

As can be seen in Abbildung 103, the signal from the troughs is difficult to differentiate from the background noise for frequencies under 156 Hz. This problem exists for all 66 kettlebell recordings, hence this analysis includes only the frequency ranges 156 – 293 Hz, 313 – 605 Hz and 625 – 1250 Hz.

Tabelle 10 shows a descriptive statistic of the calculated values.

	156 – 293 Hz		**313 – 605 Hz**		**625 – 1250 Hz**	
	Asphalt	**Buried**	**Asphalt**	**Buried**	**Asphalt**	**Buried**
Mean	0.2241	0.3271	1.0515	1.6059	14.0046	18.3393
Std	0.0535	0.0491	0.2672	0.2613	3.2777	3.0034
Max	0.3552	0.4457	1.7210	2.2418	23.0884	25.4472
Min	0.1115	0.2107	0.5843	0.9650	6.5711	10.7430

Tabelle 10: Descriptive statistics of the kettlebell recordings after normalization.

The mean of the calculated value is higher for the buried troughs for all three frequency ranges. This confirms the hypothesis that inserting rubber granulate mats between the ground and the troughs attenuate the signal reaching the optical fibre. After an analysis of variance, it can be confirmed that this difference is also statistically significant. Abbildung 108 to Abbildung 110 show the boxplots resulting from that analysis.

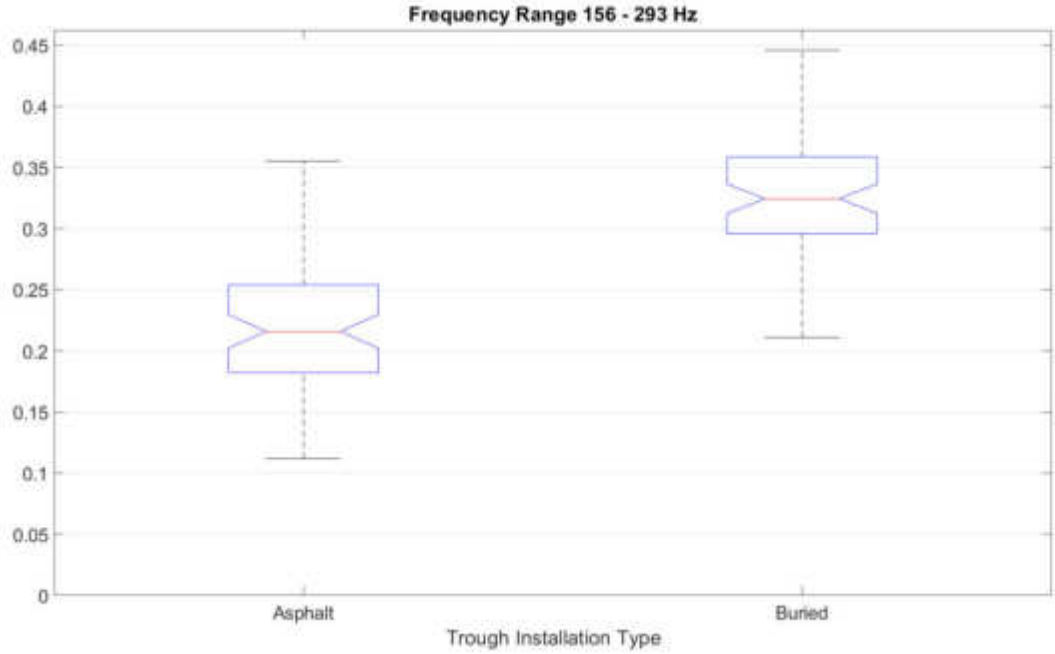

Abbildung 108: Boxplot for the signal values of asphalt and buried troughs for the frequency range 156 – 293 Hz.

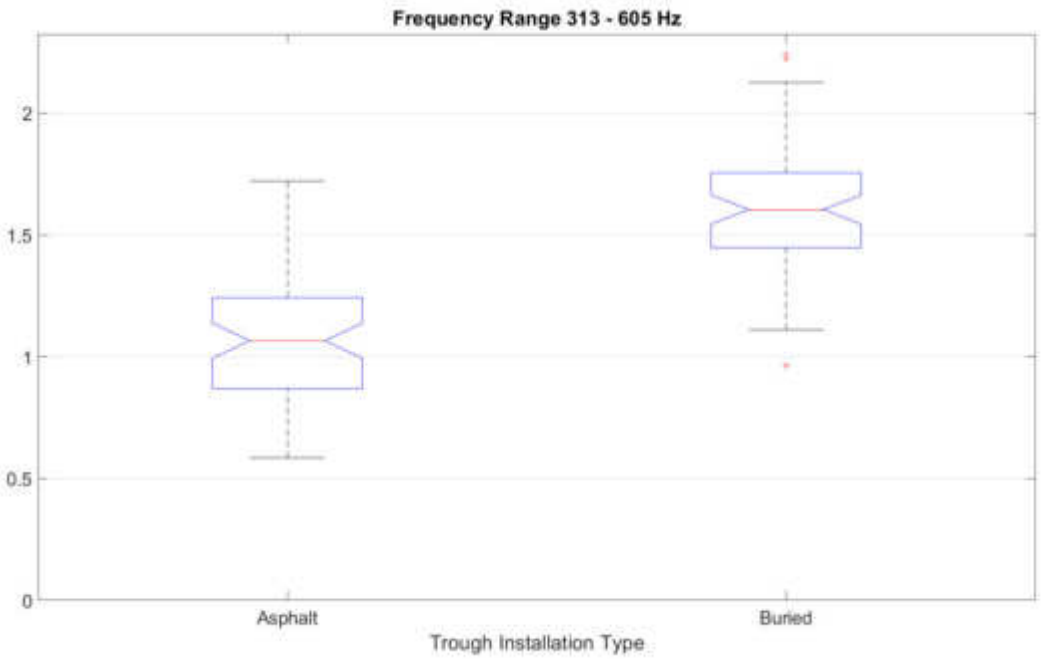

Abbildung 109: Boxplot for the signal values of asphalt and buried troughs for the frequency range 313 - 605 Hz.

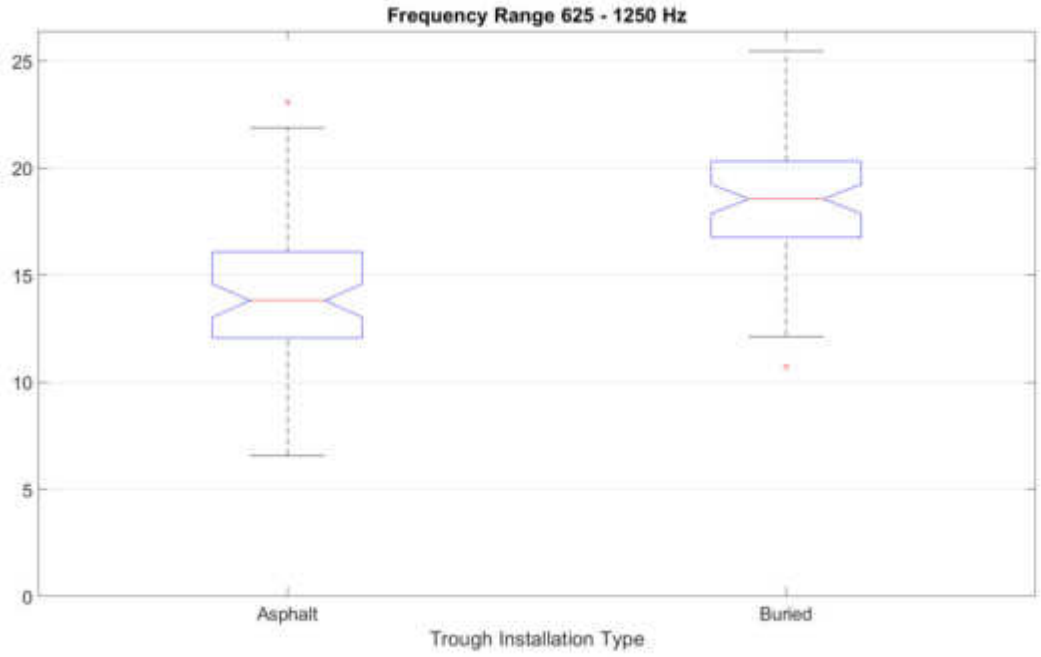

Abbildung 110: Boxplot for the signal values of asphalt and buried troughs for the frequency range 625 - 1250 Hz.

Change in Impact Energy

As mentioned before, the drop height increased from 91 cm to 98 cm during the 66 measurements, as the impact of the kettlebell compressed the ground where it hit. Hence,

there is a change in potential energy of 7.7% between the first and the last drop. The following analysis answers the question if this increase also affects the normalized values used to compare the setups. Tabelle 11, Tabelle 12 and Tabelle 13 each show the mean signal value of the first three and the last three measurements for both setups, as well as the change in percent, for the three different frequency ranges that were also used in the analysis before. It can be seen that all values, excluding the buried trough for the frequency range 313 – 625 Hz, increase over the quantity of the drops. Where the increase for the buried trough is only between 2 and 4%, the increase for the asphalt setup ranges between 12 and 45%. Even though the asphalt trough seems to react more to the increase in energy, its values were still significantly lower than the buried trough's.

156 – 293 Hz					
Start		**End**		**Change in percent**	
Asphalt	**Buried**	**Asphalt**	**Buried**	**Asphalt**	**Buried**
0.16	0.29	0.18	0.30	+12.5	+3.45

Tabelle 11: Change in the mean signal values of the first three and last three measurements for both trough setups. Frequency range 156 – 293 Hz.

313 – 625 Hz					
Start		**End**		**Change in percent**	
Asphalt	**Buried**	**Asphalt**	**Buried**	**Asphalt**	**Buried**
0.69	1.45	0.94	1.43	+36	-1.38

Tabelle 12: Change in the mean signal values of the first three and last three measurements for both trough setups. Frequency range 313 - 625 Hz.

625 – 1250 Hz					
Start		**End**		**Change in percent**	
Asphalt	**Buried**	**Asphalt**	**Buried**	**Asphalt**	**Buried**
8.56	15.55	12.42	15.92	+45	+2.38

Tabelle 13: Change in the mean signal values of the first three and last three measurements for both trough setups. Frequency range 625 – 1250 Hz.

7.4 Signal Horn

To assess if airbourne sound waves can produce a visible signal, a signal horn, shown in Abbildung 111, was actuated directly between the troughs. The horn is pumped by hand until the pressure reaches 8 bar. At this pressure-level, the horn is able to produce both a high and a low tone at frequencies of 387 +/- 10 Hz and 307 +/- 10 Hz respectively. Both tones produce

a sound level of 115 +/- 2 dbA according to the producer's official information sheet. As seen in Abbildung 112 and Abbildung 113, the higher tone was activated for 3 seconds at 09:40:11, the lower tone for 3 seconds at 11:40:13 +2GMT.

Abbildung 111: Signal horn.

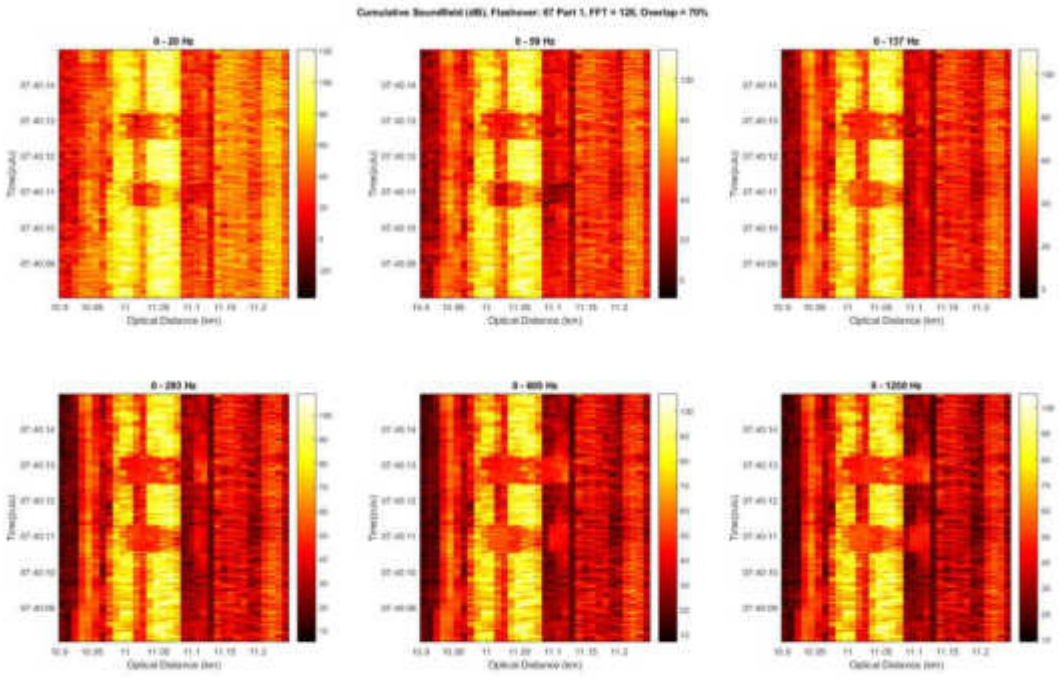

Abbildung 112: Octave plot of cumulative frequency ranges of horn measurement 1. The higher/lower (lower/higher) tones were activated at 09:40:10 and 09:40:12 CEST respectively.

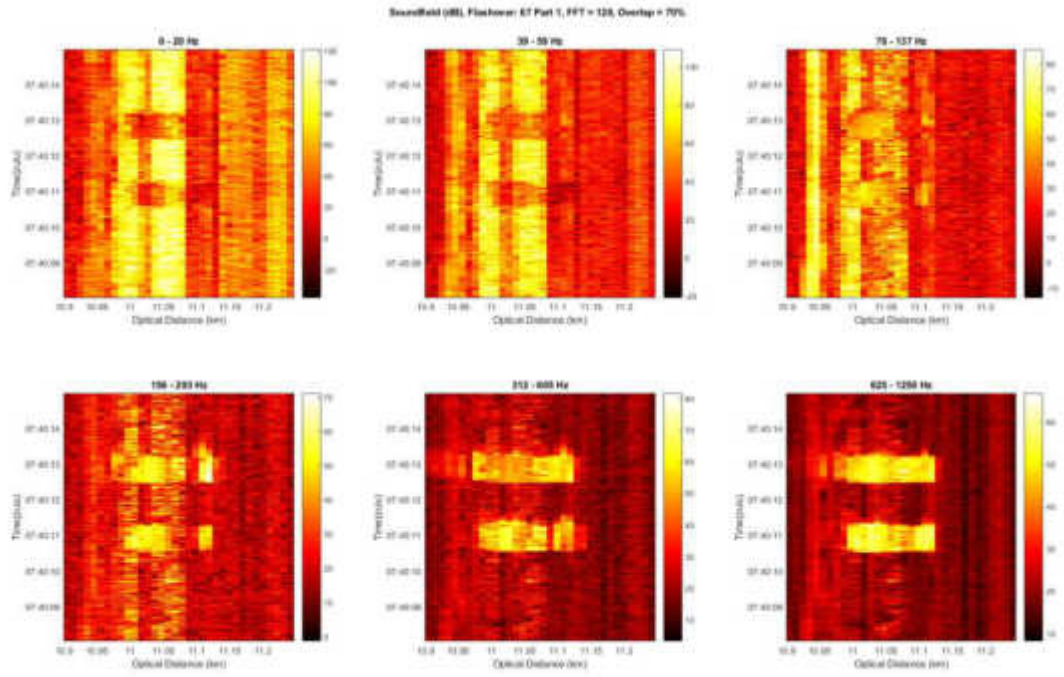

Abbildung 113: Octave plot of different frequency ranges of horn measurement 1. The higher/lower (lower/higher) tones were activated at 09:40:10 and 09:40:12 CEST respectively.

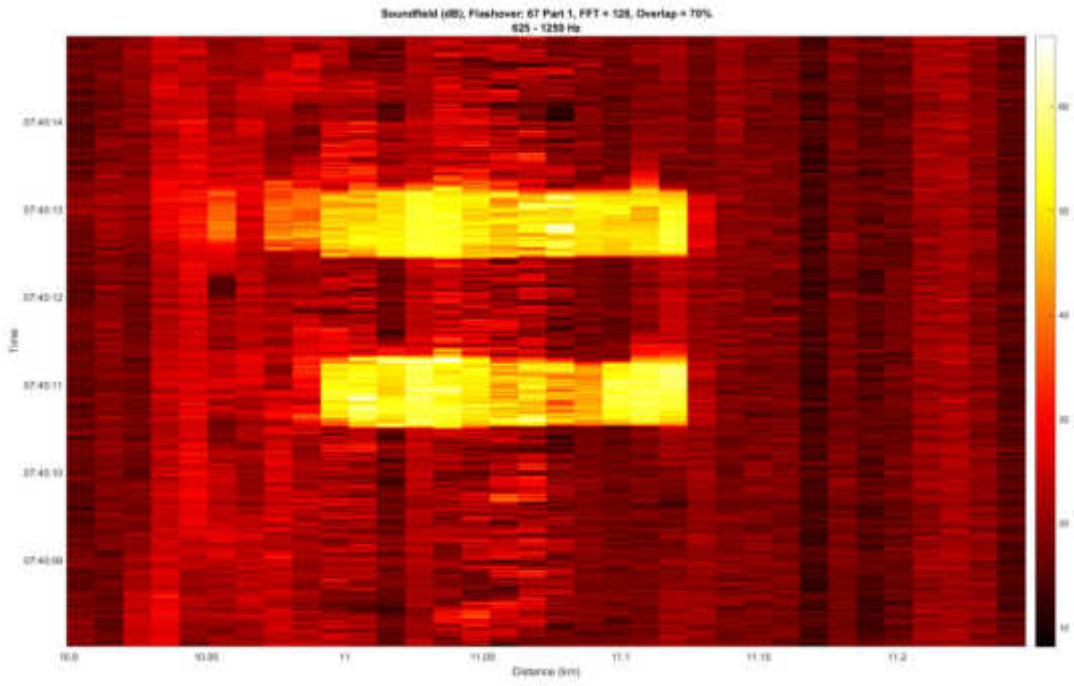

Abbildung 114: Frequency range of 625 – 1250 Hz for horn measurement 1.

Likewise, as by the drop tests, the signal inside bins 10 – 15 for the asphalt trough and 17 – 22 for the buried trough are extracted for the analysis. The analysis was only conducted using recordings 2 – 4, as the first recording was a test to ensure the tones are visible in the DAS signal. The following mean values are calculated for the frequency range 625 – 1250 Hz. On average, the high tone's signal is more visible in the asphalt trough (Asphalt: 124 – Buried: 114), the low tone's signal is more visible in the buried trough (Asphalt: 173 – Buried: 184). Hence, higher frequency sounds are more prominent in the asphalt trough setting, at least in this frequency range. Tabelle 14 to Tabelle 16 show the mean signal value of all analysed frequency ranges.

156 – 293 Hz			
High Tone		**Low Tone**	
Asphalt	**Buried**	**Asphalt**	**Buried**
45.57	128.51	348.17	712.32

Tabelle 14: Mean signal values for the signal horn's high and low tone. Frequency range 156 – 293 Hz.

312 – 605 Hz			
High Tone		**Low Tone**	
Asphalt	**Buried**	**Asphalt**	**Buried**
50.15	121.14	49.54	33.27

Tabelle 15: Mean signal values for the signal horn's high and low tone. Frequency range 312 – 605 Hz.

625 – 1250 Hz			
High Tone		**Low Tone**	
Asphalt	**Buried**	**Asphalt**	**Buried**
124.80	114.43	173.62	184.06

Tabelle 16: Mean signal values for the signal horn's high and low tone. Frequency range 625 – 1250 Hz.

Bolt

Additional drop tests were conducted with a small bolt of 42 g. It was dropped with the head looking up onto the middle of each of the trough setups 10 times. The drop height of 110 cm was defined by a wooden plank as seen in Abbildung 115: Drop tests with a bolt from a predefined height of 110 cm..

Abbildung 115: Drop tests with a bolt from a predefined height of 110 cm.

Abbildung 116 and Abbildung 117 show octave plots in the range of 156 – 293 Hz for the bolt drops for both the asphalt and the buried troughs. The drops are better visible at the asphalt troughs, at least for this frequency range. There seems to be a higher background signal at the time of the drops on the buried troughs. Over the day there were other occasions were the background noise just got louder. At this time no one was walking in range, the wind was not blowing and we did not pinpoint any other possible disturbances, hence we are not able to state the source of the increased background noise.

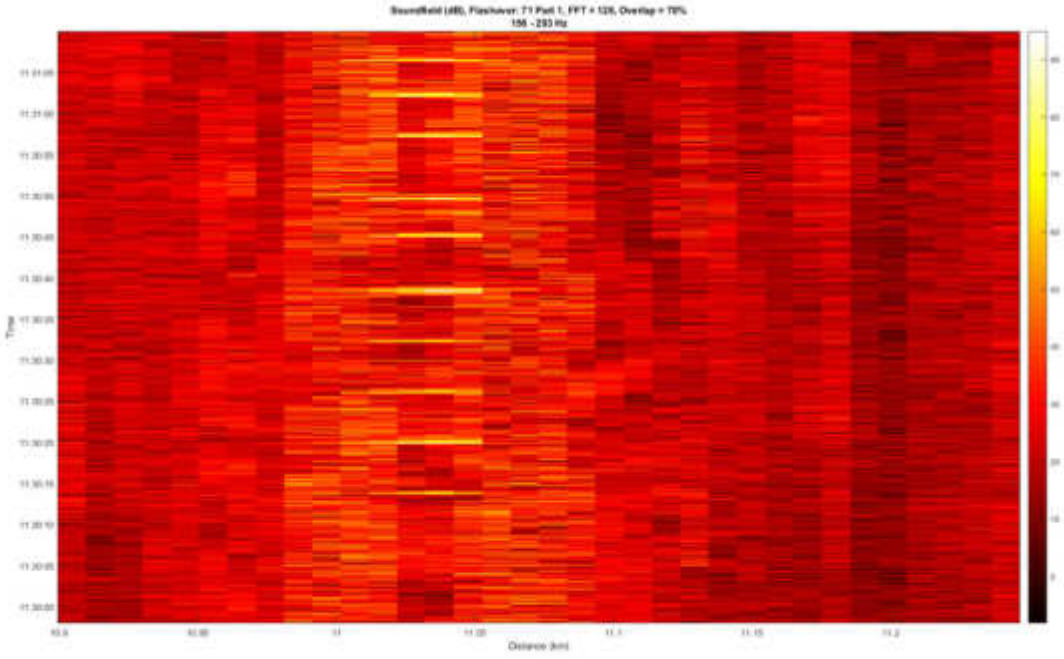

Abbildung 116: Octave plot (156 – 293 Hz) for the bolt drop on the asphalt troughs.

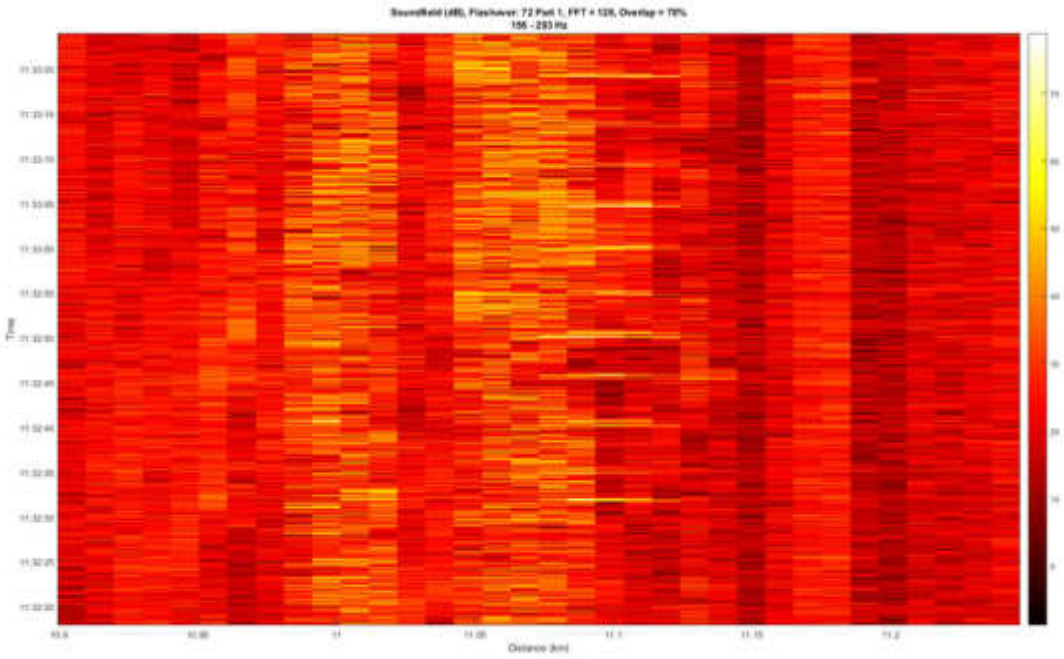

Abbildung 117: Octave plot (156 – 293 Hz) for the bolt drop on the buried troughs.

Walking

Walking from one side of the troughs to the other side was also recorded for both setups. As an example, Abbildung 118 shows walking from one side to the other on the asphalt troughs (taking three steps), turning around and walking back again (taking three steps) between the time 13:22:05 and 13:22:25 CEST. The same can be seen in the figure between 13:22:55 CEST and 13:23:35 CEST. Even with this knowledge, it is not possible to determine where or when a specific step has been taken. This is not due to the fact that walking is not traceable by DAS, but that the fibre was laid into the trough coiled up. Abbildung 118 shows the same pattern of walking between 13:24:50 and 13:25:07 CEST for the buried trough.

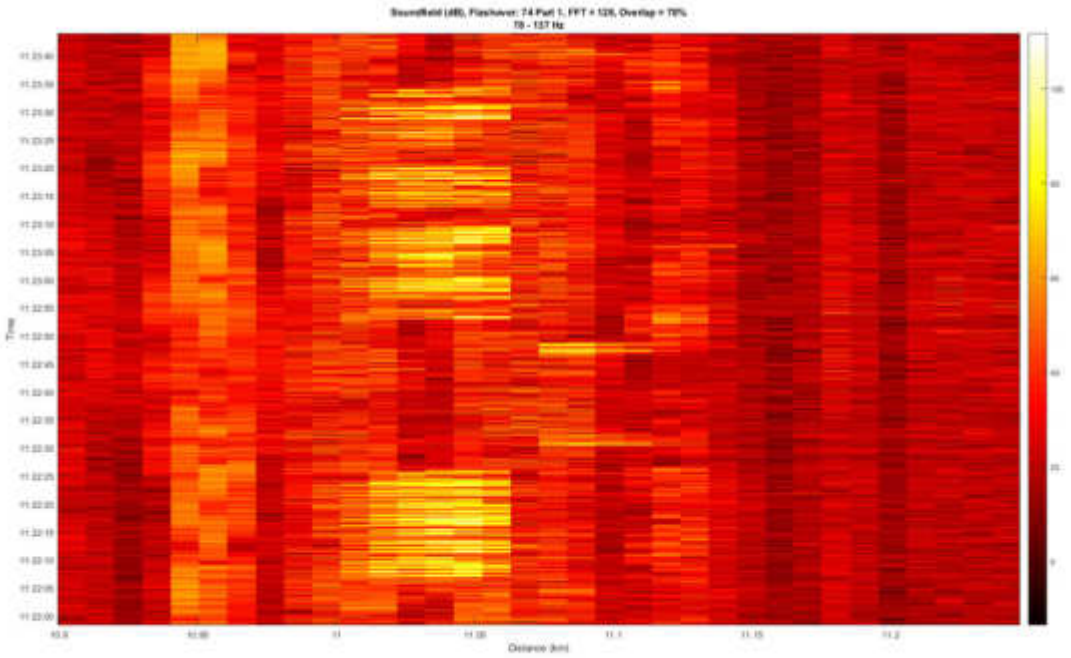

Abbildung 118: Octave plot (78 – 137 Hz) for the walking test on the buried troughs.

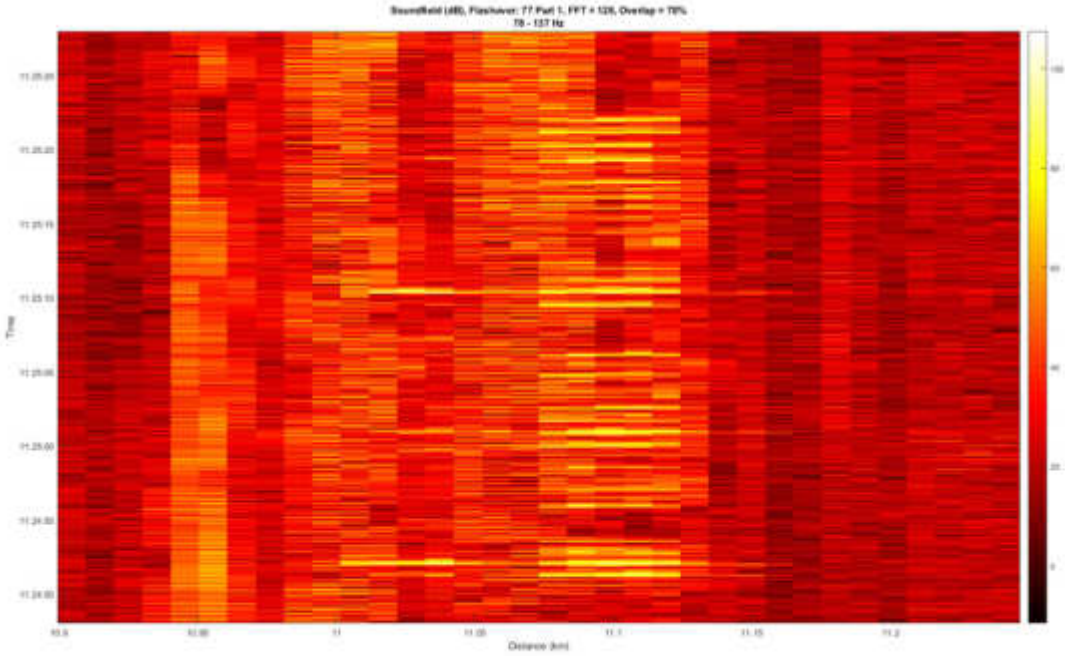

Abbildung 119: Octave plot (78 – 137 Hz) for the walking test on the buried troughs.

7.5 Conclusion

66 kettlebell drops, four horn signals, 10 bolt drops and four times walking over the troughs were recorded with an FTS system. The goal of this experiment was to support or reject the hypothesis that was formed after the second flashover trials at St. Pölten in March 201, namely that rubber granulate mats between the ground and the troughs attenuate the recorded signal more than buried troughs, making it more difficult to locate a specific event. After normalizing the data of the kettlebell drops a statistical analysis showed a significant difference in the signals' intensity between the two setups, supporting the hypothesis. The horn, bolt drops and walking measurements were recorded but not used for the analysis.

8 BESCHREIBUNG ALGORITHMUSENTWICKLUNG

8.1 Introduction

This document serves as an explainer for the first prototype Matlab algorithm written especially for the training and utilization of a RUSBoost model in order to localize catenary short circuits. The trained model is based on experiments conducted in cooperation with ÖBB in October and November 2016 in Allerding, as well as May 2017 in St. Pölten. Catenary short circuits are electrical short circuits between the high voltage (15 kV) catenary and ground typically causing an electrical spark and associated acoustic bang. These can occur for a number of reasons: faults within the locomotive, driver error, wildlife or natural occurrences such as a branch falling off a nearby tree, to name but a few. Circuit breakers in the respective substation cut the supply within a few milliseconds but in order to be able to reapply the electrical supply and resume operation, the cause of the short circuit must be found and repaired if required. In certain cases, the exact position of the short circuit is not known and a considerable amount of time and effort is required to locate it. Through FTS and DAS it is already possible to visually detect flashovers caused by short circuits. The measurable signal of a flashover depends on factors like the method the optical fibre is installed near the track (e.g. ground-buried, above the track, distance to track), the track condition (e.g. tunnel, bridge, open space) and specifics of the short circuit and flashover itself (e.g. power, decibel). The recorded flashover data are processed by signal processing techniques and plotted in different frequency bands in order to increase the signal to noise ratio. As a next step, the resulting RGB image is transformed into grayscale and then binary images to make image processing techniques, such as morphological cleaning and feature extraction by the means of boundaries, possible. The extracted features of the potential flashover are fitted with a RUSBoost model which was trained beforehand. Regions that are recognized as potential flashovers are marked in the RGB images as well as are listed in a .csv file.

8.2 Features

The recorded short circuits are classified into five groups which work similar to school grades. As the code is relying on finding a triangle-like shape through digital image processing, only the data from categories one and two can be used currently. Categories three and four are short circuits where no chevron but only excitations on different parts of the track can be seen at the same time. To date, 108 self-induced short circuits were recorded with an addition of 19 pranger shots. Twelve of those shots fall into category one; four into category two. Those are also used in the training of the models because of their similarity to the “real” short circuits in

terms of acoustic energy generated. Hence 59 out of 113 (52.21%) short circuits that are categorized can potentially be used for the purpose of training a model.

Category	Visualization	Frequency
1	large chevron	40
2	small chevron	19
3	visible	33
4	barely visible	14
5	nothing visible	7
uncategorised	-	18

Tabelle 17: Visual classification of flashovers.

The algorithm extracts properties of the regions found in a binary image. Simply put, every white object in the image is a region, the black part of the image is classified as background and is ignored. A more detailed explanation about binary images and regions will follow in this chapter. Based on the data derived from the experiments conducted with the ÖBB the algorithm is able to train a model beforehand and then classify any regions of new images into potential and non-potential flashovers. Having set the dependent variable Y as binary (flashover yes/no), the independent variables X need to be defined. These independent variables are the regions' features that may be helpful in describing a flashover. Before discussing the features, some variables and objects which are used to calculate or understand them are introduced.

bounding box The smallest rectangle that contains the region.
perimeter The distance around the border of the region.
area The area of the region.
convex hull The smallest convex polygon that contains the region.
convex area The area of the convex hull.

Once set, one can now calculate the features of the regions to obtain the independent variables X.

propDistance The distance of the region on the x-axis, in meter.

duration	The duration of the region on the y-axis, in seconds.
extent	The ratio of pixels inside the region to the total amount of pixels inside the bounding box.
shape	$\frac{4*pi*area}{perimeter^2}$ This is a factor which describes the circularity of an object. A circle has a shape factor of 1 or higher, squares have a factor of about 0.78.
extentCon	The ratio of pixels inside the convex hull of the region to the total amount of pixels inside the bounding box.
shapeCon	$\frac{4*pi*convexArea}{perimeter^2}$ The circularity of the convex hull.
density	The ratio between the region area and the convex hull area.
eccentricity	When laying an ellipse over the region, eccentricity is the ratio of the distance between its foci and the major axis length.
orientation	When laying an ellipse over the region, orientation is the angle between the x-axis and the major axis.
location	The physical location where the short circuit was recorded.

8.3 Algorithm and Functions

This chapter gives an overview of the algorithm and its functions. The aim of the algorithm is to process recorded files of new short circuits, find the short circuit (as well as all other potential ones). This is achieved by using a model that was trained by features from already known short circuits. The result should be the reported location on the track where the short circuit occurred. The main focus is about using an already trained model to find a new short circuit. Even though training said model is not part of the main code that would run at a customer's installation, it is important to first discuss how obtaining the training data and training a model works.

8.4 Training Model

As of January 2018, the two experiments mentioned in the introduction, resulted in 59 recorded short circuits of the categories 1 (40) and 2 (19) as seen in Tabelle 17. These 59 short circuits

are the training ground for the model. The following explanation of the code structure is also shown in Abbildung 120.

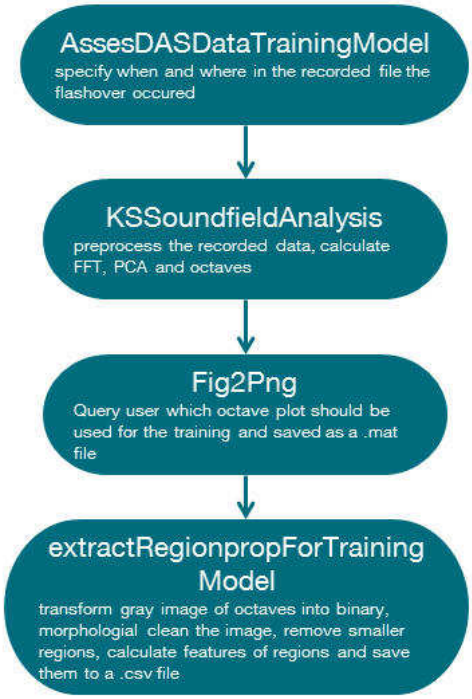

Abbildung 120: Flowchart of the code for creating a training dataset.

The model relies on features that are extracted from soundfield images, therefore the data of the recorded short circuits must first be transformed into data which can be plotted. In order to do so, the exact time (YYYY-DD-MM HH:MM:SS) and place (optical distance in m) of the short circuit must be known from the .fds file. In this file, the data matrix of the record and the information about the x- and y-scale is saved. By knowing the exact times and locations of the flashovers a window can be laid over them which is specified by four parameters (metres before and after the flashover; seconds before and after the flashover). Let us consider a model with the scaling of *4 km x 3 sec*. This requires a window of 2000 m before to 2000 m after the flashover as well as from one second before to two seconds after the short circuit. The images' x-axis is the distance; the y-axis the time. Starting the script *AssesDASDataTrainingModel*, calls the function *KSSoundfieldAnalysisTrainingModel()* which needs the four window parameters in addition to a specified frame size for the fast-fourier-transformation and an overlap rate. The standard framesize of 128, splits the whole 7500x11754 data matrix of the window *4 km x 3 sec* into 59 128x11754 matrices (the last one does not include 128 rows), performs a spatial reduction through Principle Componant Analysis (PCA) and calculates the FFT. After applying the FFT, six octave frequency bands are plotted through the resulting six 195x783 matrices. The first figure contains subplots of the frequencies 0 – 20 Hz, 39 – 59 Hz,

78 – 137 Hz, 156 – 293 Hz, 313 – 605 Hz and 625 – 1250 Hz. The second figure includes the cumulative frequency bands as seen in **Error! Reference source not found.**.The resulting soundfield figures display the flashover's chevron from which the features are calculated and saved into a predefined folder.

As a next step, running *Fig2Png()* with the path to the soundfield figures as the parameter, all flashover figures found in the folder are plotted. The user is asked which of the 12 images per figures should be used for the training data, see Abbildung 120, and the image chosen is saved as a RGB .png as well as a .mat file into the folder.

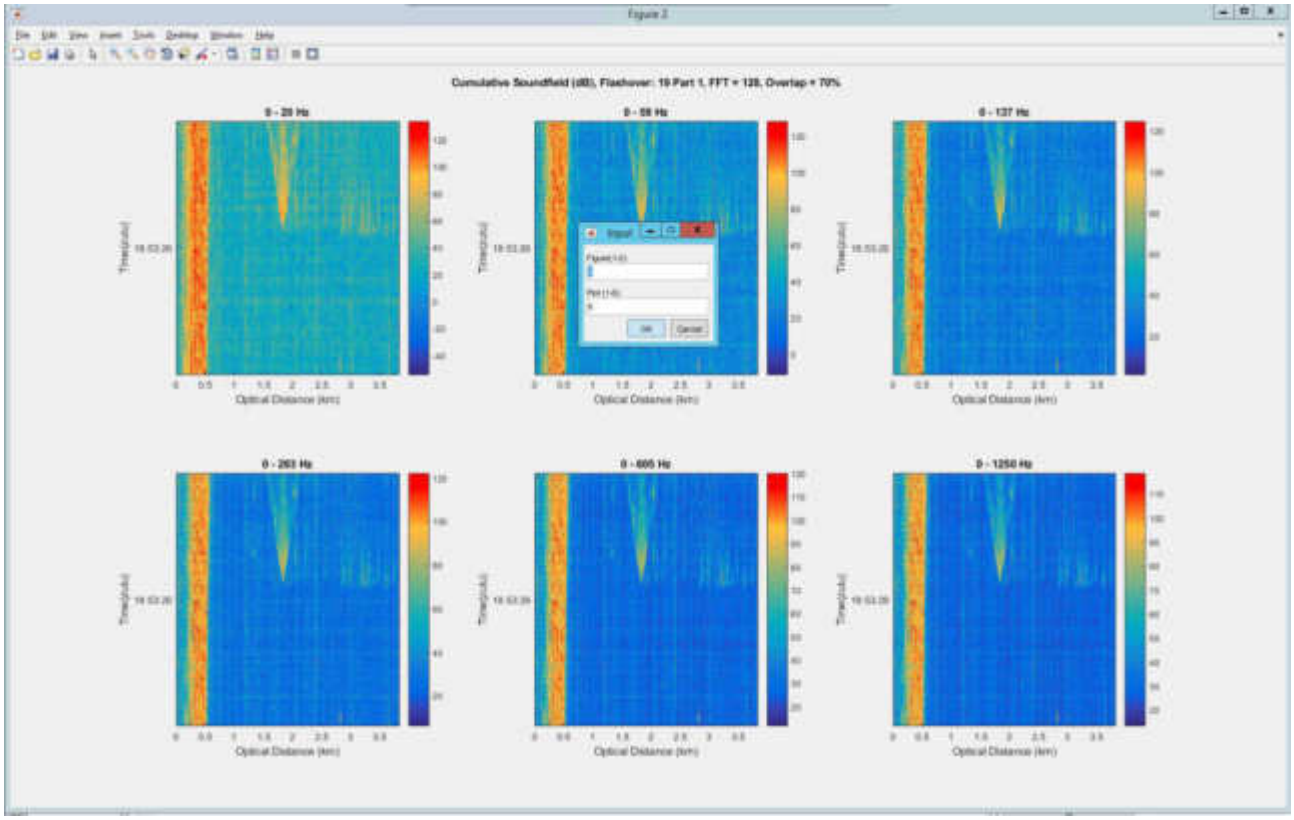

Abbildung 121: The function Fig2Png prompts the user to choose the best looking frequency band.

The last function, *extractRegionpropForTrainingModel()*, takes the .mat file of the flashover's RGB image and transforms it into a grayscale image. The grayscale image is transformed into three binary images through different thresholding approaches. The first method makes Matlab choose the threshold by Otsun's method; the second one through adaptive thresholding by the calculation of first-order statistics around every pixel. In the third the threshold is set manually to 0.45. The binary images are morphologically cleaned with square, diamond and straight line structuring elements. More information on morphological cleaning (opening, closing, erosion,

dilation) can be found in the following chapters. The user is then prompted to choose one of the three cleaned images (or discard them if none of them are fitting) and set the location where the flashover was recorded. Abbildung 122 shows the significant differences occurring between the methods of transforming the grayscale into a binary image. If an image was chosen, the region's boundaries and features are calculated through the coordinates of the pixels and saved into a Matlab data structure object. It is important to note that the features are calculated from the whole region but only from a part in time after the event occurred, which is about a third of its length. The reason for this is that short circuits can have a good triangle-like shape at the starting point, but transform into a region that is not suitable for training a model. Afterwards the user has to mark the short circuit's region with a mouse click into its bounding box as shown in Abbildung 123. Subsequently, after marking the last short circuit, minimum, maximum and mean values of all found and numbered features are calculated for every location. Both the features and descriptive statistics are saved into a excel file. With this step the creation of the dataset for training a model is complete.

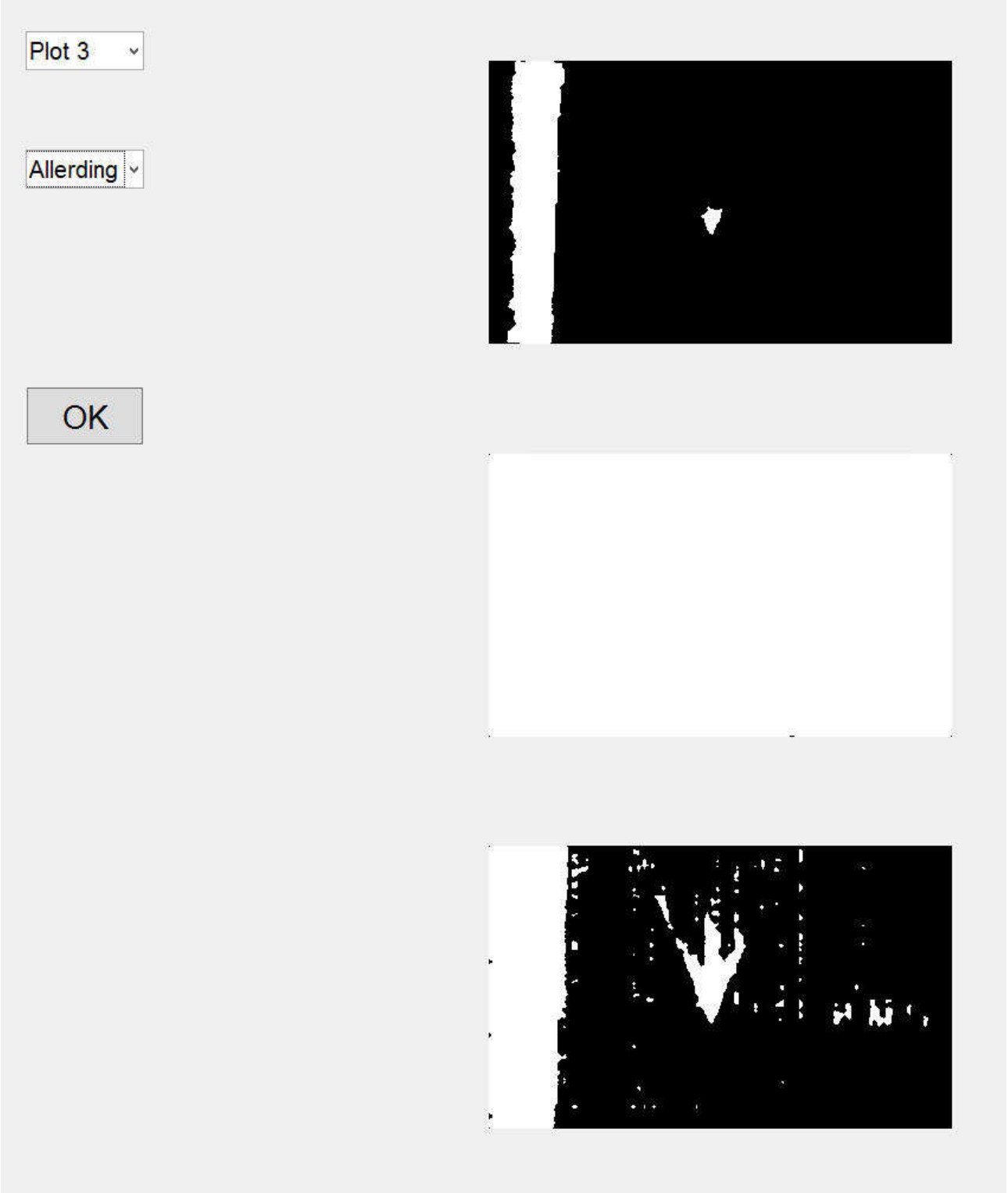

Abbildung 122: The user is prompted to choose one of the three morphologically cleaned images, measurement 19.

Top plot: Otsun's Method; middle plot: adaptive thresholding; bottom plot: threshold set to 0.45.

Abbildung 123: The user has to click into the bounding box of the flashover, measurement 19.

8.5 Fitting Data

In the same fashion, as with the training dataset, a flowchart for the structure of the detection algorithm is shown in Abbildung 124.

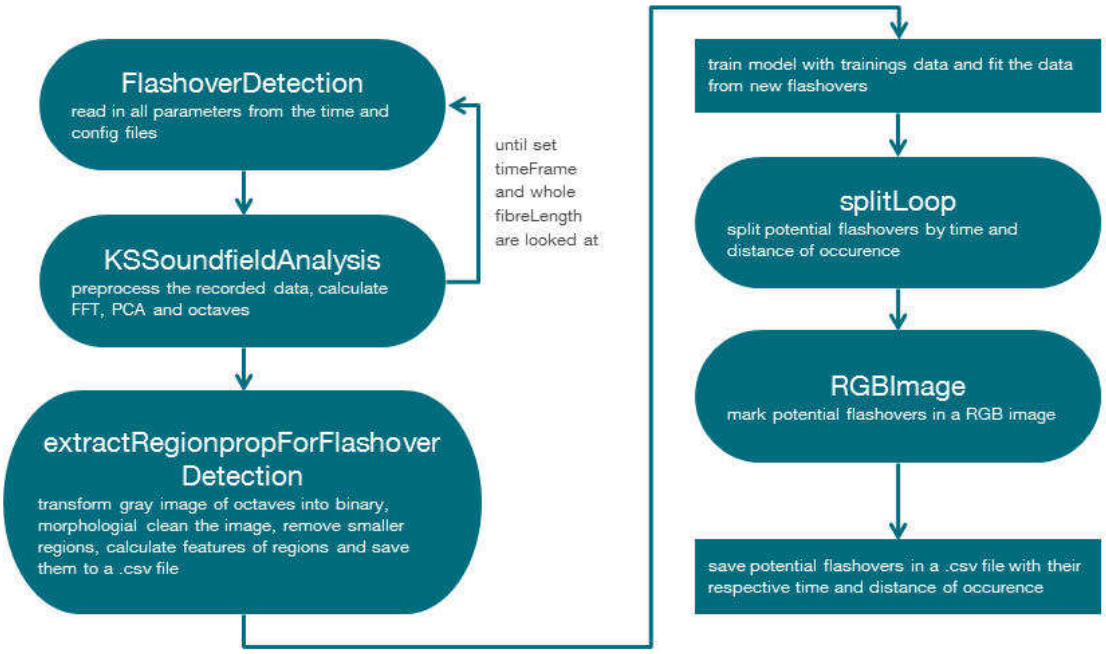

Abbildung 124: Flowchart of the detection algorithm.

FlashoverDetection() starts the processing of a newly recorded .fds file, trying to find the region of a flashover in it. The required argument is the path and name of a predefined time.csv file. This file contains the time of the short circuit and the path to the .fds file itself. A second argument, a path to a configuration file, can be specified but is optional. If it is not specified, the function will know the configuration file is in the same folder as the time file. The function imports the parameters specified below and saves them into different variables. Parts of the configuration file are shown in Abbildung 125.

date	The time of the flashover (dd,mm,yyyy,HH,MM,SS) in format datenum.
filepath	The path and name of the .fds file of the flashover.
location	The location of the track where the FTS system is installed
timeFrame	The window of time the algorithm looks for the flashover. It starts at timeFrame/2 seconds before the time of the flashover and stops after reaching timeFrame/2 after it.
fibreLength	The complete length of the fibre.
plotPath	The path where the folder for the results is created. It is also the path where the training data excel file is located.

trainingData	The name of the training data.
excelfileAllBlobs	The resulting excel file of all regions that were found in the black and white images.
excelfileOnlyFlashovers	The resulting excel file of only potential flashovers that were found in the black and white images.
fibreFilepath	The path and name of the .csv file which states the destinations which must be cut out of the file due to spools.
subSheet	Defines if the frequency band or the cumulative frequency band figure should be used for extracting plots.
sub	Defines which of the frequency plots should be extracted.
sec	The amount of seconds the search-windows should have → scaling of the y-axis of the images
meter	The amount of metres the search-windows should have → scaling of the x-axis of the images

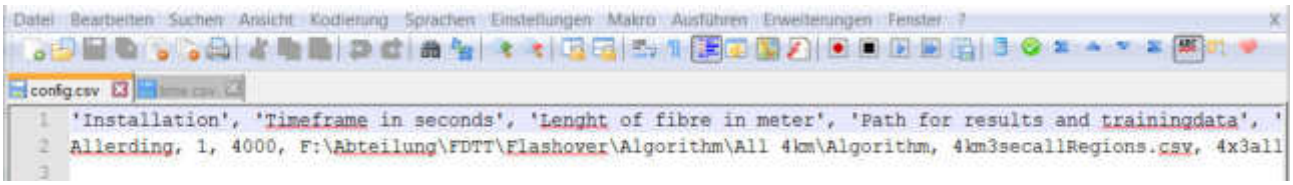

Abbildung 125: Parts of the configuration file.

The .fds file of the recorded short circuit is then processed identically to the .fds files for the training data by calling *KSSoundfieldAnalysisDetection()*, resulting in the soundfield plots of the different frequency ranges. The only difference is instead of only calculating and plotting the soundfield of one part of the file where the short circuit is known to be, the complete length of the track must be analysed. With the data models of *4 km x 3 sec*, a timeframe of six seconds and a track length of 30 km would require the calculation of 40 windows. The parameter *timeFrame* indicates the number of seconds before and after the time of the reported short circuit that will be analysed. A *timeFrame* equal to 6 seconds, a fixed overlap of 1 second and a y-axis scaling of 3 seconds results in four windows for the 4 km window. On the x-axis, we also have a fixed overlap of 1 km which produces ten windows for 30 km.

The plots of the frequency range specified in the configuration file are saved as .mat files, read in by the function *extractRegionpropForFlashoverDetection()* and transformed into three grayscale and binary pictures each, with the same methods as described earlier. The regions and their features are calculated from every image and all regions that are smaller than a

specified threshold regarding the distance and time are removed from the binary image. The threshold is set to 90% of the minimum value reached by the trainings data. This is repeated for each location individually. Hence, if the smallest flashover region in Allerding would be 1 km long after the morphological cleaning, every region that is smaller than 0.9 km would be deleted from the binary images. As a consequence of this, new flashovers on a specific track that are smaller than the already recorded flashovers on that track will be deleted and cannot be found. All the features are saved into the variable *flashover*. The previously saved trainings data is imported into the variable *data*, the RUSBoost model is trained with it and fitted on the features in the variable *flashover*.Depending on the regions' features, the region is labelled with a 0 (= not a flashover) or 1 (= flashover). After the fit, every region with label 0 is deleted from the variable, leaving only the potential short circuits. These are then divided into groups by their .mat filename. *splitLoop()* splits those groups further into subgroups depending on their time of occurrence. Potential short circuits are fused together if the distance between each of them and their mean distance is not greater than 10 m. *RGBImageTable()* marks all potential short circuits in the appropriate image as seen in Abbildung 126. As a last step, the variables inside *flashover* are saved into a .csv file and are moved into a folder named with the current system time, together with the marked images.

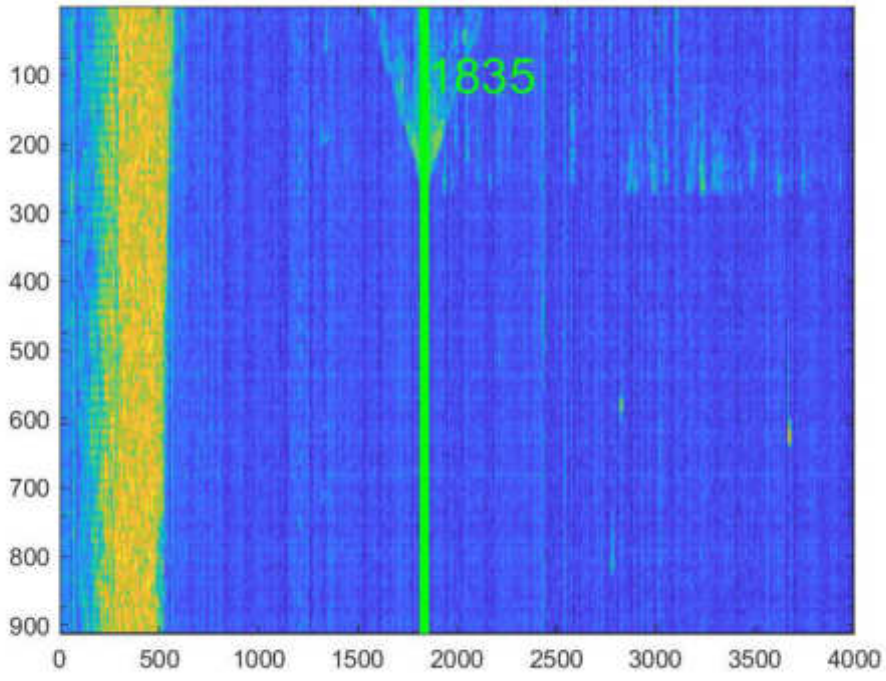

Abbildung 126: RGB image of a marked flashover region.

8.6 Model Performance and Selection Criterions

It is important to identify which of the defined parameters are needed to describe a flashover's region in mathematical terms. Matlab's Statistics Toolbox offers a wide selection of classifier models. The graphical interface allows for an easy calculation and comparison of different models like nearest neighbour, decision trees or linear models with different parameters included, by just a few clicks. As a performance check, it offers a confusion matrix, the Receiver Operator Curve (ROC)-curve as well as the accuracy of the fitted models.

8.7 Confusion Matrix

The confusion matrix is a 2x2 table of the true positive, true negative, false positive and false negative observations from which one can easily derive the True Positive Rate (TPR) and False Positive Rate (FPR). These rates describe the percentage of observations that were correctly and incorrectly classified into class A. The higher the true positive rate and the lower the false positive rate, the better the model. As an example, Abbildung 127shows the confusion matrix of a model with a true positive rate of 95% and a false positive rate of 1%. So 95% of the observations that were predicted as class 1 are really from class 1, 1% of the positively predicted are not from class 1 but class 0.

Abbildung 127: Confusion matrix.

8.8 ROC-curve

The receiver operating characteristic curve graphs the true positive vs. the false positive rate and hence shows the trade-off between detection and false alarm. The Area under this Curve (AUC) provides a value ranging from 0 to 1 which makes it comparable to other models. The higher the AUC value, the better the model.

8.9 RUSBoost

The tricky part is finding a well suited model that does not overfit the data or implements some other kind of error. As there is always only one flashover region, if at all, but often more than fifty non-flashover regions per image, the data is heavily skewed. The problem with heavily skewed data is that most of the models classify observations as belonging to the omnipresent class. Our researches investigate two approaches in order to tackle this situation; data sampling and boosting. There are two kinds of data sampling techniques, random undersampling (RUS) and random oversampling. Random oversampling duplicates observations of the minor group until the desired ratio is achieved. Random undersampling does the same by randomly deleting observations from the major group. Both methods have a drawback, by undersampling information is lost, by oversampling the model could be overfitted.

The most commonly used boost algorithm is called AdaBoost and builds models iteratively. Each iteration weighs the observations, in the following iteration the observations that were falsely classified are weighted more heavily. After the last iteration, all defined models vote on how to classify unlabelled observations. We test different sampling, boosting and combinations of these models. They conclude that RUSBoost models, a combination of random undersampling and the AdaBoost algorithm, are perfect for situations where one class greatly outnumbers the other one. This can be confirmed for the flashover dataset with a scaling of *4 km x 3 sec*, hence the main focus lies in the comparison of RUSBoost models.

RUSBoost in Matlab

Abbildung 128shows the input that is needed in Matlab in order to train a classifier model.

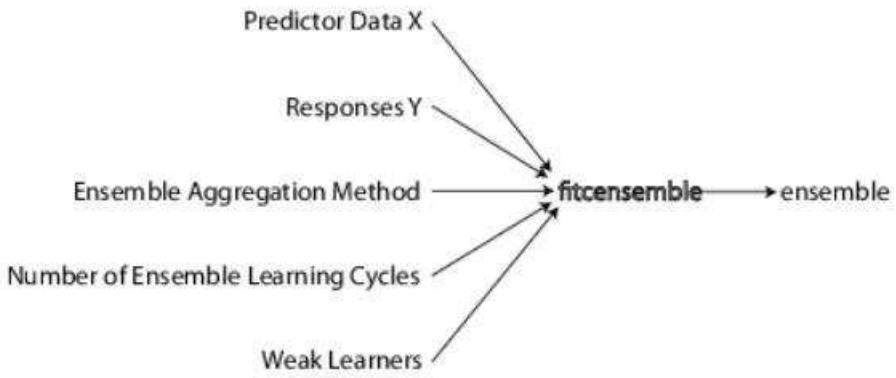

Abbildung 128: Input for training a classifier model in Matlab.

Source: https://de.mathworks.com/help/stats/framework-for-ensemble-learning.html

Predictor Data X are the features used to describe a flashover's region. *Responses Y* is a binary variable for the flashover. *Ensemble Aggregation Method* describes the boost method that is used. *Number of Ensemble Learning Cycles* balances the act between speed and accuracy. A large amount of cycles can lead to overfitting. The standard procedure is to check at which amount of cycles the classification error is not getting smaller anymore. Matlab does this without a user input and terminates the iterations by itself. Nonetheless, the maximum number of cycles is set to 30. *Weak Learners* are defined as trees. Tree branches are created that differentiate the values of a specific parameter and combinations of parameters. Hence, depending on what combination of parameter values a observations has, and the branches created by the model, it is classified into class 0 or 1. The number of maximum splits balances training time and memory usage. Fewer splits lead to less branches. The more branches the more specific the model gets, but it also takes longer for the model to be trained. The number of maximum splits is set to 555.

8.10 Model Selection

In order to choose a good model, different combinations of parameters were calculated and compared by the aforementioned TPR, FPR and AUC. The dataset that was used for the calculation included data from images with a distance of 8 km (scale of x-axis; defined by variable *meter*) and a duration of 3 seconds (scale of y-axis; defined by variable *sec*) where a flashover appeared in the image. 28 from the 55 flashovers were useable for this scaling to train the model after transforming the RGB images into binary ones. After the morphological cleaning the other 27 flashover images did not show a good chevron to train the model on. As

there exists multiple models due to different combinations of parameters, only a sample is shown in Tabelle 18 where either the TPR is higher than 95% or the FPR is lower 3%.

Nr	Parameters	TPR	FPR	AUC
1	All	96	1	1
2*	propDistance, duration, extent, extentCon, orientation, location	96	1	1
3	propDistance, duration, shape, shapeCon, orientation, location	96	3	0.99
4	propDistance, duration, extent, extentCon, location	96	1	1
5	propDistance, duration, shape, shapeCon, location	96	2	0.99
6*	propDistance, duration, extent, extentCon, density, location	100	1	1
7	propDistance, duration, shape, shapeCon, density, location	93	2	1
8	propDistance, duration, extent, extentCon, eccentricity, location	96	1	1
9	propDistance, duration, shape, shapeCon, eccentricity, location	96	2	1
10*	propDistance, duration, location	100	4	0.99

Tabelle 18: Sample models tested with different parameters.

Even though Model 1 has good results on all three criterions, it is ignored for further tests as the risk of overfitting is fairly high when fitting a small dataset with many parameters. Model 6 and 10 achieved the maximum TPR, meaning that all of the flashovers were correctly classified as flashovers. Additionally model 2 is taken into consideration as one of the three models with a TPR of 96% and a FPR of 1%.

8.11 Simulations and Performance

Models 2, 6 and 10, called *Orientation*, *Density* and *DistDur,* are used to train and simulate RUSBoost models. This time not only on data from images with the scale *8 km x 3 sec*, but also

- 4 km x 3 sec (regions removed)
- 4 km x 3 sec
- 4 km x 2 sec (regions removed)
- 4 km x 2 sec
- 2 km x 3 sec (regions removed)
- 8 km x 3 sec (regions removed)
- 8 km x 3 sec (median-cleaned colormap)

The median-cleaned colormap models are a different approach to using Matlab built-in colormaps. It normalizes the data and instead of using the median, it takes 0 as the reference point for the colourbar. This, on the one hand, results in a clearer and more easily readable image (both for the human eye and the machine) as seen in Abbildung 129, but on the other hand also takes longer to process.

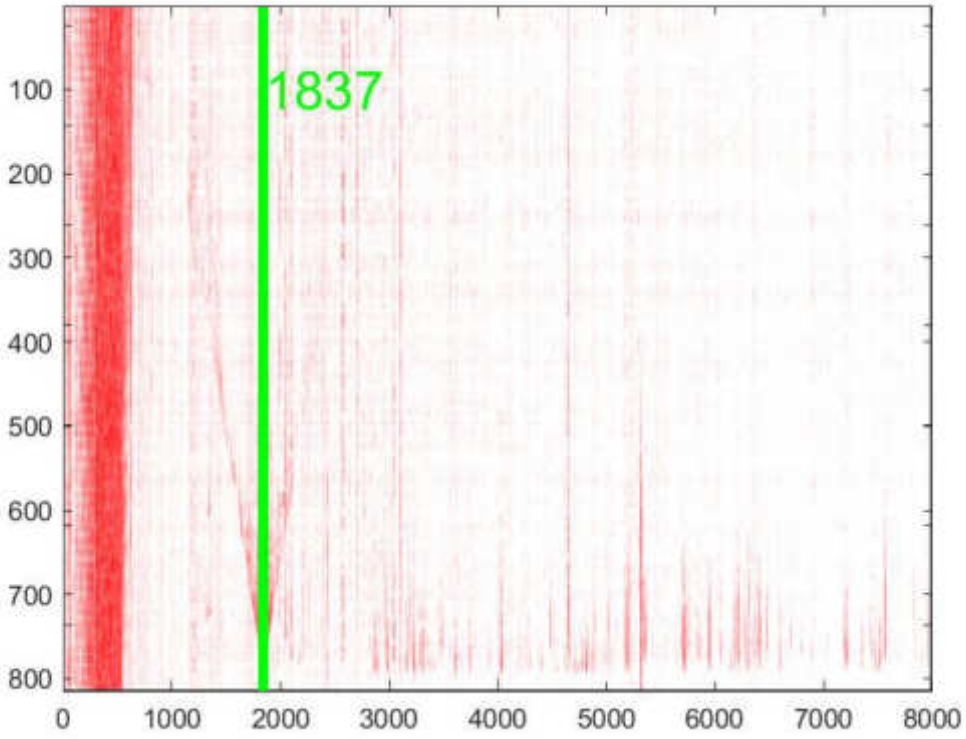

Abbildung 129: Median-cleaned colormap of a flashover, measurement 19.

The *4 km x 3 sec (region removed)* models are an exception as they were trained not only with images from one frequency per flashover, but all frequencies. This resulted in more acceptable binary images. Hence, the model has 59 different flashover images on which it is trained on. Testing was performed by splitting every dataset into two random samples with a ratio of ~50:50. E.g. the dataset for the scaling *8 km x 3 sec* contains 1462 observations from 29 short circuits that are usable; both samples therefore contain 731 observations. Sample A is used to train the model, sample B is used to fit the trained model and calculate the TPR and FPR. As a reminder, the true positive rate describes the amount of regions marked as potential flashovers that are really flashovers; the false positive rate describes the amount of regions

marked as potential flashovers that are not flashovers. In order to obtain a more reliable result from these simulations, random sampling, training and fitting is repeated 2000 times and the means of all rates are calculated. Tabelle 19 shows the mean rates of the specified models.

Scaling	TPR	FPR	FO	Regions
Model Orientation				
4 km x 3 sec (regions removed)	81.60%	9.28%	59	286
4 km x 3 sec	95.27%	1.48%	38	4085
4 km x 2 sec (regions removed)	79.69%	12.23%	37	227
4 km x 2 sec	95.38%	1.86%	33	4780
2 km x 3 sec (regions removed)	82.95%	8.95%	35	249
8 km x 3 sec (regions removed)	84.48%	9.86%	28	127
8 km x 3 sec (median-cleaned colormap)	98.86%	1.22%	31	2573
8 km x 3 sec	95.57%	2.81%	28	1462
Model Density				
4 km x 3 sec (regions removed)	83.21%	9.01%	59	286
4 km x 3 sec	94.86%	1.33%	38	4085
4 km x 2 sec (regions removed)	80.91%	10.72%	37	227
4 km x 2 sec	95.43%	1.82%	33	4780
2 km x 3 sec (regions removed)	82.86%	8.41%	35	249
8 km x 3 sec (regions removed)	85.53%	9.35%	28	127
8 km x 3 sec (median-cleaned colormap)	99.10%	1.24%	31	2573
8 km x 3 sec	95.87%	2.94%	28	1462
Model DistDur				
4 km x 3 sec (regions removed)	78.37%	16.32%	59	286
4 km x 3 sec	94.87%	1.77%	38	4085
4 km x 2 sec (regions removed)	70.25%	18.62%	37	227
4 km x 2 sec	95.35%	2.03%	33	4780
2 km x 3 sec (regions removed)	82.52%	9.05%	35	249
8 km x 3 sec (regions removed)	70.25%	21.77%	28	127
8 km x 3 sec (median-cleaned colormap)	98.57%	1.96%	31	2573
8 km x 3 sec	96.00%	4.99%	28	1462

Tabelle 19: TPR, FPR, number of flashovers and amount of regions from the different models.

All models without reduced amounts of regions perform better than their region-removed counterparts. In addition, median-cleaned colourmaps always perform slightly better still. As an example, the model *Orientation* with the scaling *8 km x 3 sec* and a median-cleaned colourmap has a TPR 98.86% and a FPR of 1.22%. This means that on average 31 (31*0.9886

= 30.65) out of the 31 usable flashovers are seen correctly as a flashover. On the other hand, on average 16 (2573/2*0.0122 = 15.7) out of the 2573 regions that are not flashovers are seen as a flashover.

8.12 Runtime

Not only the TPR and FPR are important to assess the performance of a model, but also the time it takes the whole code to run in its entirety. It is important to consider that by now the algorithm produces 12 images. Six images for octave frequency ranges (e.g. 39 – 59 Hz, 303 – 605 Hz) and six for the accumulation of these frequency ranges (e.g. 0 – 605 Hz, 0 – 1250 Hz). The reason for doing this is that after the experiments in Allerding and St. Pölten, the hypothesis was formed that every track produces the best image of the flashover on a different frequency range. Before knowing the right frequency range for a specific track, more data must be analysed. Hence, the time of how long the code runs for a specific scaling of a model is divided into a test where all 12 ranges are calculated but only one is used and one where six ranges are used. The *fibrelength* is set to 30 km and the timeframe around the flashover to 6 seconds. Tabelle 20 shows the runtime in minutes.

Scaling	**Duration (s), 1 Frequency**	**Duration (s), 6 Frequencies**
4 km x 3 sec	42.55	65
4 km x 2 sec	48.27	85.52
8 km x 3 sec	38.62	50.67
8 km x 3 sec (median-cleaned colormap)	54.53	73.42

Tabelle 20: Runtime of the code in minutes.

It shows a trend that was to be expected. The lower the scaling of the distance/time, the more images must be plotted and the longer it takes for the code to run., It also seems that, independently of the track from which the data originated, the accumulated frequency range 0 – 1250 Hz gives the best image. This on the one hand may spare us the act of finding the best frequency range for a new track; on the other hand this might give rise to problems when other noise sources (e.g. passing trains) are nearby. Although the median-cleaned colourmap model takes the longest it also produces better images for low frequency bands which would counter the noise source problem.

Matlab has a built in function (profiler) to track how long code, and every function used in it, requires to run. Abbildung 130 shows a part of that profiler for the scaling *8 km x 3 sec* and one frequency image used. The functions are ordered descending by their execution time. The calculation of the PCA (Principal Components Analysis) consumes about 38% of the total time the code runs. The PCA is a common technique used for pattern recognition in high dimensional data. As the PCA is needed for the pre-processing of the data, little can be done on this part of the code to make it faster without significant research.

Function Name	Calls	Total Time	**Self Time***	Total Time Plot (dark band = self time)
pca>localSVD	923940	583.792 s	480.899 s	
pca	923940	1905.807 s	391.399 s	
statset	923940	187.506 s	187.506 s	
parseArgs	925632	177.710 s	127.317 s	
getParamVal	1847880	197.220 s	120.274 s	
wnanmean	923940	117.426 s	117.426 s	
KSSoundfieldAnalysisDetection	20	2256.436 s	94.186 s	
Decimator>Decimator.process	1180	2006.800 s	86.259 s	
cellstr	1848080	76.962 s	76.962 s	
parseArgs	925632	233.368 s	55.658 s	
removenan	923941	55.121 s	55.121 s	
num2cell	924888	50.432 s	50.432 s	
removenan	923941	102.895 s	47.774 s	
isString	925612	51.682 s	38.532 s	
RawFDSFile>RawFDSFile.readData	1180	38.905 s	38.274 s	
getParamVal	1847880	235.004 s	37.785 s	

Abbildung 130: Profiler for 8 km x 3 sec, ordered by Self Time.

8.13 Further Work

Choosing the Optimal Model and Additional Tests

After the simulation and the runtime tests, another test is required to find correctly classified flashovers. By always excluding one of the flashovers from the trainings data set and allowing the algorithm to look for this flashover in its .fds file, we get a list for every model that tells which one of the flashovers was found.

Reducing Runtime

- Decreasing the length of the time frame. Setting it to one second, results in only one image per 8 km distance, reducing the time from 38 minutes to 9 minutes. The only risk to consider is that if the time of the flashover and the time the algorithm is provided with are not synchronous, the flashover may not fall into the specified time frame and is not seen at all.
- Reducing the amount of methods to transform RGB images. When there is only one method instead of three (or even four as in the case of median-cleaned colourmaps) to transform RGB images into grayscale images, less time is consumed to transform the images, find their regions and calculate the features.
- Instead of only extracting one frequency range from the 12 figure plots, really just calculate the only frequency range needed.
- Optimising or replacing the PCA function

➔ All three approaches would additionally most probably lead to fewer entries into the list of potential flashovers.

Additional Region Properties

Even though plenty of research has been done on feature extraction from the regions, this has not been exhaustive and there may still exist others that could influence the models in a positive way.

Alternatives to Image Processing

As stated, the PCA takes the most time of the processing. Research should be done on methods other than image processing where a PCA may not be needed or which are generally better suited for the task of finding a short circuit.

Reducing and Ordering Entries

By now the only way of reducing entries in the list of potential flashovers is the fusion of events that happened at the same time and are not further than 10 m from their mean distance value. A better solution than this should be implemented into the code. Additionally a comparison between events that happened at the same time and at the same distance but in different images must be likewise implemented.

Marking Flashovers

The function for marking flashovers for the training data is still not able to differentiate between regions which bounding boxes are overlapping. As this happens only in a few special cases, this does not have high priority.

struct2table

The Matlab built-in function *struct2table* exits with an error if the structure contains only one observation for every field. Currently, there are still more potential flashovers in the result list, which is why this was not a high priority problem.

Generally Improve Code

- The function *extractRegionpropForTrainingModel()* still produces one excel file with two sheets, one for the features and one for the descriptive statistics. This should be changed into two separate .csv files.
- Extracting features of new flashovers saves them into a new .csv file and they must be added to the existing training data file by hand. This process should be automated. Separate script files exist which have to run for the median-cleaned colourmaps. If they should be used in the future, this must be implemented in the main scripts.

8.14 Conclusion

Making use of the data we gathered from experiments in Allerding and St. Pölten, a Matlab algorithm was written with the purpose of finding the location of short circuits. After plotting the soundfield of every flashover, they were categorised into five groups. By definition, only category 1 and 2 show flashover with a prominent chevron or “V”. As the main part of the code relies on image processing to find this chevron only the data from those two categories have been used. The recorded flashovers are transformed into binary images by different methods and the features of the still existent regions are extracted. These features are used to train models typically of the scaling *8 km x 3 sec*. As the data is heavily skewed, due to the fact that an image may only contain one flashover or even none, the logical choice fell on RUSBoost models. Several models with different combinations of parameters were trained and the three best performing were simulated 2000 times with different scaling in order to get the TPR and FPR for every simulation. Further, the runtime of the various models with distinct scaling and colourmaps was also analysed. The combination of TPR, FPR and runtime helped to decide

which parameters, scaling and colourmap optimised the results. The trained model was fitted to recorded data in order to find potential regions of flashovers and to determine the location of a short circuit. This information was marked in RGB images of the flashovers and saved. The features of the recorded flashovers are, if useable, added to the training data in order to increase the models accuracy over time.